Università degli Studi di Palermo *Université Claude Bernard Lyon-1*

DIPARTIMENTO DI CHIMICA E FISICA DELLA TERRA
ED APPLICAZIONI ALLE GEORISORSE E AI RISCHI NATURALI C.F.T.A. (Palermo)

INSTITUT GÉNIE DE L'ENVIRONNEMENT ET ECODÉVELOPPEMENT
& DÉPARTEMENT SCIENCES DE LA TERRE (Lyon)

Co-supervision Ph.D. in Geochemistry

DOTTORATO DI RICERCA IN GEOCHIMICA- XXII Cycle (GEO/08)

DOCTORAT DE RECHERCHE EN GÉOCHIMIE

The behaviour of trace elements during the volcanic ash-liquid interaction. Example of marine and human systems.

Ph.D. thesis by

Loredana Antonella Randazzo

Ph.D Coordinator:

Prof. F. Parello
(Ph.D director, University of Palermo)

Supervisors:

Prof. P. Censi (University of Palermo)

Prof. P. Zuddas (University of Lyon)

Jan 2008 – Dec 2010

Università degli Studi di Palermo *Université Claude Bernard Lyon-1*

DIPARTIMENTO DI CHIMICA E FISICA DELLA TERRA
ED APPLICAZIONI ALLE GEORISORSE E AI RISCHI NATURALI C.F.T.A. (Palermo)

INSTITUT GÉNIE DE L'ENVIRONNEMENT ET ECODÉVELOPPEMENT
& DÉPARTEMENT SCIENCES DE LA TERRE (Lyon)

Co-supervision Ph.D. in Geochemistry

DOTTORATO DI RICERCA IN GEOCHIMICA- XXII Cycle (GEO/08)
DOCTORAT DE RECHERCHE EN GÉOCHIMIE

THE BEHAVIOUR OF TRACE ELEMENTS DURING THE VOLCANIC ASH-LIQUID INTERACTION. EXAMPLE OF MARINE AND HUMAN SYSTEMS.

Ph.D. thesis by

Loredana Antonella Randazzo

Ph.D Coordinator:

Prof. F. Parello

(Ph.D director, University of Palermo)

Supervisors:

Prof. P. Censi (University of Palermo)

Prof. P. Zuddas (University of Lyon)

Reviewers:

Prof. R. Hannigan (University of Massachusetts, Boston)

Prof. R. Petrini (University of Trieste, Italy)

Dr. S. Speziale (Deutsches GeoForschungsZentrum, Germany)

Board of examiners:

Prof. A. Aiuppa (University of Palermo)

Prof. R. Cirrincione (University of Catania)

Prof. P. Allemand (University of Lyon)

Prof. A.M Aucour (University of Lyon)

Jan 2008 – Dec 2010

CONTENTS

PREFACE

ABSTRACT……..1

Chapter I. - INTRODUCTION

1.1. The scientific problem ……....8
1.2. Plume composition and pyroclastic products of Etna's 2001 eruption ……...9
1.3. Consequences of volcanic ash delivery on marine system ……...10
1.4. The fate of inhaled particles ……..11
1.5 Objectives of this study ……..13
1.6 Rare Earth Elements (REEs) ……....14
References ……...19

Chapter II - THE BEHAVIOUR OF RARE EARTH ELEMENTS DURING THE VOLCANIC ASH DISSOLUTION IN SEAWATER SOLUTION.

2.1. Introduction ……....26
2.2. Materials and Methods ……....27
2.2.1. Starting materials ……27
2.2.1.1. Solid phase ……..…..27
2.2.1.2. Seawater solutions ……29
2.2.2 Experiments ……..30
2.2.2.1. Volcanic ash ……..30
2.2.2.2. Kinetic experiments …….……..31
2.2.3. Analyses……32

2.2.3.1. Solid phase ……32
2.2.3.1.1. Gravimetric and magnetic bulk separation ……....32
2.2.3.1.2. Morphological investigations ……33
2.2.3.2. Dissolved phase ……33
2.2.3.2.1. pH measurement …...……..33
2.2.3.2.2. SiO_2 measurement ……..……33
2.2.3.2.3. Ultrafiltration ……..34
2.2.3.2.4. YLn determination ……..34
2.3. Results and discussions ……...34
2.3.1. Evolution of the interacting solution ……34
2.3.1.1. VG-Sw ……..……..35
2.3.1.2. (Ol-Px)-Sw ……..……...35
2.3.1.3. Ash-Sw ……..35
2.3.1.4.Ash-CS and Ash-HAS…….35
2.3.1.5. Rare Earth Elements ……..43
2.3.2. SEM observations ……50
2.4. Conclusions …….....53
References …….....54

Chapter III - YTTRIUM AND LANTHANIDES IN HUMAN LUNG FLUIDS, PROBING THE EXPOSURE TO ATMOSPHERIC FALLOUT.

Abstract ……..60
3.1. Introduction ……..……60
3.1.1. Briefly description of alveoli anatomy ……61
3.2. Experimental section ……...62
3.2.1. Briefly characterization of the particulate emitted by Etna volcano in summer 2001 ……..62
3.2.2. BAL extraction and chemical processing of the samples…….63

3.2.3. Thermodynamic modelling ……..66
3.3. Results ……71
3.4. Implications ……73
References ……..75

Chapter IV - ORIGIN OF TRACE ELEMENTS IN HUMAN BRONCHOALVEOLAR LAVAGES DURING THE ETNA 2001 ERUPTION.

Abstract …….....80
4.1. Introduction ……..... 80
4.2. Experimental section …….. 81
4.2.1. Fine particulate emitted by Etna volcano in summer 2001 ……. 81
4.2.2. BAL extraction and chemical sample processing ……82
4.3. Results and discussion ……85
4.3.1. BAL composition ……85
4.3.2. Enrichment factors (EFs) ……87
4.3.3. Contribution of the anthropogenic sources ……..89
4.4.Conclusions ……..91
References ……..92

Concluding remarks …….……..……96

PREFACE

This Ph.D. thesis deals with chemical investigations on the processes occurring at suspended matter-liquid interface. The thesis consists of a general introduction presented in Chapter I, and three stand-alone papers, from Chapters II to IV. Each of the chapters contains a separate introduction, description of methods, presentation of data, discussion and a separate reference list. The independent papers are submitted for publication, as well as in preparation for submission to international journals.

A summary of topic and aim of each one is reported as following.

CHAPTER II

The behaviour of Rare Earth Elements during the volcanic ash dissolution in seawater solution.

Authors: **Randazzo L.A.**, Saiano. F., Zuddas P., Censi P.

Status: to be submitted.

This paper presents the results of a study on solid-liquid interaction in a simulated marine system. We carried out dissolution kinetic experiments and we focused our attention on the release of yttrium and lanthanides (YLn) from the glass and crystalline components of volcanic ash. In addition, we experimentally investigated how the competing ligand species present in seawater affect trace elements fractionation between dissolved and solid phases. Furthermore morphological investigations were carried out on solids before and during kinetic experiments in order to evidence the alteration structures and as support to chemical data.

CHAPTER III

Yttrium and lanthanides in human lung fluids, probing the exposure to atmospheric fallout.

Autors: Censi P., Tamburo E., Speziale S., Zuddas P., **Randazzo L.A.,** Punturo R., Cuttitta A., Aricò P.

Status: in press on *Journal of Hazardous Materials.*

This study investigates the ash-liquid interaction in a human system. The normalised YLn pattern distribution was studied in bronchoalveolar lavages (BAL) collected from selected individuals that, just after the exposure to strong delivery of atmospheric ash of volcanic origin, showed respiratory problems. This study highlights the capacity to use a typical geochemical investigation tool to investigate the consequences of erupted volcanic ash on human health.

CHAPTER VI

Origin of trace elements in human bronchoalveolar lavages during the Etna 2001 eruption.

Autors: P. Censi, P. Zuddas, L.A. **Randazzo**, E. Tamburo, A. Cuttitta, R. Punturo, P. Aricò, R. Santagata,.

Status: submitted to *Environment International*.

On the bronchoalveolar lavages (BAL) of the same patients were analysed minor and trace element concentrations in order to provide information about the exact origin and nature of inhaled particulate.

ABSTRACT

The solid-liquid interaction processes regulate the mechanisms governing the availability of trace elements in liquid phase. In this paper, these processes have been studied through the use of the Rare Earth Elements (REE) since they are excellent tracers of geochemical processes.

The purpose of the first part of this work was to study the reactivity of volcanic particulates during the interaction with synthetic seawater. This investigation was carried out through batch experiments for a maximum period of 6 months. Further investigation was carried out by adding NaHCO3 (160 mg/L) and humic acids (5 mg/L) to the synthetic seawater, in order to test the possible effects on the solid and on the elements behaviour in the solution. Since the volcanic ash (in this study from the eruption of Etna in 2001) consists mainly of glass (70%), olivine and clinopyroxene, it was also considered the reactivity both of glass and mineral fractions interacting with the synthetic solution without ligands. The results show that concentrations of REE measured in the solution interacting with volcanic glass, are about 2 times greater than experiments with mineral fraction, suggesting that these elements are mainly released by the glassy fraction. In all experiments REEs show concentration increases in solution but there are intervals where concentrations tend to decrease. This trend suggests that apart from the dissolution, which is the main process, a surface adsorption process also occurs, probably on the surface of newly formed crystals. The supposed presence of these minerals is suggested by the temporal variation of the Y/Ho ratio. In the solution with minerals the Y/Ho ratio, for example, at the end of the experiment rising, suggesting the formation on the mineral surfaces consisting of Al and Fe oxy-hydroxides, where Ho is preferably adsorbed. On the contrary, in the solution with glass the Y/Ho ratio decreases suggesting the presence of clay minerals on the surface, where Y is preferentially scavenged. The presence of the above mentioned newly formed minerals, is confirmed by SEM observations and XRD analysis. Finally the addition of ligand species to dissolved media does not increase dissolution rate of volcanic particles but modify the YLn distribution in liquid phase.

In the second part of this work, the Rare Earth study was applied to a human system. These elements were used, in fact, to investigate the effects due to the interactions between the inhaled atmospheric particulate matter and the lung fluids (BAL), in people exposed to fallout of volcanic ash. The observed concave shale of normalised YLn patterns in BAL is very similar to those recognised in parent solutions that experienced co-precipitation of YLn-phosphates. This result suggests that phosphate precipitation occurs in lungs as a consequence of inhalation of volcanic particles and their interactions with lung fluids. This process is confirmed by thermodynamic and kinetic simulations indicating that crystallisation of YLn-phosphates and other authigenic phases occurs as a consequence of the soluble ash fraction dissolution. Finally, in the same biological system, minor and trace element concentrations were analysed in order to identify the origin and the nature of inhaled particulate matter. This study was carried out taking in account the enrichment factor (EF) in bronchoalveolar fluids with respect to the composition of the parent magma, the upper continental crust and the road dust. The effects of partial dissolution of a volcanic component in contact with lung fluids is recognised as the source of V, Cr, Mn, Fe, Co and U delivered to pulmonary system. Nevertheless the inhaled particle budget is also influenced by the presence of anthropogenic particles that interact with bronchial fluids enriching Ni, Cu, Cd and Pb in the fluid. Moreover the occurrence of the further industrial input is detected by means of La enrichment in BAL solutions. The combination of YLn fractionation in bronchial fluids can represent a potential tracer of exposure to atmospheric fallout and is suitable as a diagnostic parameter of environmental contaminant exposure.

RIASSUNTO

I processi d'interazione solido-liquido sono alla base dei meccanismi che governano la disponibilità degli elementi in tracce in fase liquida. In questo lavoro tali processi sono stati studiati attraverso l'utilizzo degli elementi delle Terre Rare (REE) che come serie di elementi, per le loro peculiari caratteristiche sono degli ottimi traccianti di processi geochimici.

Lo scopo della prima parte di questo lavoro è stato quello di studiare la reattività di un particolato vulcanico durante l'interazione con un'acqua marina sintetica. Tale indagine è stata effettuata attraverso esperimenti di tipo batch, per un periodo massimo di 6 mesi. Ulteriori indagini sono state effettuate aggiungendo NaHCO3 (160 mg/L) e umati (5 mg/L) alla soluzione salina, al fine di testare l'eventuale effetto sia sul solido che sul comportamento degli elementi in soluzione. Dal momento che l'ash vulcanico (proveniente dall'eruzione dell'Etna del 2001) è costituito principalmente da vetro (70%), olivina e clinopirosseno, è stata inoltre studiata anche la reattività delle singola frazione vetrosa e mineralogica a contatto con la soluzione salina senza leganti. I risultati mostrano che e concentrazioni di Terre Rare misurate nella soluzione a contatto con il vetro vulcanico sono maggiori mediamente di 2 volte rispetto alla frazione mineralogica, suggerendo che tali elementi sono principalmente rilasciati dalla frazione vetrosa. In tutti gli esperimenti le Terre Rare mostrano un aumento delle concentrazioni in soluzione intervallato da concentrazioni che tendono a diminuire. Questo andamento suggerisce che a parte la dissoluzione, che è il principale processo, si realizza anche un processo di adsorbimento superficiale, probabilmente su cristalli di neoformazione. La presunta presenza di tali minerali è suggerita dalle variazioni temporali del rapporto Y/Ho. Nella soluzione a contatto con i minerali si hanno, ad esempio, valori del rapporto Y/Ho in aumento nelle ultime fasi temporali, suggerendo che sulla superficie dei minerali si formano ossi-idrossidi di Al e Fe, dove l'Ho è preferibilmente adsorbito. Al contrario nella soluzione a contatto con il vetro il rapporto tende a diminuire suggerendo la presenza sulla superficie di minerali argillosi dove si ha di preferenza scavenging di Y. La presenza dei minerali di neoformazione sopracitati è inoltre

confermata da osservazioni al microscopio elettronico a scansione (SEM) e da analisi in XRD. Infine l'aggiunta di specie leganti in soluzione non determina un aumento della dissoluzione ma ha un effetto sulla distribuzione degli elementi in tracce in fase liquida.

Nella seconda parte del lavoro lo studio delle Terre Rare è stato applicato ad un sistema umano. Le Terre Rare sono, infatti, state utilizzate per indagare gli effetti causati dall'interazione tra particolato atmosferico inalato e fluidi broncoalveolari (BAL). Tale indagine è stata eseguita su soggetti esposti ad un intenso fallout di particolato vulcanico. Il pattern delle Terre Rare normalizzate presenta una forma concava nei BAL che è molto simile a quello osservato in soluzioni che presentano co-precipitazione di Terre Rare con i fosfati. Questo dato suggerisce che nei polmoni si ha precipitazione delle Terre Rare con i fosfati, come conseguenza dell'inalazione di particelle vulcaniche e della loro interazione con i fluidi polmonari. Questo processo è confermato da simulazioni termodinamiche e cinetiche indicanti la cristallizzazione di fosfato di Terre Rare e altre fasi autigene come conseguenza della dissoluzione della frazione solubile della cenere vulcanica. Nello stesso sistema biologico sono infine state analizzate anche le concentrazioni di elementi minori ed in tracce, al fine di identificare l'esatta origine e la natura del particolato inalato. Tale studio è stato affrontato calcolando il fattore di arricchimento (EF) nei fluidi broncoalveolari rispetto a materiale di diversa origine. La presenza di V, Cr, Mn, Fe, Co e U nel sistema polmonare indica l'effetto della parziale dissoluzione della componente vulcanica a contatto con i fluidi polmonari. Tuttavia il budget di particolato inalato è anche influenzato dalla presenza di particelle di origine antropica che interagendo con i fluidi bronchiali portano ad un arricchimento in Ni, Cu, Cd e Pb. Arricchimenti in La nei BAL suggeriscono inoltre l'effetto di un ulteriore input di particolato inalato, riconducibile a quello industriale. La combinazione del frazionamento delle Terre Rare nei fluidi bronchiali può rappresentare un potenziale tracciante dell'esposizione al fallout atmosferico ed è un buon parametro diagnostico di esposizione a contaminati ambientali.

RÉSUMÉ

Les processus d'interaction solide-liquide réguler les mécanismes qui régissent la disponibilité des oligo-éléments en phase liquide. Dans cet article, ces processus ont été étudiés grâce à l'utilisation des éléments de terres rares (REE), car ils sont d'excellents traceurs des processus géochimiques.

Le but de la première partie de ce travail était d'étudier la réactivité des particules volcaniques lors de l'interaction avec l'eau de la mer synthétique. Cette enquête a été réalisée grâce à des expériences batch pour une période maximale de 6 mois. Une enquête plus poussée a été réalisée par l'ajout de NaHCO3 (160 mg/L) et d'acides humiques (5 mg/L) à l'eau de la mer synthétique, afin de tester les effets possibles sur le solide et sur les comportement de l'éléments dans la solution. Depuis les cendres volcaniques (dans cette étude de l'éruption de l'Etna en 2001) est principalement constitué de verre (70%), d'olivine et de clinopyroxène, il a été considéré la réactivité de verre et des minérales au cours de l'interaction avec la solution synthétique sans ligands. Les résultats montrent que les concentrations de terres rares mesurés dans la solution après l' interactions avec de verre volcanique, sont environ 2 fois plus que les expériences avec la fraction minérale, ce qui suggère que ces éléments sont principalement rejetés par la fraction vitreux. Dans toutes les expériences les terres rares montrent une augmentation des concentrations en solution, mais il y'a des intervalles où les concentrations ont tendance à diminuer. Cette tendance suggère que, en dehors de la dissolution, qui est le processus principal, un procédé d'adsorption de surface se produit également, probablement sur la surface des cristaux nouvellement formé. La présence supposée de ces minéraux est suggéré par la variation temporelle de l' Y/Ho. Dans la solution avec les minéraux, le rapport Y/Ho, par exemple, à la fin de l'expérience augmente, suggérant la formation sur les surfaces de oxy-hydroxydes de Al et Fe, où Ho est de préférence adsorbés. Au contraire, dans la solution avec le verre le rapport Y/Ho diminue suggérant la présence de minéraux argileux en surface, où Y est préférentiellement piégé. La présence des minéraux mentionnés ci-dessus, est confirmée par des observations SEM et analyse XRD.

Enfin, l'ajout des ligand dissous ne pas augmenter le taux de dissolution des particules volcaniques, mais modifiant la distribution de REE en phase liquide.

Dans la deuxième partie de ce travail, l'étude des terres rares a été appliquée à un système humain. Ces éléments ont été utilisés, en fait, d'enquêter sur les effets dus aux interactions entre les particules atmosphériques inhalées et les fluides du poumon (BAL) chez les personnes exposées aux retombées de cendres volcaniques. Les modèles normalisés des terre rare montre une forme concave dans le BAL qui est très similaire à ceux qui sont reconnus dans les solutions parent qui a connu la co-précipitation des phosphates-YLn. Ce résultat suggère que la précipitation du phosphate se produisent dans les poumons à la suite de l'inhalation de particules volcaniques et de leurs interactions avec des fluides du poumon. Ce processus est confirmé par des simulations thermodynamiques et cinétiques indiquant que la cristallisation de YLn-phosphates et d'autres phases authigènes apparaît comme la conséquence de la dissolution de la fraction solubles de cendres. Enfin, dans le même système biologique, les concentrations des éléments mineurs et en traces ont été analysés afin d'identifier l'origine et la nature des particules inhalées. Cette étude a été réalisée prenant en compte le facteur d'enrichissement (EF) dans les liquides du poumon en ce qui concerne la composition du magma, la croûte continentale supérieure et de la poussière de la route. Les effets de la dissolution partielle d'un composant volcaniques en contact avec les fluides du poumon est reconnu comme la source de V, Cr, Mn, Fe, Co et U livré au système pulmonaire. Cependant, le budget des particules inhalées est également influencée par la présence de particules anthropiques qui interagissent avec des liquides bronchiques enrichir Ni, Cu, Cd et Pb dans le liquide. Enrichissement le La dans BAL suggère également l'effet d'un apport supplémentaire de particules par inhalation, en raison de l'industrie. La combinaison de fractionnement des REE dans les fluides bronchique peut représenter un potentiel marqueur de l'exposition aux retombées atmosphériques et est approprié comme un paramètre diagnostic de l'exposition aux contaminants environnementaux.

Chapter I

Introduction

1.1 - The scientific problem
1.2 - Plume composition and pyroclastic products of Etna's 2001 eruption
1.3 - Consequences of volcanic ash delivery on marine system
1.4 - The fate of inhaled particles
1.5 - Objectives of the study
1.6 - Rare Earth Elements (REE)

1.1. The scientific problem

Solid-liquid reactions *lato sensu* are mainly responsible of chemical changes in the hydrosphere. The geochemical approach to the investigation of these processes works in marine systems (Jinkel et al., 2005; Sauthou et al., 2007), both in open oceanic environment (Greaves et al., 1999) and especially in limited semi-closed basin such as the Mediterranean Sea (Guieu et al., 1997; 2002). In seawater, speciation of many minor and trace elements is mainly related to carbonate-bearing species. This evidence is also true for yttrium and lanthanides (YLn), although in coastal areas organic species can play an important role (Censi et al., 2010). According to geochemical investigations of YLn their distribution is one of the best proxies to investigate solid-liquid interface processes due to the capability to fractionate during both dissolved and surface complexation processes. In the Mediterranean Sea, atmospheric fallout can originate also from volcanic activity and only recent investigations have focused on the delivery of freshly-erupted volcanic ash to seawater as the cause of changes in the water column (Censi et al., 2007; 2010). This is despite complexation effect of YLn in seawater after dissolution of volcanic dust which have also to clarified.

Therefore this is the scope of this study and we suggest that the used geochemical approach can be borrowed to study not only processes occurring between volcanic dusts and water, but also to study other solid-liquid interfaces such us biological fluids exposed to interactions with the same solids. The eruption of Etna in Summer 2001 gave us the possibility to study the interaction between seawater with volcanic ash and investigate the kinetic evolution of these interactions. This eruption was the largest pyroclastic phenomena of Etna since about 200 years ago (Viccaro et al., 2006) and the fallout impacted Catania, the most anthropised area in Sicily. The combinating natural and anthropogenic aerosols gave us the possibility to apply the geochemical approach also to the solid-liquid reactions occurring in human lungs of people who inhaled volcanic particles. It represents the first worldwide investigation of this topic and demonstrates that the geochemical approach is suitable to investigate solid-liquid interface process independently of the nature of involved liquids.

1.2. Plume composition and pyroclastic products of Etna's 2001 eruption

Mount Etna, the most active and extensively degassing volcano in Europe (Chester et al., 1985; Allard et al., 1991; Tanguy et al., 1997; Schiano et al., 2001), has been in a persistent active state for the last 200,000 years, with frequent paroxysmal episodes separated by passive degassing periods (Aiuppa et al. 2005). Between July 17 and August 9 2001 Mt. Etna produced a complex eruption involving both a summit and a significant flank eruption (Acocella and Neri, 2003, INGV, 2001), after a long phase of degassing with intermittent small-scale eruptions at the summit Craters (Aiuppa et al. 2002). During eruptive episodes Etna released gases and particles that were dispersed in the atmosphere constituting the volcanic plume, a peculiar physical/chemical system. The emitted gas phase mainly consisted of water vapour (that represents 70–90%), carbon dioxide (that is likely to be relatively inert during atmospheric dilution), acidic gaseous volatile species (SO_2, H_2S), hydrogen halides (HCl, HF, HBr) and H_2, CO, N_2, CH_4 (Symonds et al., 1994, Bardintzeff, 1998).

As reactive species are emitted from the vent, cooled and mixed with atmospheric gases, they are available to take part in both homogeneous (gas-only) and heterogeneous (gas-liquid-solid) reactions (Aiuppa et al. 2006). Because the annual CO_2 and SO_2 emission from Etna are about 12 and 2 Mt, respectively (Allard et al., 1991; Allard, 1997; Aiuppa et al., 2006), this volcano is recognized as the greatest emitter of volatiles on Earth. The mixing of the atmospheric gases (especially atmospheric oxygen) with the high-temperature volcanic plume gases followed by dilution and fast cooling has the potential to alter the composition of the volcanic material emitted from the volcano (Gerlach & Nordlie 1975; Martin et al. 2006).

In addition to the release of several gases, molten and solid rock fragments (tephra) were emitted into the air. The ash (rock fragments with diameter <2 mm) rising into the air formed an eruption column (Grainger and Highwood, 2003) and together with solid sulfur-derived particles, represent the dominant component. Ash materials produced during the pristine stage were the richest in glass and this fraction decreased from sideromelane to tachylites (the two different end-members produced during

explosive activity of Mt. Etna, 2001) that represent the final stage of the pyroclastic episode (Taddeucci et al 2004). Tephra are porphyritic with large variability in phenocryst content (15–39% vol) consisting of plagioclase, clinopyroxene, olivine and Ti-magnetite (Corsaro and Pompilio 2004c). On the whole, large microlites enclosed in both sideromelane and tachylite are euhedral: plagioclases are usually tabular with minor skeletal (i.e., swallow-tail) shapes; olivine and Ti-magnetite form blocky or sub-rounded crystals; pyroxene microlites are, everywhere, prismatic (Taddeucci et al., 2004).

Clinopyroxene and olivine are more abundant than plagioclase in the material emitted from the lower volcanic vents. This feature is typical for Etnean "eccentric" (or peripheral) eruptions (Rittmann 1965; Armienti et al. 1988; Pompilio et al. 1995), so defined because they are fed by dikes that are independent of the plumbing system involved in summit crater activity (Viccaro et al.2007). Clinopyroxene is the most abundant mineral (8–14% vol.) and, when measured in the inner and outer zone of cognate xenoliths, extend to a wider compositional range from augite to fassaite. Most crystals are subhedral, sub-millimeter in size, and frequently enclose Ti-magnetite; others range from 3 to 10 mm, are euhedral and enclose Ti-magnetite, olivine, and, more rarely, plagioclase and glass. Olivine (1–3% vol.) is generally sub-rounded and sub-millimeter in size; crystals up to 7 mm are euhedral and show complex compositional zoning. Within this group, the most frequent compositions are between Fo 75–67 (Corsaro et al. 2007).

1.3. Consequences of volcanic ash delivery on marine system

It was widely demonstrated that the chemical weathering of silicate minerals influences the chemistry of natural waters both in terms of release of trace elements and determining scavenging processes onto surfaces of newly-formed alteration minerals (Berner, 1980; Schott et al., 1981; Berner and Schott, 1982; Schott and Berner, 1983, 1985; Spivack e Staudigel, 1994; Brady e Gislanson, 1997; Chester, 2000; Kump et al., 2000). Thus it is, on the whole, the most important factor affecting the geochemical behaviour and cycling of various elements (Louvat, 1997; Moulton et al., 2000;

Stefansson e Gislason, 2001).

Volcanic ash can come into contact with many atmospheric, terrestrial and oceanic systems and undergo a range of processes once deposited (Cronin et al., 2003; Frogner et al., 2001; Frogner Kockum et al., 2006). Recently there has been interest on impact of volcanic ash on terrestrial and marine ecosystem as the ash may fertilize the marine environment, and so directly impact the marine primary productivity (MPP), the biological carbon pump and climate (Censi et al., 2010b; Olgun et al., 2010; Duggen et al., 2007; Jones and Gislason, 2008; Frogner et al., 2001; Langmann et al., 2010, Duggen et al., 2010).

Volcanic eruptions can induce complex environmental effects as many cycles in the Earth system are affected simultaneously. An important consideration is the release of gases, aerosols, and metal salts during an eruption, which have the ability to initiate rapid biogeochemical changes upon deposition (Jones and Gislason, 2008) such as seawater fertilization and, subsequently, phytoplanktonic growth, after dissolution (Duggen et al., 2010; Censi et al. 2010). Therefore, the reaction of minerals and glasses with aqueous fluids at low temperatures is one of the major geochemical processes on the Earth's surface (Stumm and Morgan, 1996). The alteration of glass has become a subject of growing interest in geochemistry (Berger et al., 1987; Crovisier et al., 1987; Ghiara et al., 1993; Gieskes and Lawrence, 1981; Gíslason and Eugster, 1987; Guy et al., 1992; Oelkers and Gíslason, 2001; Seyfried and Bischoff, 1979; Wolff-Boenisch et al., 2004; Yokoyama and Banfield, 2002), since volcanic glass, having a relatively rapid dissolution rate, plays a major role in the global flux and cycling of numerous elements.

1.4. The fate of inhaled particles

Depending upon their aerodynamic diameter, inhaled particles migrate to the alveoli in the deep lung if they are not retained in the upper airways. Generally the mucosa present in the pharynx can block particles with a diameters between 10 and 6 μm; if particles have a diameter between 6 and 3 μm they do not go into the bronchiole while particles with an aerodynamic diameter less than 1 μm enter the alveoli causing

serious damage. In particular, nanoparticles can pass through the epithelial layer and reach other organs via blood circulation. In the alveoli, several events may follow, depending upon the particles form, size, chemical composition and surface state. Particles can damage epithelial cells that constitute the alveoli wall though which gaseous exchanges can occur (Figure 1.1).

The particles also activate immune defenses, sending signals to alveolar macrophage (AM) cells, which engulf (phagocytose) and remove the foreign substances. If the AM are successful (clearance), there will be no harm; conversely, the activated macrophage can eventually die, releasing around the particles and many other substances, including factors to recruit new immune-defences cells (Fubini and Fenoglio, 2007). A continuous cycle of recruitment and cell death will be established, which causes sustained inflammation that lasts as long as the particles reside in the lung. The causes of the inflammation are the substances released during AM activation, cytokines, ROS (Reactive Oxygen Species) and growth factors, all of which contribute to damaging the surrounding epithelial cells and stimulating abnormal growth of fibroblasts, for example. The long term consequences may be very serious.

The surface chemistry of the particles plays a fundamental role in governing most mechanisms of interaction. Their reactivity, and hence potential toxicity, is directed by:

- mineral habit; a fibrous habit, for example, is relevant for toxicity, because macrophages cannot engulf them successfully, while amorphous silica causes little damage;
- sharp edges;
- fractured surfaces;
- surface defects;
- poorly coordinated ions.

Volcanoes produce nano- to micro- particles, including crystalline silica, with a toxic potential. As recently demonstrated (Schooner et al. 2006), some minerals, including forsterite, generate oxygenated free radicals in solution, with a tested toxic effect. Nevertheless, according to epidemiological and toxicological studies, the health

risk of volcanic ash does not correlate with the crystalline silica content, probably due to the presence of other minerals such as clay minerals (Horwell and Baxter, 2006) with a protective effect against silicosis (that is caused by inhalation of crystalline silica dust, and is marked by inflammation and scarring in forms of nodular lesions in the upper lobes of the lungs) (Wallance et al. 1994). Conversely, iron in volcanic ash can impart a high reactivity by generating hydroxyl free radicals through the Fenton reaction (Horwell et al, 2003).

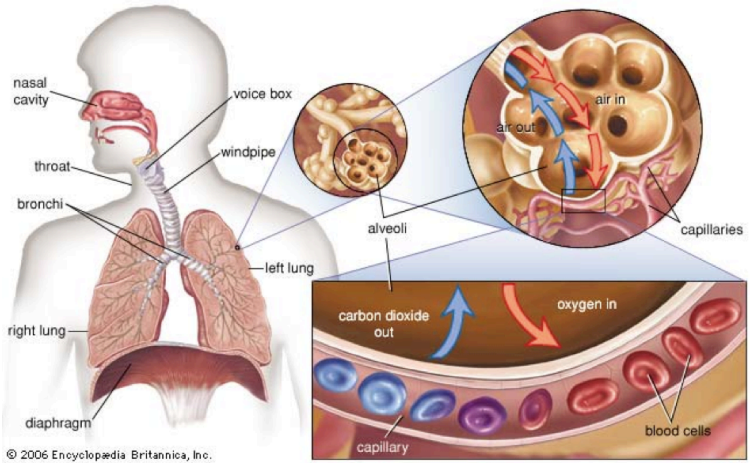

Figure 1.1 – Pulmonary alveoli representation.

1.5. Objectives of the study

This study, part of a wider research project, contributes to knowledge about trace elements release from fresh volcanic particulates in both marine and broncoalveolar fluids. The first process is studied on model system while the second is natural. This last study is designed to probe the human exposure to atmospheric fallout using a typical geochemical investigation tool as the shale-YLn normalized patterns.

For the study of ash-seawater solutions interaction:

- mineralogical characterization of the fresh volcanic ash;
- ash separation in to two components: glass and mineral;

- morphological investigation of minerals;
- experimental study of the kinetic of volcanic ash, volcanic glass and minerals for a period of six months, in saline solution;
- evaluation of the trace elements distribution in presence of carbonate and humic acid in seawater solution;
- morphological investigations of the volcanic ash during kinetic experiments and glass mineralogical characterization after six months of interaction.

For the study of inhaled ash-alveolar fluids:

- trace elements analyses on Broncoalveolar liquid (BAL) to assess the nature and source of inhaled particulate matter;
- determination of shale-YREE normalized pattern on the same BAL to probe the possible effects of Etna eruption on human health.

Rare Earth Elements were broadly used in these studies as useful investigation tools since, due to their peculiar chemical characteristics (see section 1.6), represent useful tracers of a wide range of geochemical processes leading to detailed descriptions of processes occurring at the solid-liquid interface. Moreover the study of YREE fractionation in bronchial fluids can represent a potential tracer of environmental stress.

1.6. Rare Earth Elements (REEs)

Lanthanides (Ln) consist of a coherent group of fourteen elements, from La (Z=57) to Lu (Z=71), that occur in a trivalent oxidation state in natural environments (except Ce and Eu). They can be divided into light (from La to Nd), middle (from Sm to Ho) and heavy (from Er to Lu). Pm, which can be produced by nuclear reactions, does not exist in nature in significant concentrations thus usually light lanthanides are comprise from La to Nd. Due to similarity of chemical behaviour induced by the same charge and similar atomic dimensions, also yttrium (Y) is associated to lanthanides (in particular heavy) during geochemical investigations (YLn).

The large interest in these elements is related to their behaviour derived from chemical

coherence, mainly due to the same external electronic configuration, as result of the progressively filling of the *f*-electron shell that is closer to the nucleus than *s*- and *p*-electron shells (Fig.1.2). The lanthanides with quite similar chemical behaviour and the large sensibility to record modifications of their coordination polyhedra, both in dissolved and surface environment, allowed several investigators to use lanthanides as geochemical tracers in the marine environment in order to obtain information about processes involving them along the water columns (de Baar et al., 1985; German et al., 1995; Zhang and Nozaki, 1996; Alibo and Nozaki, 2003; 2004).

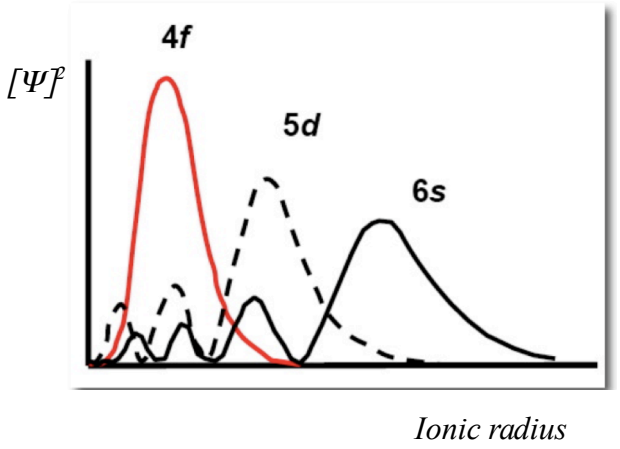

Figure 1.2 – Amplitude of wave functions of 4f, 5d and 6s shells

The effective ionic radii of REEs decreases systematically with increasing atomic number from La to Lu according to a phenomenon defined as "lanthanide contraction" (Shannon, 1976) (Fig.1.3). The REE's CHarge and RAdius-Controlled (CHARAC) behaviour (Bau, 1996) generates well-known smoothed patterns when they are normalized to average shale and/or chondrite. The occurrence of irregular features generally indicates that REEs are involved in non-CHARAC processes that differently influence their concentrations causing a sub-partition of the their normalized pattern into four "segments" called tetrads: La-Nd, Sm-Gd, Gd-Ho, Er-Lu (Masuda et al., 1987; Monecke et al., 2002).

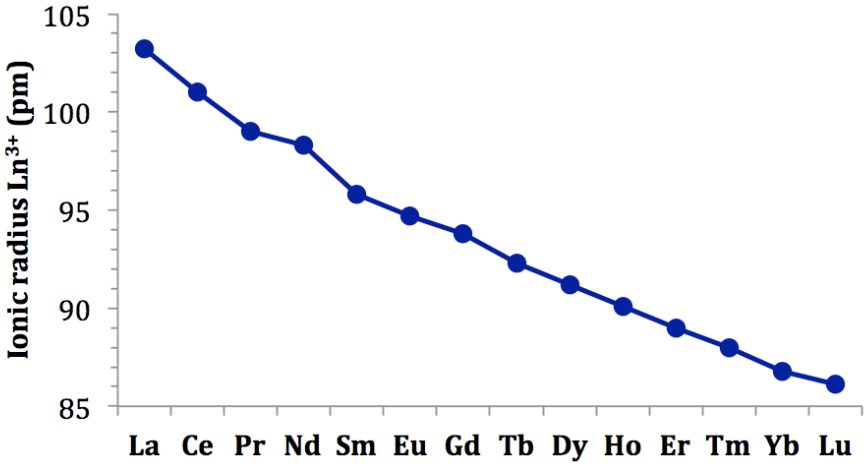

Figure 1.3 –Ionic radius across the Lanthanide series.

According to this view, tetrad effects are observed in the normalized REEs distributions of sediments and water when adsorption, co-precipitation, dissolution, complexation and/or ligand-exchange reactions occur (Masuda and Ikeuchi, 1979; Masuda et al., 1987; Kawabe, 1992).

From a theoretical point of view, tetrad effects are attributed to the incomplete filling of the 4f orbitals characteristic of the different lanthanides: the tetrads are produced by the "half-filled" effect for Gd^{3+} (with the ground-level electronic configuration of $[Xe](4f)^7$), the "one-quarter-filled" effect for Nd^{3+} ($[Xe](4f)^3$), and the "three-quarter-filled" effect for Er^{3+} ($[Xe](4f)^{11}$) and the full-filled effect for Lu^{3+} ($[Xe](4f)^{14}$). To explain the tetrad effect, a direct relationship between the electronic configuration of REE^{3+} ions $[Xe](4f)^q$ and the heterogeneous equilibria in seawater was invoked. According to Jørgensen (1970; 1979) and Nugent (1970) the tetrad effect could be clearly explained with "the refined spin-pairing energy theory (RSPET). Since a complete understanding of the tetrad effect is impossible taking into account only simple electrostatic forces involved in changes of the bonding energy of the lanthanide ions and their interaction with ligands, it can be better explained using the ligand-field theory.

Specifically, different free ions have different energies in relation to the variations in electron-electron repulsion and these different energies can be expressed using a small

number of electrostatic parameters (the Racah constants). These parameters are linear combinations of Coulomb and exchange integrals pertaining to the free metal ions related to the extent of electron-electron repulsion, and are determined empirically. The larger they are, the greater the repulsion is. Moreover, the Racah repulsion parameters for a metal complex vary in relation to changes of ligands or on the covalency of the coordination polyhedron. Spectroscopic observations suggest that the Racah parameters decrease slightly from the gaseous free ion values as a function of the anionic ligands involved in the formation of REE(III) complexes (Reisfeld and Jørgensen, 1977; Jørgensen, 1979). This effect is known as the nephelauxetic effect in the ligand-field theory and is explained by a reduction of the effects of repulsion as covalency increases. Therefore the covalency of the products and substrates involved in complexation and/or adsorption reactions influences the features and shapes of the tetrad effects.
The quantification of the tetrad effect can be expressed by the equation:

$$t_i = \sqrt{\frac{[REE]_2 \times [REE]_3}{[REE]_1 \times [REE]_4}} \quad (1)$$

(Monecke et al., 2002) where t_i is the amount of tetrad effect and $[REE]_{1\text{-}4}$ are the normalized REE concentrations of the first, second, third and fourth elements of a given tetrad. When $t_i > 1$ a downward convex, M-shaped tetrad effect is recognised in a given tetrad; when $t_i < 1$ a upward convex, w-shaped tetrad effect occurs; if $t_i = 1$ REE have a tetrad effect-free pattern. Tetrad effects with W-shaped features are indicative of adsorption mechanisms corresponding to lanthanide ion – ligand weaker covalence or dissolution processes, whereas upward convex or M-shaped patterns correspond to stronger covalence of the REE–O bond onto solid surfaces, or scavenging phenomena (Kawabe, 1992, Bau, 1999).

Similar to the tetrad effect, yttrium decoupling with respect to Ho also represents an indicator of non-CHARAC processes. Actually, Y shows large geochemical similarities with heavy lanthanides (mainly Ho) when are involved in CHARAC processes. In non-Radius controlled reactions its behaviour is substantially different, allowing us to use the Y/Ho ratio as proxy for these processes. The explanation of this phenomenon is due to the close similarity of Y and Ho ionic radii that plays a

fundamental role in determining their coupling during processes driven by differences in the ionic radii. During non-CHARAC processes, the most important feature of the Y-Ho behaviour consists of the differences in their electronic configuration ([Kr]$4d^0$ and [Xe]$4f^0$ (respectively for triply charged ions) that induces decoupling.

In oceanic seawater, the behaviour of shale-normalised lanthanides is always characterised by constant HREE enrichment and LREE depletion with a strong negative Ce anomaly. This feature is explained by the preferential Ce scavenging, as Ce (IV) is less soluble in superficial waters, and larger stability of HREE dissolved complexes then LREE complexes. At the same time, Y which has a similar distribution as Ho in crustal materials, is decoupled with respect to the Ho enriched in water. This phenomenon reflects the preferential removal of Ho by particulate matter from surface to deep seawater (Nozaki et al., 1997).

Modifications of YREE distribution with respect to this behaviour are considered to be an "anomaly". The amplitude can be quantified based on the REE shale-normalised concentrations according to the following expression:

$$\frac{[REE_i]}{[REE_i]^*} = \frac{2*[REE_i]_n}{[REE_{i-1}]_n + [REE_{i+1}]_n} \qquad (2)$$

where $[REE_i]_n$ represents the normalised content of some REE, $[REE_{i-1}]_n$ and $[REE_{i+1}]_n$ represent the REE contents of the previous and the next REE and $[REE_i]^*$ is the expected value of some REE calculated as average between the previous and the next element.

References

Acocella, V., Neri, M. (2003). What makes flank eruptions? The 2001 Etna eruption and its possible triggering mechanisms. Bull. Volcanol. 65, 517– 529.

Aiuppa, A., Federico, C., Paonita, A., Pecoraino, G., and Valenza, M. (2002). S, Cl and F degassing as indicator of volcanic dynamics, Geophys. Res. Lett. 29 (11), 10.1029/2002GL015032.

Aiuppa, A., Federico, C., Franco, A., Giudice, G., Gurrieri, S., Inguaggiato, S., Liuzzo, M., McGonigle, A. J. S. & Valenza, M. 2005a Emission of bromine and iodine from Mount Etna volcano. Geochem. Geophys. Geosyst. 6, Q08008. (doi:10.1029/2005GC000965).

Aiuppa, A., Bellomo, S., Brusca, L., D'Alessandro, W., Di Paola, R., Longo, M., (2006). Major ion bulk deposition around an active volcano (Mt. Etna, Italy). Bull. Volcanol. 68, 255–265.

Alibo D.S. and Nozaki. Y. (2004). Dissolved rare earth elements in the eastern Indian Ocean: chemical tracers of water masses. *Deep-Sea Res.* **51**, 559-576.

Allard P., Carbonelle J., Metrich N., and Zettwoog P. (1991). Eruptive and diffuse emissions of carbon dioxide from Etna volcano. Nature 351, 38–391.

Allard, P., 1997: Endogenous magma degassing and storage at Mount Etna, Geophys. Res. Lett. 24 (17), 2219–2222.

Armienti, P., Innocenti, F., Petrini, R., Pompilio, M., Villari, L., 1988. Sub-aphyric alkali basalt from Mt Etna: inferences on the depth and composition of the source magma. Rend. Soc. Ital. Mineral. Petrol. 43, 877–891.

Bardintzeff, J.M., 1998. Volcanologie, second ed. Dunod Editeur.

Bau, M., 1996. Controls on the fractionation of isovalent trace elements in magmatic and aqueous systems: evidence from Y/Ho, Zr/Hf, and lanthanide tetrad effect. Contributions to Mineralogy and Petrology 123, 323-333.

Berger G., Schott J., and Loubet M. (1987) Fundamental processes controling the first stage of alteration of a basalt glass by seawater: An experimental study between 200 and 320°C. Earth and Planetary Science Letters 84, 431-445.

Brady P. V., & Gislason S. R. (1997). Geochimica et Cosmochimica Acta 61, 965–973.

Censi P., Zuddas P., Randazzo L.A., Saiano F., Aricò P., Cuttitta A, Punturo R. (2010a). Influence of dissolved organic matter on Rare Earth Elements and Yttrium

distributions in coastal waters. Chemistry and Ecology 26 n 2, 123-135

Censi P., Randazzo L.A., Zuddas P., Saiano F., Aricò P., Andò S., Mazzola S. (2010b). Trace element behaviour in seawater during pyroclastic Etna's activity in 2001. Concurrent effects of nutrients and formation of alteration minerals. Journal of Vulcanology and Geothermal Research193, 106-116.

Chester, D.K., Duncan, A.M., Guest, J.E., Kilburn, C.R.J., 1985. Mount Etna: The anatomy of a volcano. Chapman andHall, London. 404 pp.

Corsaro, RA., Miraglia, L., Pompilio, M. (2007). Petrologic evidence of a complex plumbing system feeding the July–August 2001 eruption of Mt. Etna, Sicily, Italy. Bull Volcanol (2007) 69: 401–421.

Cronin, S.J., Neall, V.E., Lecointre, J.A., Hedley, M.J., Loganathan, P., 2003. Environmental hazards of fluoride in volcanic ash: a case study from Ruapehu volcano, New Zealand. J. Volcanol. Geotherm. Res. 121, 271–291.

Corsaro RA, Pompilio M (2004a) Buoyancy-controlled eruption of magmas at Mt Etna. Terra Nova 16(1):16–22

Crovisier J.-L., Honnorez J., and Eberhart J. (1987) Dissolution of basaltic glass in seawater: Mechanism and rate. Geochimica et Cosmochimica Acta 51, 2977-2990.

de Baar, H.J.W., Bacon, M.P., Brewer, P.G., Bruland, K.W., 1985. Rare earth elements in the Pacific and Atlantic Oceans. Geochimica et Cosmochimica Acta 49, 1943– 1959.

Duggen, S., Croot, P., Schacht, U., Hoffmann, L., 2007. Subduction zone volcanic ash can fertilize the surface ocean and stimulate phytoplankton growth: evidence from biogeochemical experiments and satellite data. Geophys. Res. Lett. 34, 1–4.

Frogner Kockum, P.C., Herbert, R.B., Gislason, S.R., 2006. A diverse ecosystem response to volcanic aerosols. Chem. Geol. 231, 51–66.

Fubini e Fenoglio (2007). *Toxic Potential of Mineral Dusts*. Elements 3, 407-414.

Gieskes, J., Lawrence, J., 1981. Alteration of volcanic matter in the deep sea sediments: evidence from the chemical composition of interstitial waters from deep sea drilling cores. Geochimica et Cosmochimica Acta 45, 1687–1703.

Gislason S. R., and Eugster H. P. (1987a) Meteroic water-basalt interactions. I: A laboratory study. Geochim. Cosmochim. Acta 51, 2827–2840.

Gerlach, T. M. & Nordlie, B. E. 1975 The C–O–H–S gaseous system, part II: temperature, atomic composition, and molecular equilibria in volcanic gases. Am. J. Sci. 275, 377–394.

German, C.R., Masuzawa, T., Greaves, M.J., Elderfield, H., Edmond, J.M., 1995. Dissolved rare earth elements in the Southern Ocean: cerium oxidation and the influence of hydrography. Geochimica et Cosmochimica Acta 59 (8), 1551–1558.

Ghiara M. R., Franco E., Petti C., Stanzone D., and Valentino G. M. (1993) Hydrothermal interaction between basaltic glass, deionized water, and seawater. Chem. Geol. 104, 125-138.

Greaves, M.J., Elderfield, H., Sholkovitz, E.R. (1999). Aeolian sources of rare earth elements to the Western Pacific. Ocean Marine Chemistry, 68 (1-2), pp. 31-38.

Guieu, C., Chester, R., Nimmo, M., Martin, J. M., Guerzoni, S., Nicolas, E., Mateu, J., Keyse, S. (1997). Atmospheric input of dissolved and particulate metals in the NW Mediterranean, Deep-Sea Research H 44, N. 3-4, 655-674.

Guieu, C., Bozec, Y., Blain, S., Ridame, C., Sarthou, G., Leblond, N. (2002). Impact of high Saharan dust inputs on dissolved iron concentrations in the Mediterranean Sea. Geophysical Research Letters, 29 (19), pp. 17-1.

Guy, C., Schott, J., Destrigneville, C., Chiappini, R., 1992. Low-temperature alteration of basalt by interstitial seawater, Mururoa, French Polynesia. Geochimica et Cosmochimica Acta 56, 4169–4189.

INGV-Staff, Sezione di Catania, 2001. Multidisciplinary approach yields insight into Mt. Etna 2001 eruption. EOS Trans. AGU 82 (52), 653–656.

Jones, M.T., Gislason, S.R., 2008. Rapid releases of metal salts and nutrients following the deposition of volcanic ash into aqueous environments. Geochim. Cosmochim. Acta 72, 3661–3680.

Hannigan, R.E. and E.R. Sholkovitz 2001. The development of middle rare earth element enrichments in freshwater: weathering of phosphate minerals. Chem. Geol. 175: 495-508.

Horwell, C.J., Baxter, PJ. (2006). The respiratory health hazards of volcanic ash: a review for volcanic risk mitigation. Bulletin of Volcanology 69, 1-24.

Horwell, C.J., Fenoglio, I., Ragnarsdottir, K.V., Sparks, R.S.J., Fubini, B., 2003. Surface reactivity of volcanic ash from the eruption of Soufrière Hills volcano, Montserrat, with implications for health hazards. Environ. Res. 93, 202–215.

Jickells, T. D., An, Z. S., Andersen, K. K., Baker, A. R., Bergametti, C., Brooks, N., Cao, J. J., Boyd, P.W., Duce, R. A., Hunter, K. A., Kawahata, H, Kubilay, N., LaRoche, J., Liss, P. S., Mahowald, N., Prospero, J. M., Ridgwell, A. J., Tegen, I., Torres, R. (2005). Global iron connections between desert dust, ocean biogeochemistry, and climate. Science 308, pp. 67–71.

Jørgensen, C.K., 1970. The "tetrad effect" of Peppard is a variation of the nephelauxetic ratio in the third decimal. Journal of Inorganic Nuclear Chememistry 32, 3127– 3128.

Jørgensen, C.K., 1979. Theoretical chemistry of rare earths. In: Gschneider, K.A., Eyring, L. (Eds.), The Handbook of Physics and Chemistry of Rare Earths, 3, 111-169, North-Holland, Amsterdam.

Kawabe I. 1992. Lanthanide tetrad effect in the Ln3+ ionic radii and refined spin-pairing energy theory. Geochem. J. 26: 309–335.

Kump L. R., Brantley S. L., Authur M. A. (2000). Annual Rev. Earth Planet. Sci. 28, 611 667.

Langmann, B., Zakˇsek, K., Hort, M., and Duggen, S.: Volcanic ash as fertiliser for the surface ocean, Atmos. Chem. Phys. Discuss, 10, 711–734, 2010, http://www.atmos-chem-phys-discuss.net/10/711/2010/.

Louvat P. (1997). Ph.D. thesis. University of Paris.

Martin, R. S., Mather, T. A. & Pyle, D. M. 2006 High-temperature mixtures of magmatic and atmospheric gases. Geochem. Geophys. Geosyst. 7, Q04006. (doi:10.1029/2005GC001186)

Masuda, A., Kawakami, O., Dohomoto, Y., Takenaka, T., 1987. Lanthanide tetrad effects in nature: two mutually opposite types, W and M. Geochemical Journal 21, 119-124.

Masuda and Ikeuchi, 1979. Lanthanide tetrad effect observed in marine environment. Geochemical Journal 13, 19–22.

Monecke, T., Kempe, U., Monecke, J., Sala, M., Wolf, D., 2002. Tetrad effect in rare earth element distribution patterns: A method of quantification with application to rock and mineral samples from granite-related rare metal deposits. Geochimica et Cosmichimica Acta 66, 1185-1196.

Monecke, T., Kempe, U., Monecke, J., Sala, M., Wolf, D., 2002. Tetrad effect in rare earth element distribution patterns: A method of quantification with application to rock and mineral samples from granite-related rare metal deposits. Geochimica et Cosmichimica Acta 66, 1185-1196.

Moulton K. L., West J., & Berner R. A. (2000). Am. J. Sci. 300, 539–570.

Nozaki Y., Zhang J., and Amakawa H. (1997) The fractionation between Y and Ho in the marine environment. Earth Planet. Sci. Lett. 148, 329–340.

Nugent, L.J., 1970. Theory of the tetrad effect in the lanthanide(III) and actinide(III) series. Journal of Inorganic Nuclear Chemistry 32, 3485– 3491.

Oelkers, E.H., Gislason, S.R., 2001. The mechanism, rates, and consequences of basaltic glass dissolution: I. An experimental study of the dissolution rates of basaltic glass as a function of aqueous Al, Si, and oxalic acid concentration at 25 °C and pH=3 and 11. Geochim. Cosmochim. Acta 65, 3671–3681.

Olgun, N., Duggen, S., Croot, P. L., Delmelle, P., Dietze, H., Schacht, U., O´ skarsson, N., Siebe, C., and Auer, A.: Surface ocean iron fertilization: The role of airborne volcanic ash from subduction zone and hotspot volcanoes and related fluxes into the Pacific Ocean, Global Biogeochem. Cy., in review, 2010.

Pompilio M, Coltelli M, Del Carlo P, Vezzoli L (1995) How do basaltic magmas, feeding explosive eruptions, rise and differentiate at Mt. Etna? Period Mineral 64:253–254.

Reisfeld, R., Jørgensen, C.K., 1977. Lasers and Exited States of Rare Earths, Sprinter-Verlag, Berlin, 226pp.

Rittmann, A., 1965. Notizie sull'Etna. Nuovo Cim. I (3), 1117–1123.

Sholkovitz, E.R., W. M. Landing, B. L. Lewis. 1994. Ocean particle chemistry: the fractionation of rare earth elements between suspended particles and seawater. Geochim. Cosmochim. Acta 58:1567-1579.

Saladin, Kenneth S. (2007). *Anatomy and Physiology: the unity of form and function*. New York, N.Y.: McGraw Hill.

Sarthou, G., Baker, A.R., Kramer, J., Laan, P., Laës, A., Ussher, S., Achterberg, E.P., de Baar, H.J.W., Timmermans, K.R., Blain, S. (2007). Influence of atmospheric inputs on the iron distribution in the subtropical North-East Atlantic Ocean. Marine Chemistry, 104 (3-4), pp. 186-202.

Schiano, P., Clocchiatti, R., Ottolini, L., Busà, T. (2001): Transition of Mount Etna lavas from a mantle-plume to an island-arc magmatic source. Nature, 412, 900-904.

Seyfried J., W.E., Bischoff, J., 1979. Low temperature basalt alteration by seawater: an experimental study at 70 °C and 150 °C. Geochimica et Cosmochimica Acta 43, 1937–1947.

Spivack A. J., & Staudigel H. (1994). Chem. Geol. 115, 239–247.
Stefansson A., & Gislason S. R. (2001). Am. J. Sci. 301, 513–556.

Stumm, W. and Morgan J. J. (1996) Aquatic Chemistry. third ed. Wiley-Interscience, 1040.

Schooner, MAA, Cohn, CA, Roemer, E., Laffers, R., Simon, SR., O'Riordan, T. (2006). Mineral-induced formation of reactive oxygen species. In: Sahai N, Shoonen

MAA (eds). Medical Mineralogy and Geochemistry, Reviews in Mineralogy & Geochemistry 64, 179-221.

Shannon, R.D., 1976. Revised effective ionic radii and systematic studies of interatomic distances in halides and chalcogenides. Acta Crystallographica B25, 925-946.

Symonds, R.B., Rose, W.I., Bluth, G.J.S., Gerlach, T.M., 1994. Volcanic gas studies: methods, results and applications. In: Carroll, M.R., Hollaway, J.R. (Eds.), Volatiles in Magmas, Rev. Mineral., vol. 30. Mineralogical Society of America, pp. 1–66.

Spivack A. and Staudigel H. (1994) Low-temperature alteration of the upper oceanic crust and the alkalinity budget of seawater. Chemical Geology 115, 239-247.

Taddeucci, J., Pompilio, M., Scarlato, P., 2004. Conduit processes during the July–August 2001 explosive activity of Mt. Etna (Italy): inferences from glass chemistry and crystal size distribution of ash particles. J. Volcanol. Geotherm. Res. 137, 33–54.

Tanguy, J.C., Condomines, M., Kieffer, G. (1997): Evolution of Mount Etna magma: Constraints on the present feeding system and eruptive mechanism. J. Volcanol. Geotherm. Res., 75, 221-250.

Viccaro M., Ferlito C., Cortesogno L., Cristofolini R. and Gaggero L. (2006) Magma mixing during the 2001 event at Mount Etna (Italy): effects on the eruptive dynamics. J. Volcanol. Geotherm. Res. 149, 139–159.

Viccaro, M., Ferlito, C., Cristofolini, R. (2007). Amphibole crystallization in the Etnean feeding system: mineral chemistry and trace element partitioning between Mg-hastingsite and alkali basaltic melt. Eur. J. Mineral. 2007, 19, 499–511.

Wolff-Boenisch, D., Gíslason, S., Oelkers, E.H., Putnis, V., 2004. The dissolution rate of natural glasses as a function of their composition at pH 4 and 10.6, and temperatures from 25 and 74 °C. Geochimica et Cosmochimica Acta 68 (23), 4843–4858.

Yokoyama, T., Banfield, J., 2002. Direct determination of the rates of rhyolite dissolution and clay formation over 52,000 years and comparison with laboratory measurements. Geochimica et Cosmochimica Acta 66 (15), 2665–2681.

Wallance, WE., Harrison, JC., Grayson, RL., Keane, MJ., Bolsaitis, P., Kennedy, RD., Wearden, AQ., Attfield, MD. (1994). aluminosilicate surface contamination of respirable quartz particles from coal mine dusts and from clay works dusts. Annals of Occupational Hugiene 38, 439-445.

Zhang, J., Nozaki, Y., 1996. Rare earth elements and yttrium in seawater: ICP-MS determinations in the East Caroline, Coral Sea, and South Fiji basins of the western South Pacific Ocean. Geochimica et Cosmohimica Acta 60 (23), 4631– 4644.

Chapter II

The behaviour of rare earth elements during the volcanic ash dissolution in seawater solution.

Randazzo L.[A,B,C], Saiano F.[D], Zuddas P.[B], Censi P.[A,C,E].

A. *Dipartimento C.F.T.A., Università di Palermo, Via Archirafi, 36 90123 Palermo, Italy*
B. *Institut de Génie de l'Environnement Ecodéveloppement and Département Sciences de la Terre, UMR 5125, Université Claude Bernard Lyon 1, 2 rue R. Dubois, Bat GEODE 69622 Villeurbanne Cedex (France).*
C. *En.Bio.Tech. – Via Aquileia, 35 90100 Palermo (Italy)*
D. *Dipartimento I.T.A.F., Università di Palermo, Viale delle Scienze, 13, 90128 Palermo, Italy*
E. *I.A.M.C.-Consiglio Nazionale delle Ricerche, Via faro, 1, 91021 Torretta Granitola, Campobello di Mazara (Tp), Italy*

2.1. Introduction

During the last 25 years several studies focused processes driving the Y and lanthanide (YLn) distributions in marine systems (Goldberg et al, 1963; Cantrell and Byrne, 1987; Elderfield, 1988; Goldstein and Jacobsen, 1988; Greaves et al., 1991). These were carried out in order to evaluate YLn solution complexation (Cantrell and Byrne, 1987; Koeppenkastrop et al., 1991; Koeppenkastrop and De Carlo, 1992; Lee and Byrne, 1992; Millero, 1992), to track the delivery of anthropogenic and lithogenic materials from river and atmospheric input (Elderfield et al., 1990; Alibo and Nozaki, 1999; Tachikawa et al., 1999; Quinn et al., 2004) and to describe YLn behaviour in mouth environment under variable ionic strength conditions (Sholkovitz, 1993; Sholkovitz et al., 1999; Hannigan and Sholkovitz, 2001; Aubert et al. 2002). YLn are probably the best geochemical indicator for processes occurring at solid-liquid interfaces. However, we have a limited knowledge of their behavior during dissolution of solid particles in high saline media in presence of different competing ligand species.

In Mediterranean Sea trace element contents in the water column are mainly related to external input from surrounding areas. In particular, atmospheric fallout both from Sahara and the Arabian peninsula in the south-eastern basin, riverine and atmospheric inputs from western Europe in the north-western basin play an important role to drive trace element contents along the water columns (Greaves et al., 1991; Molinaroli et al. 1999). On the contrary only a limited literature exists about the effects of volcanic activity of Mount Etna on YLn distribution in marine system. Here we will evaluate the effects induced by the pyroclastic activity of Mt. Etna that produced one of the most significant eruptive episode during summer 2001, involving large deposition of volcanic ash on central mediterranean area.

In order to investigate the effects that freshly erupted volcanic particles could have on chemistry of shallow water was carried out a detailed laboratory study of features of YLn release from freshly erupted volcanic ash to synthetic seawater under close-system conditions. This investigation was carried out evaluating features of trace element leaching from volcanic ash as a whole, from glass ash fraction, from Fe-Mg rich mineral fraction both in absence and in the presence of carbonate and humate ligand species, to

simulate the effects of dissolved YLn complexation, besides under closed system conditions. Weathering experiments were investigated during a 6 months period and modifications induced by these processes on the solid phase were quantitatively characterized with SEM observations and X-ray analyses.

2.2. *Materials and methods*

2.2.1. *Starting materials*

2.2.1.1 Solid phase

The volcanic ash was collected using a polyethylene plate with a surface area of 1 m^2 located on the roof of the Department of Geology of the University of Catania for five days (from 21 July to 26 July 2001). During this period no rainfall event occurred and at the end of the collection period, a thickness of about 2 cm of volcanic ash was measured.

Mineralogical composition of the bulk samples was investigated by X-ray diffractometry (Siemens 5500 X-ray spectrometer).

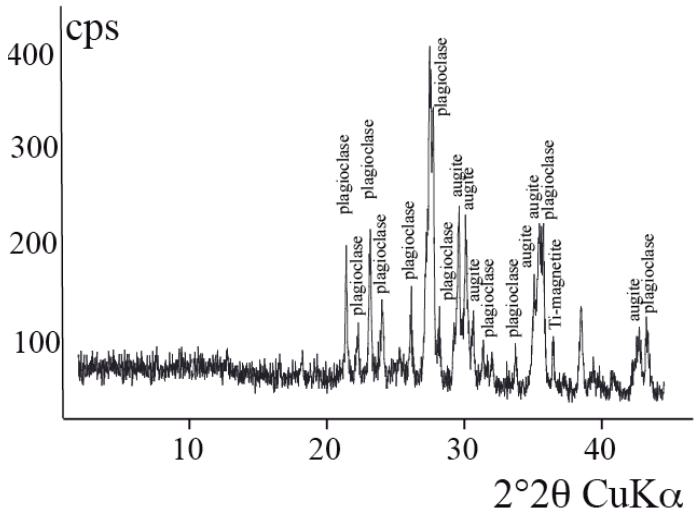

Figure 2.1 - XRD patterns of investigated volcanic ash.

Optical examinations of rock fragments indicate the presence of porphyritic texture with phenocrystals contents less than 30 %. Glass fraction, having density lower than 2.90 g/cm^3, is about 80% w/w of the material and represents the main component of the ash fraction (Tab. 2.3).

Sample	**Weight (g)**	**%**
Total sample	131.251	100
Light	101.921	78
Heavy	29.330	22

Table 2.3 – Light and heavy ash composition (% w/w)

Optical observations on glass fragments showed irregular surfaces rich of grooves and embayments suggesting the occurrence of early alteration episodes during rising in the volcanic plume. Corrosions signs, as well as cleavage, are recognised also on the investigated minerals (Fig. 2.2). Even if these features are not widely seen, on the whole, they are dominant in the crystal face parallel to *c* axis while the face orthogonal to *c* axis shows a knurled feature.

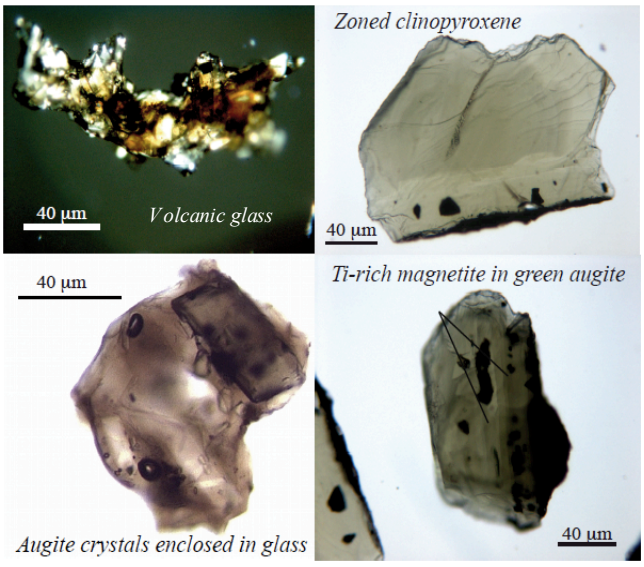

Figure 2.2 – Glass and minerals optical images. Glass fragment shows embayments, grooves such as minerals inclusions. Euhedral clinopyroxene crystal is enclosed in volcanic glass matrix. Green augite shows areas with zonation, magnetite inclusion and dentate terminations.

These evidences are justified through the crystallographic character of each

mineral, thus the natural presence of channels on the (100) and (010) faces make them rich of cleavages and (001) such as (111) surface, in which these planes are projected, result the surfaces with the most particular features such “hacksaw”.

SEM observations show that volcanic glass has a very irregular surface with random signs of alteration and many grooves and conchoidal fractures. Minerals, on the contrary, show dissolution structures, cleavage and incipient etch pits on the surface, although slightly marked. Moreover these features are developed mainly in a particular crystal direction that is parallel to the *c*-axis and their side-by-side coalescence explains a more advanced weathering and results in the formation of early sawtooth (Velbel 1993; Velbel, 1999), or denticulated margin (Fig. 2.3). Crystals show the anisotropic behaviour with respect to dissolution.

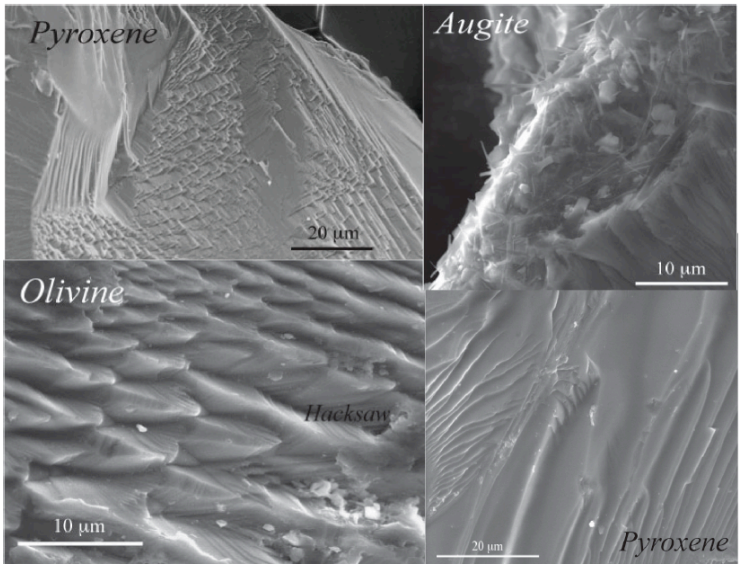

Figure 2.3 – Evidences of alteration effects in Olivine and Pyroxene surface that occur into volcanic plume.

2.2.1.2. Seawater solutions

Artificial seawater solution with a salinity of 35 $^{o}/_{oo}$ (Doe,1994), was prepared as reported in Tab. 2.1. This solution is indicated as *Sw*.

Components	Moles	Weight (g)
NaCl	0.42570	24.8835
KCl	0.01058	0.7900
$MgCl_2 \cdot 6H_2O$	0.05480	11.1175
$CaCl_2$	0.01145	1.2685
Na_2SO_4	0.02940	4.1760

Tab. 2.1 - Simplified artificial seawater composition (1 liter).

$NaHCO_3$ (0.00183 moles, 0.1537 g) was added only for kinetic experiments testing the YLn behaviour in presence of carbonate (*CS*). Moreover to examine the competition effects on the YLn elements release in solution, further investigations were carried out in seawater solution added of Humic Acid (Alfa Aesar) with a concentration of 5 mg/l (*HAS*). All reagents used in the experiments were ultrapure grade or of the highest available purity. Water was always ultrapure grade (18.2 MΩ).

2.2.2. *Experiments*

2.2.2.1. Volcanic ash

Freshly erupted volcanic ash was sieved and the granulometric fraction 63-125 μm was selected for kinetic experiments. Volcanic ash was ultrasonically cleaned and shaked in water for 1 hour, to remove more soluble salts adsorbed onto particle surfaces. The sample was then dried in an oven at 110 °C, cooled to room temperature in a dry box and then stored in a sealed plastic bottle. The geometric specific surface area of the ash was estimated at 0.03 $m^2\ g^{-1}$ assuming a spherical grain shape based on optical microscopic observations (e.g, Gautier et al. 2001).

In order to study the reactivity both of volcanic ash and components (glass (VG), olivine and clinopyroxene (Ol-CPX)), gravimetric and magnetic separation methods were applied. The first separation was carried out in order to obtain two fractions called “light” and “heavy”. A further gravimetric separation of the light fraction was carried out in order to isolate the volcanic glass.

Magnetic separation both of “light” and “heavy” fractions was performed using a

magnet for a coarse selection and then, limiting to heavy fraction, using a *Frantz* separator (Rikers et al., 1998) for a more precise mineralogical separation. Finally, three different samples for kinetic experiments were obtained:

- ash sample not differentiated (ASH);
- volcanic glass (VG);
- mineralogical component ([Ol+CPX]).

The morphology of glass and minerals was investigated by both optical microscope and Scanning Electronic Microscope (SEM).

2.2.2.2 Kinetic experiments

The solid-liquid interaction batch experiments were carried out for a maximum of 4320 hours (table 2.2.) at temperatures of 25 ±1 °C, using a solution/solid ratio of 10:1 vol/wt. The experiments were performed with 4 g aliquots of each sample placed in 50 ml Nalgene® bottles. In particular 10 ash samples were placed in 40 ml of Sw, 10 in 40 ml of CS and 10 in 40 ml of HAS for 1, 3, 5, 7, 24, 48, 360, 720, 2160, 4320 hours.

Similarly, 5 aliquots of each volcanic glass sample and 5 aliquots of each minerals sample were treated with Sw, until 1, 5, 24, 720, 4320 hours respectively. All the experiments were carried out in triplicate.

	1h	3h	5h	7h	24h	48h	15d	30d	90d	180d
Ash-Sw	x	x	x	x	x	x	x	x	x	x
Ash-CS	x	x	x	x	x	x	x	x	x	x
Ash-HAS	x	x	x	x	x	x	x	x	x	x
VG-Sw	x		x		x			x		x
[Ol+CPX]-Sw	x		x		x			x		x

Tab. 2.2 - Summary table of kinetic experiments. Column headings are the duration of solid-liquid interaction (h: hours, d: days). Headers of the lines refer to the characteristics of experiments (Ash: volcanic ash, Sw: seawater as reported in Tab 2.1, CS: seawater with carbonates, HAS: seawater with carbonates and Humic Acid, VG: volcanic glass, Ol: Olivine, CPX: Augite).

After every experiment, pH was immediately measured, the solutions were separated by filtration using 0.45 μm Millipore® filters and the volume was brought to

50 ml by Millipore. Then the amount of SiO_2 was spectrophotometrically measured in order to estimate the bulk dissolution rate from the surface that is the rate determining step for the overall dissolution process.

In regard to kinetic experiments with HAS, the YLn eventually complexed by HAS were quantitatively separated from the solution by ultrafiltration. The amounts of YLn complexed with HAS correspond to the difference between the YLn concentration in CS seawater solution and the remaining YLn concentration in the < 3.5 kDa HAS ultrafiltrates. Finally the concentrations of Y and REEs in all samples have been obtained by Inductively Coupled Plasma Mass Spectrometry (ICP-MS) measurements after pre-concentration with CHELEX-100® resin.

2.2.3. Analyses

2.2.3.1 Solid phase

Mineralogical composition of the ash samples was determined by X-ray diffractometry (Siemens 5500 X-ray spectrometer), using a Ni-filtered CuKa radiation both on fresh ash and after six months.

2.2.3.1.1 Gravimetric and magnetic bulk separation

Gravimetric separation was carried out centrifugating volcanic ash, for 3 minutes at 2500 rpm, in a solution of sodium metatungstate, density 2.90 g/cm^3, and sodium metatungstate at 2.60 g/cm^3 (to obtain the only glassy fraction). After centrifugation the bottom part of the vials was frozen by immersion in liquid nitrogen for few minutes and the surnatant was removed.

Magnetic separations were carried out by using both a magnet (ferrite) and Frantz iso-dynamic magnetic separator, Model L-1, at 0.05 A with inclination of 5° and 0.20 A/20°.

Geometrical parameters were calculated assuming a spherical grain shape, whereas densities of 2.72 g cm^{-3}, 2.50 g cm^{-3} and 3 g cm^{-3} were used for volcanic ash, glass fraction and minerals, respectively. According to these parameters the whole surface area of 1400 cm^2, 1525 cm^2 and 1270 cm^2 was calculated for volcanic ash, glass

and minerals, respecively.

2.2.3.1.2 Morphological investigations

Optical observations were carried out using LEICA DM EP optic microscope. SEM observations and EDS analyses were carried out by means of a LEO 440 equipment at the Dipartimento CFTA., University of Palermo. Both volcanic ash samples and selected particles of different fractions were resin-mounted, polished and gold coated and their features were examined by SEM using the secondary electron (SE) imaging signal and a beam voltage of 20 kV. Selected glass particles, olivine and clinopyroxene phenocrysts were resin-mounted, polished, and coated with a thin layer of carbon, and examined by X-ray quantitative microprobe techniques using a Si (Li drifted) EDS. X-ray localized quantitative determinations of major chemical components were carried out using a standard based ZAF correction program. Further SEM observations were carried out at University of Milano Bicocca, with a Tescan Vega TS5136XM SEM (High voltage 20kV; middle heating), calibrating an appropriate mix of detector (15% BSE and 85% SE), to optimize the quality picture.

2.2.3.2 Dissolved phase

2.2.3.2.1 pH measurement

The pH values were measured using a METTLER TOLEDO MA 130 Ion Meter, calibrated with appropriate buffers from 6 to 10 pH units under synthetic seawater media. The accuracy of the pH measurement was ± 0.1 pH unit.

2.2.3.2.2 SiO_2 measurement

SiO_2 concentrations were determined by UV-VIS spectrophotometer (Genesys10) as follows. Dissolved H_4SiO_4 reacts with molybdate ions to form a yellow heteropoly acid in sulphuric solution; the reaction product is then reduced to silicomolybdenum blue and photometrically determined (Standard Methods for the Examination of Water and Wastewater, 1992). Silica concentrations was determined by external calibration using Na_2SiF_6 solution in seawater, in a range of 0.1 - 5.00 mg l^{-1} Si. Analytical uncertainties,

expressed as standard deviation, are ± 0.03 mg l^{-1} Si.

2.2.3.2.3 Ultrafiltration

Ultrafiltrations were carried out by centrifugating solutions in 20 ml dialysis tubes of pore size 3.5 kDa (Novagen, D-Tube Dialyzer Mega) at 5000 rpm for 30 minutes.

2.2.3.2.4 YLn determination

In order to increase the accuracy of the synthetic seawater YLn analyses, each sample (45 ml) was pre-concentrated with CHELEX-100® (200-400 mesh), previously cleaned and conditioned according to Paulson (1986). Chelex-100® resin is a styrene divinylbenzene copolymers containing iminodiacetate ions which act as chelating groups in binding metal ions. It is classed as weakly acidic cation exchange resins by virtue of its carboxylic acid groups, but it differs from ordinary exchangers because of its high selectivity for metal ions and its much higher bond strength.

In each seawater sample pH value was adjusted to 6.5 with CH_3COONH_4 as described by Möller et al. (1992). The sample was loaded into an 5-cm long column previously filled with CHELEX-100 (0.5 g) through a peristaltic pump to checking flux (0.5 ml/min). REEs were then eluted with 5 ml of HNO_3 3.5 M yielding a 9-fold enrichment factor. Details of the procedures are reported in Paulson, 1986 and Möller et al., 1992. Concentrations of Y and lanthanides in all samples have been obtained by an Inductively Coupled Plasma Mass Spectrometry (ICP-MS) (Agilent Technologies 7500 Series) using 10 nmol l^{-1} YLn and Tl as internal standards.

2.3. Results and discussions

2.3.1. Evolution of the interacting solution

pH changes during experiments are reported in Tables 2.3 and presented in

Figures 2.3, whereas the evolution of SiO_2 concentration is reported in Table 2.4 and Figure 2.4.

2.3.1.1 VG-Sw

pH values start from 5.8, progressively change to 6.7 after one hour and then progressively decrease to 5.5 until the end of experiments (Figure 2.3 a). At the same time dissolved SiO_2 reaches 5.5 µmol l^{-1} after one hour, attaining 72.7 µmol l^{-1}at the end of experiments.

2.3.1.2 (Ol-CPX)-Sw

Here pH values start from 5.8 attaining 7.7 after 240 hours. Then, pH decreases, to 6.2 after 480 hours, remaining quite constant to the end of the experiments (Figure 2.3 a). Dissolved SiO_2 concentrations monotonously increase during these experiments reaching 6.7 µmol l^{-1} after 6 months.

2.3.1.3 Ash-Sw

pH value starting from 5.8 attain 6.3 after one hour and reaching 6.6 after 48 hours and remaining constant to the end of experiments (Figure 2.3 a). Dissolved SiO_2 concentration increases to 14 µmol l^{-1} after 48 hours and then reaches 36 µmol l^{-1} at the end of experiments.

2.3.1.4 Ash-CS and Ash-HAS

pH values start from 7.6 in these solutions remaining quite constant during all the experiments under the effect of the bicarbonate/carbonate buffer (Figure 2.3 b). The rate of the SiO_2 release is influenced by concurrent occurrence of carbonate and humate species that induce a faster release during the first 360 hours (from 0.4 to 14.2 µmol l^{-1} for Ash-CS and from 0.8 to 16.2 µmol l^{-1} for Ash-HAS, respectively) when the investigated systems attain the steady state.

Time (hours)	pH VG-Sw	±σ	pH [Ol+CPX]-Sw	±σ
1	6.7	0.1	7.4	0.1
5	6.2	0.3	7.5	0.0
24	5.8	0.1	7.7	0.0
240	5.6	0.1	7.5	0.1
480	5.5	0.1	6.2	0.2
720	5.5	0.1	5.9	0.0
1080	5.5	0.1	5.8	0.1
4320	6.1	0.1	6.2	0.1

Table 2.3a - pH values during kinetic experiments. Sw: synthetic seawater; VG: volcanic glass; Ol: Olivine, CPX: Augite.

Time (hours)	pH Ash-Sw	±σ	pH Ash-CS	±σ	pH Ash-HAS	±σ
1	6.3	0.1	7.6	0.2	7.6	0.1
3	6.3	0.1	7.6	0.1	7.6	0.1
5	6.3	0.0	7.5	0.0	7.6	0.0
7	6.4	0.1	7.5	0.1	7.6	0.1
24	6.4	0.1	7.6	0.0	7.5	0.0
48	6.6	0.1	7.6	0.1	7.4	0.1
360	6.1	0.1	7.3	0.1	7.2	0.0
720	6.1	0.1	7.4	0.1	7.0	0.1
2160	6.1	0.1	7.3	0.1	7.2	0.0
4320	6.4	0.1	7.6	0.1	7.5	0.1

Table 2.3b - pH values during ash–seawater kinetic experiments. Ash: volcanic ash, Sw: synthetic seawater; CS˚: synthetic seawater plus carbonates; HAS: synthetic seawater plus carbonates and Humic Acid.

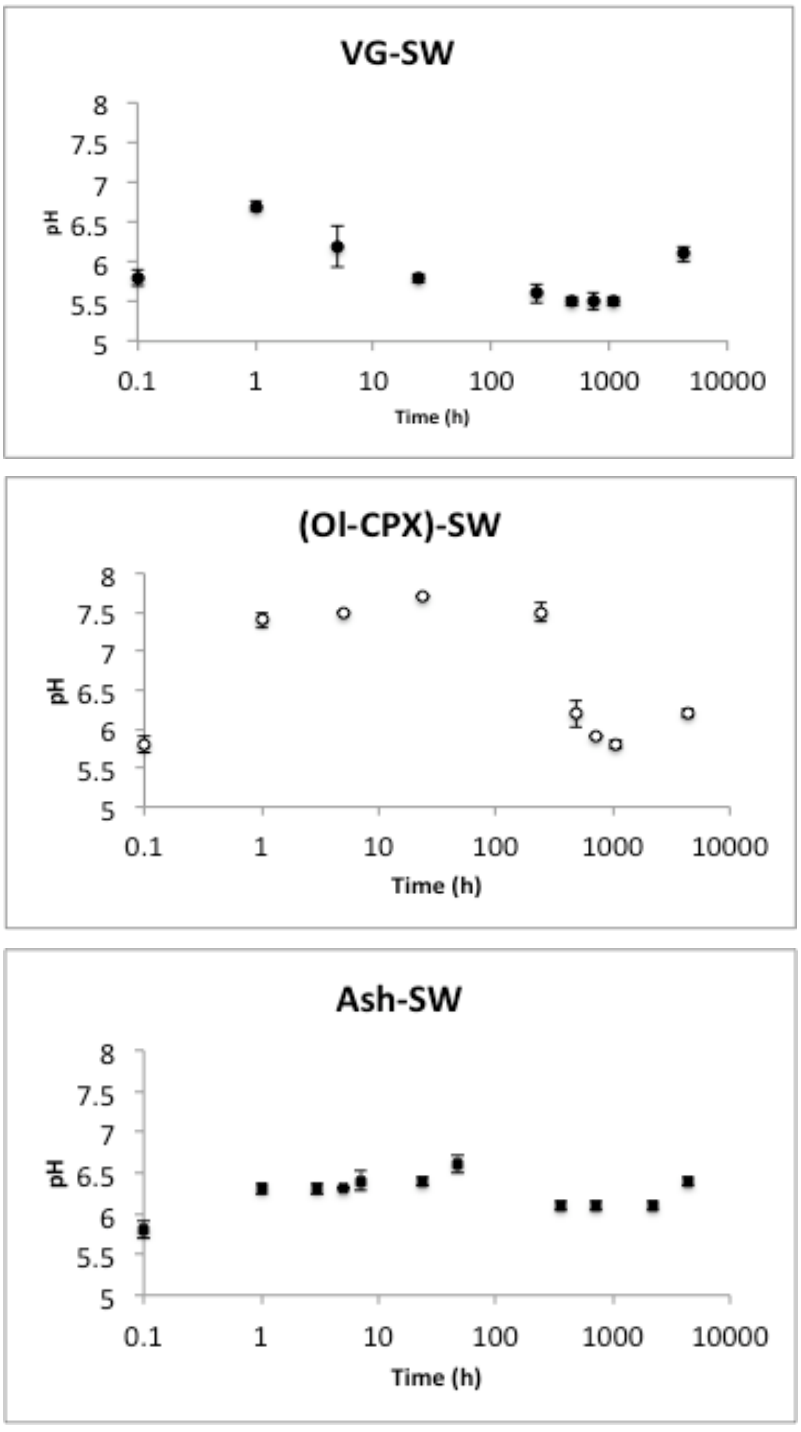

Figure 2.3a: Evolution of pH values during ash–seawater kinetic experiments in VG-Sw, (Ol-CPX)-Sw, Ash-Sw. VG: Volcanic glass; Ol: Olivine, CPX: Augite; Ash: volcanic ash; Sw: synthetic seawater.

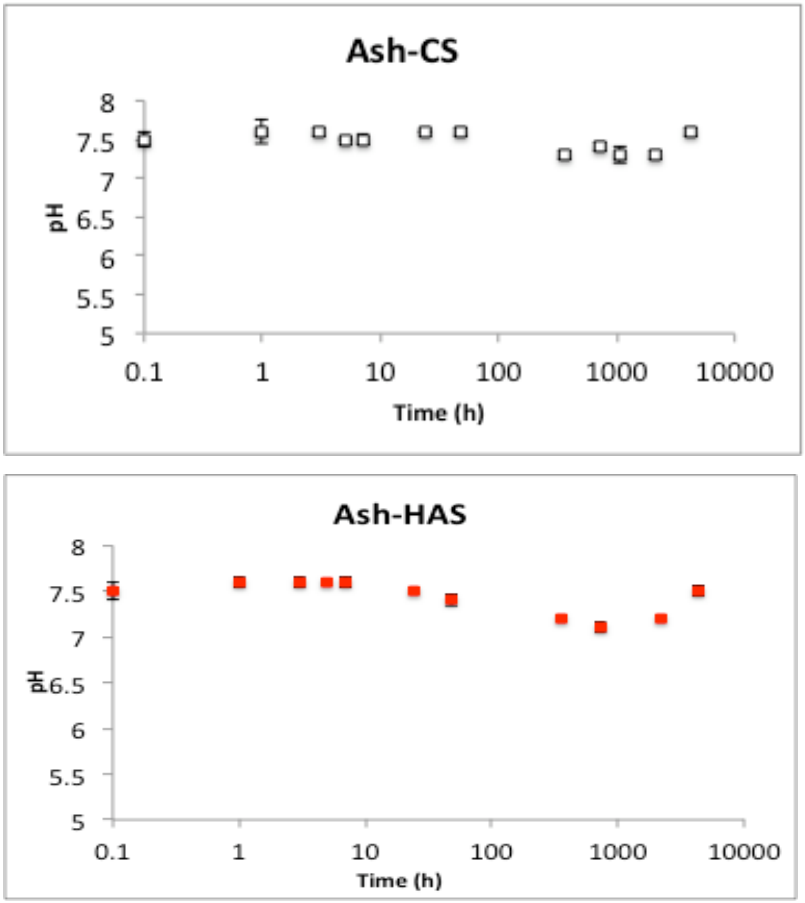

Figure 2.3b: Evolution of pH values during ash–seawater kinetic experiments in Ash-CS and Ash-HAS. Ash: volcanic ash; Sw: synthetic seawater; CS¯: synthetic seawater with carbonates; HAS: synthetic seawater with carbonates and Humic Acid.

Time (hours)	VG-Sw	±σ	(Ol-CPX) -Sw	±σ	Ash-Sw	±σ	Ash-CS	±σ	Ash-HAS	±σ
1	3.6	0.2	0.7	0.0	2.6	1.4	0.3	0.2	0.6	0.3
3	-	-	-	-	2.9	0.6	1.5	0.4	2.7	0.4
5	7.4	0.3	1.3	0.2	4.1	0.3	2.2	0.3	2.9	0.4
7	-	-	-	-	4.9	0.5	3.3	0.6	3.8	0.4
24	15.0	0.6	2.9	0.3	6.2	0.1	4.3	0.4	5.3	1.5
48	-	-	-	-	10.0	0.5	6.9	0.5	6.9	0.2
360	-	-	-	-	16.1	0.7	10.1	0.8	11.6	1.5
720	38.9	0.4	4.9	0.3	22.6	1.8	13.0	1.2	11.4	1.3
2160	-	-	-	-	27.0	0.5	15.0	0.9	19.9	0.5
4320	47.7	0.9	5.2	0.1	25.6	3.0	13.2	1.1	14.9	3.2

Table 2.4 - Silica concentration (nM cm^{-2}) in kinetic experiments. Ash: volcanic ash, Sw: synthetic seawater; CS: synthetic seawater plus carbonates; HAS: synthetic seawater plus carbonates and Humic Acid, VG: volcanic glass; Ol: Olivine, CPX: Augite.

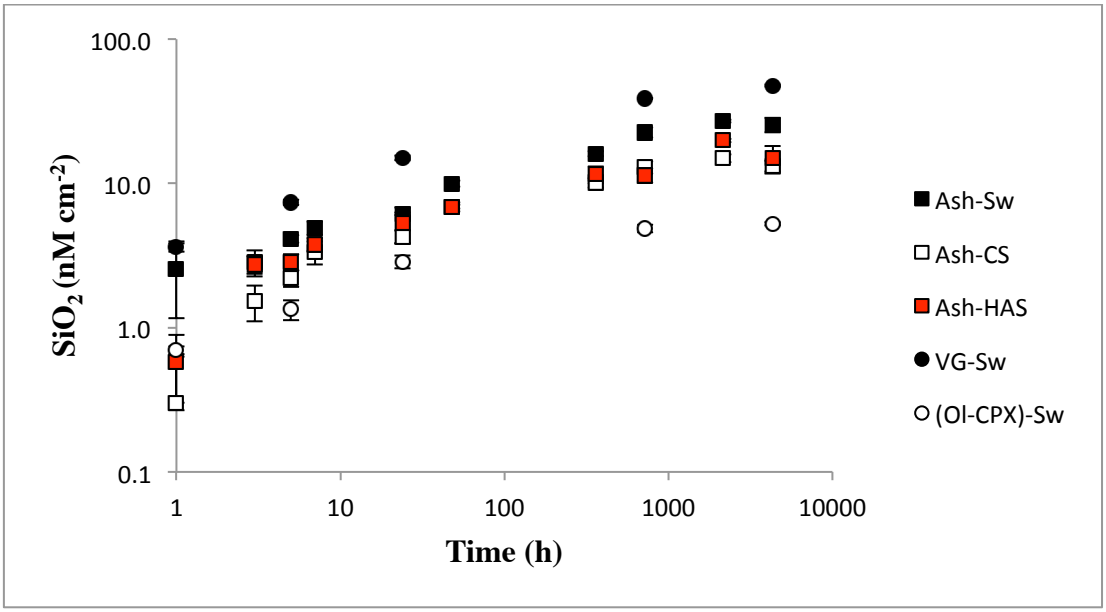

Figure 2.4 - Evolution of SiO_2 concentration as function of time. Ash: volcanic ash, Sw: synthetic seawater, CS: synthetic seawater with carbonates, HAS: synthetic seawater with carbonates and Humic Acid, VG: volcanic glass, Ol: Olivine, CPX: Augite.

The silica release from the three selected solids under experimental conditions is in accordance with the following first order rate equation (Lerman and Mackenzie, 1975):

$$dc/dt = K_1 (C_s - C_0); \quad (1)$$

$$C = C_s + (C_0 - C_s) \exp \{-K_1(t - t_0)\} \quad (2)$$

where dc/dt is the rate of the change of concentration C, in solutions; C_s is the steady-state concentration; C_0 is the initial concentration at time t_0.
In this study t_0=0 thus the equation can be written as the following simplified expression:

$$[S_i]_{sw} = m_1 [1 - \exp (-m_2 t)] \quad (3)$$

where $[S_i]_{sw}$ represents the Si concentration value in the leaching solution, m_1 is the concentration at steady-state and m_2 represents the kinetic rate constant for the overall leaching process of dimension time^{-1}.
The kinetic evolution of SiO_2 concentrations in the dissolved phase during the experiments is shown in Fig. 2.5, while the values for kinetic constant m_2 is given in Table 2.5. The equations show a faster SiO_2 release in the "(Ol-CPX)-Sw" system, whereas in the other experiments kinetic rate constants are in the same order of magnitude. This behaviour suggests the higher reactivity of the structural defects occurring on the mineral surface. In the "VG-Sw" experiment the kinetic rate constant is slower even if the amount of Si released is greater because the dissolution process is not delocalized such us occurs for minerals. As a consequence of different reactivity of these materials, larger silica dissolution occurs from glassy ash fraction than from minerals. In the other experiments Si release is comparable to the glass, being the ash composed mainly of glass.

Si (nmol cm^{-2})	m_2	±σ	r
VG-SW	0.0030	0.0018	0.93
(Ol-CPX)-SW	0.0356	0.0074	0.98
Ash-SW	0.0030	0.0008	0.93
Ash-CS	0.0045	0.0017	0.89
Ash-HAS	0.0020	0.0007	0.80

Table 2.5 – Kinetic constant value in all experiments (t^{-1}).

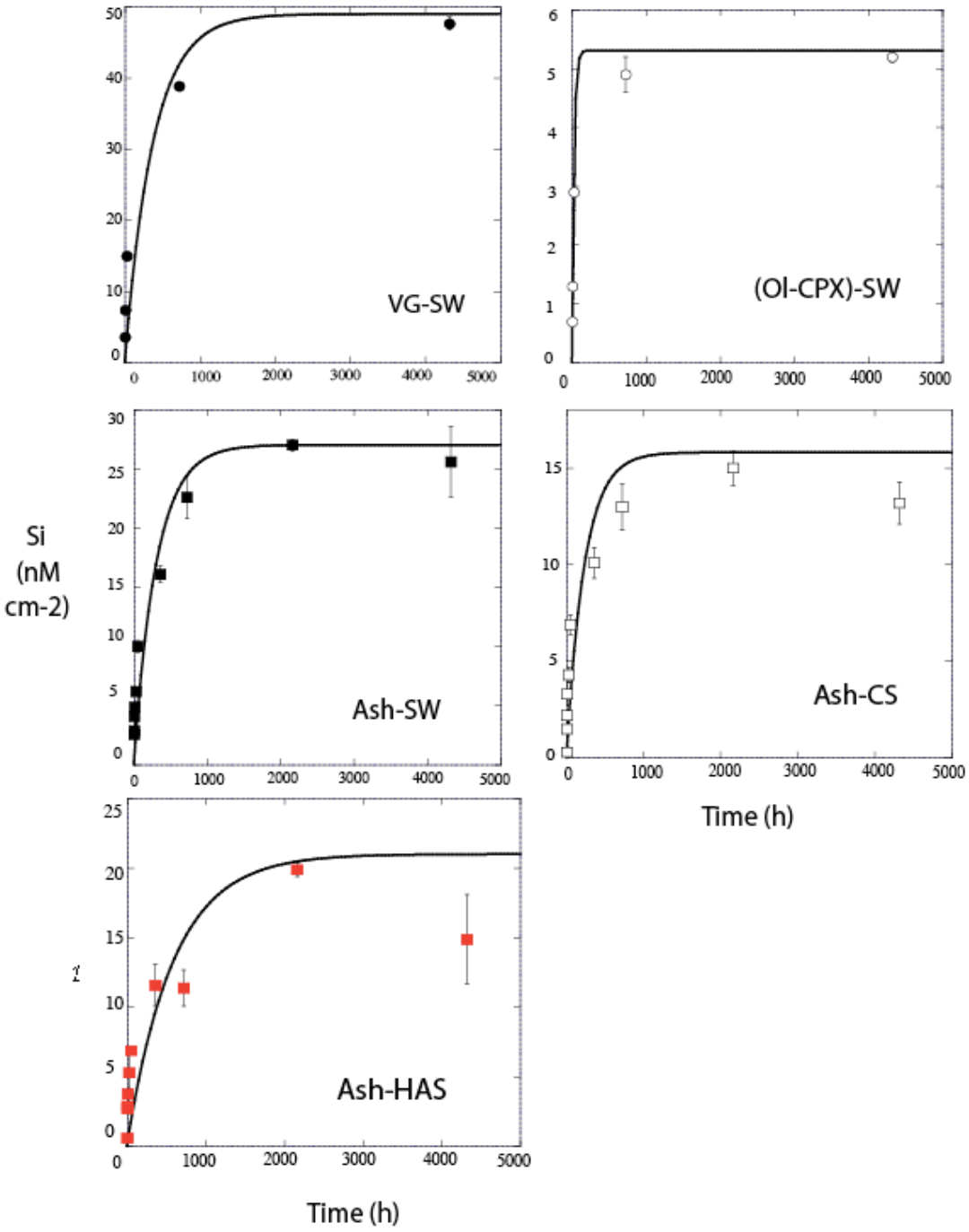

Figure 2.5 - Variation of silica concentrations in dissolved phase during kinetic experiments.

Mineral–water interactions occur primarily at the external mineral surfaces. These

processes are typically "surface controlled" since the reaction rate is limited by the basic molecular processes that finally lead, in the case of crystal dissolution, to the detachment of a molecule from the bulk crystal structure into the solution (Lasaga, 1998).

Apart from carbonate-bearing solutions, where pH is almost constant at 7.5, in the other samples pH progressively decreases, especially in volcanic glass-seawater sample. This feature suggests crystallization of possible smectite-like secondary phases, as previously reported under similar physical-chemical conditions (Ghiara et al.,1993; Seyfried and Bischoff, 1977; Hajash and Archer, 1980; Seyfried and Mottl, 1982; Thornton and Seyfried, 1985). According to Ghiara et al.,(1993), smectite formation in seawater occurs according to the following reaction:

basaltic glass + Mg^{2+} + H_2O = smectite + H^+ (4).

This mechanism justifies pH and SiO_2 leaching rate observed during kinetic experiments after a rapid SiO_2 release during the early interaction period. In the same conditions and with the same solution in fact the SiO_2 released from volcanic glass is 3 orders of magnitude higher compared to minerals and 1-3 times enriched than in volcanic ash. Just during the first hour of interaction pH seem to increase due to a quick solid hydratation. The formation of secondary minerals is confirmed by SEM observations (Fig. 2.11) and XRD analysis after 6 months.

The mechanism of formation of alteration layers on silicates has most commonly been attributed to simple leaching accompanied by surface condensation and reconstruction reactions (Brantley, 2004). This dissolution process is generally followed by precipitation. Crystal dissolution will preferentially take place at kinks and edges, due to a lower activation energy thus the dissolution of such structure then implies the breaking of only one Si-O linkage, comparable with the situation of the dissolution of some reaction complexes in imperfections at the minerals surface. These defects play an important role in the dissolution behaviour of minerals. The presence of defects in the structure creates the possibility that some Si tetrahedra are only singly linked to the solid.

2.3.1.5 Rare Earth Elements

The amount of YLn released during kinetic experiments is reported in Table 2.6 and Figure 2.6. Higher YLn amounts were released from glass sample, where elements are preferentially enriched due to their geochemical behaviour. On the contrary the leaching amplitude was lower from the minerals where YLn are preferentially retained on the surface rather than in crystal lattice (Rollinson, 1993).

YLn release in glass-Sw system reaches the maximum after 7 hours. Therefore, concentrations decrease to the end of experiments. Subsequently concentrations. On the contrary, if Sw reacts with Fe-Mg crystals concentrations progressively decrease during the first 7 hours and then moderately increase or remain quite constant to the end of experiments. After carbonate addition to the seawater solution YLn concentrations remain quite constant or slowly decrease to 7 hours and then increase reaching the maximum after 15 days. Then progressively decrease to the end of experiments. If YLn-humate complexes are removed from Sw (Ash-HAS), concentrations of residual dissolved YLn remain quite constant under carbonate-complexes form. Only random variations are shown during experiments.

A detained scenario of YLn behaviour in the studied system is mirrored by features of Y/Ho changes vs. time (Fig. 2.7 a). Y/Ho values generally increase with time always spanning on superchondritic values, in agreement with a large scavenging tendency for Ho with respect to Y as evidenced in Fig. 2.7 b. Carbonate addition emphasizes these features allowing to Y/Ho values close to those typically occurring in seawater.

These features cannot related to different leaching rate for Y and Ho because during CHARAC processes they behave similarly due to the closest values of their ionic radii and their solution complexation is quite similar in SO_4 and Cl^- media (Wood, 1990; Byrne and Sholkovitz, 1996). But superchondritic Y/Ho values in Sw system can involve a different behaviour during weathering, as suggested by Bau et al. (1995), due to the larger Y mobility with respect to Ho. Therefore, rare lower Y/Ho values during interactions can reflect deposition of alteration phases onto solid surfaces, as corroborated by Takahashi et al. (2004) who evidenced a larger Y capability to scavenge onto montmorillonite-like surfaces only under low ionic strength conditions, whereas this behaviour is tipped in high saline media (Coppin et al., 2002).

ppt	Y	La	Ce	Pr	Nd	Sm	Eu	Gd	Tb	Dy	Ho	Er	Tm	Yb	Lu
VG-Sw 1 h	11.93	16.48	18.05	2.51	11.61	2.74	0.87	2.92	0.34	1.99	0.35	0.99	0.08	0.79	0.08
VG-Sw 5 h	17.08	36.47	50.50	5.06	21.14	4.05	1.35	4.70	0.60	3.29	0.60	1.68	0.19	1.54	0.17
VG-Sw 24 h	17.78	27.00	25.71	3.79	17.31	4.29	1.51	4.77	0.58	3.41	0.63	1.76	0.18	1.37	0.18
VG-Sw 1 m	13.73	79.86	31.13	3.47	12.36	1.74	0.71	2.50	0.24	1.42	0.28	0.77	0.06	0.62	0.05
VG-Sw 6 m	8.14	42.14	15.32	1.79	6.56	1.15	0.53	1.55	0.17	0.98	0.18	0.54	0.03	0.48	0.06
(Ol-Px)-Sw 1 h	8.52	17.01	15.43	1.97	8.09	1.46	0.71	1.66	0.17	1.02	0.18	0.56	0.06	0.49	0.05
(Ol-Px)-Sw 5 h	7.02	16.51	16.31	1.83	6.99	1.03	0.47	1.29	0.11	0.80	0.12	0.37	0.01	0.36	0.02
(Ol-Px)-Sw 24 h	4.41	9.56	8.42	1.08	4.63	0.70	0.30	0.84	0.13	0.55	0.11	0.30	0.03	0.31	0.02
(Ol-Px)-Sw 1 m	6.93	22.72	14.55	1.69	6.27	0.91	0.41	1.23	0.24	0.71	0.19	0.40	0.07	0.38	0.08
(Ol-Px)-Sw 6 m	3.82	23.26	8.83	0.97	3.11	0.49	0.26	0.65	0.05	0.35	0.05	0.17	0.01	0.16	0.01
Ash-Sw 1 h	6.33	38.30	29.61	2.82	14.71	7.55	0.95	0.98	3.21	1.24	0.16	0.63	0.08	0.34	0.02
Ash-Sw 3 h	6.73	35.86	22.28	2.40	11.89	6.57	1.06	1.11	2.75	1.33	0.21	0.72	0.12	0.39	0.04
Ash-Sw 5 h	8.60	41.31	30.70	3.00	14.58	7.35	1.18	1.41	3.24	1.58	0.19	0.86	0.11	0.49	0.02
Ash-Sw 7 h	8.87	61.75	38.39	4.38	20.34	10.45	1.10	1.78	5.92	1.81	0.22	0.93	0.18	0.49	0.08
Ash-Sw 24 h	10.53	35.66	27.85	3.02	14.39	8.17	1.66	1.55	3.57	2.10	0.29	1.36	0.20	0.74	0.07
Ash-Sw 48 h	5.23	34.15	17.20	1.62	7.71	3.84	0.71	1.02	1.91	0.83	0.10	0.44	0.05	0.25	0.02
Ash-Sw 15 d	10.54	76.85	41.09	4.13	20.14	10.71	1.36	1.39	5.45	2.10	0.22	1.04	0.14	0.54	0.03
Ash-Sw 1 m	8.41	66.91	34.40	3.17	15.88	7.76	0.89	1.07	4.46	1.48	0.16	0.64	0.09	0.36	0.01
Ash-SW 3 m	6.04	59.47	22.12	2.13	10.19	5.22	0.68	0.89	2.94	1.05	0.09	0.49	0.05	0.26	0.01
Ash-Sw 6 m	5.02	46.81	20.72	1.99	9.31	4.22	0.60	0.86	2.58	0.88	0.08	0.37	0.04	0.19	0.01
Ash.CS 1 h	4.62	11.79	10.16	1.13	5.35	3.03	0.57	0.85	1.40	0.70	0.08	0.45	0.05	0.29	0.01
Ash-CS 3 h	5.29	10.30	8.51	1.05	4.52	2.66	0.57	0.95	1.14	0.71	0.07	0.49	0.05	0.30	0.02
Ash-CS 5 h	4.49	11.13	8.30	1.01	4.47	2.53	0.49	0.89	1.07	0.63	0.07	0.38	0.04	0.22	0.01
Ash-CS 7 h	4.26	8.46	7.95	0.95	4.08	2.23	0.51	0.99	0.93	0.58	0.07	0.38	0.03	0.28	0.02
Ash-CS 24 h	3.53	6.89	6.25	0.78	3.59	2.05	0.34	0.87	0.91	0.52	0.04	0.34	0.02	0.18	0.01
Ash-CS 48 h	4.13	8.46	7.66	0.87	3.94	1.86	0.42	1.15	0.80	0.53	0.06	0.36	0.02	0.23	0.02
Ash-CS 15 d	8.55	14.62	17.12	2.11	9.59	5.98	1.28	1.45	2.72	1.62	0.21	1.09	0.14	0.61	0.04
Ash-CS 1 m	4.42	9.82	9.62	1.15	4.86	2.72	0.50	0.97	1.15	0.66	0.11	0.40	0.07	0.29	0.05
Ash-CS 3 m	4.14	9.38	7.04	0.89	3.83	2.20	0.42	0.94	0.95	0.55	0.05	0.36	0.02	0.17	0.01
Ash-CS 6 m	3.32	23.68	26.32	1.29	9.65	3.04	0.40	1.08	3.14	0.68	0.04	0.26	0.00	0.15	0.01
Ash-HAS 1h	3.17	12.34	12.02	1.08	4.90	2.48	0.58	0.64	0.88	0.56	0.05	0.33	0.02	0.14	0.01
Ash-HAS 3 h	2.89	36.85	41.99	1.75	14.84	3.76	0.38	0.38	3.33	0.73	0.04	0.22	0.00	0.11	0.01
Ash-HAS 5 h	3.10	9.06	6.83	0.77	3.49	2.03	0.43	0.58	0.70	0.47	0.04	0.30	0.04	0.16	0.01
Ash-HAS 7 h	2.82	11.44	10.62	0.91	4.84	2.31	0.50	0.67	0.99	0.46	0.04	0.26	0.01	0.11	0.01
Ash-HAS 24 h	3.09	10.57	7.57	0.87	3.82	2.20	0.61	1.25	0.77	0.45	0.05	0.34	0.02	0.16	0.01
Ash-HAS 48 h	2.29	9.99	8.90	1.64	4.01	2.06	0.44	0.69	0.73	0.43	0.04	0.27	0.01	0.11	0.01
Ash-HAS 15 d	3.43	14.75	10.35	1.24	4.46	2.49	0.66	1.20	0.90	0.56	0.05	0.35	0.03	0.16	0.01
Ash-HAS 1 m	2.26	13.33	8.85	0.97	4.16	2.16	0.34	0.72	0.76	0.35	0.03	0.17	0.00	0.05	0.01
Ash-HAS 3 m	4.11	22.84	12.72	1.40	5.59	2.86	0.50	0.77	1.08	0.58	0.06	0.37	0.04	0.22	0.01
Ash-HAS 6 m	1.29	16.57	10.25	1.19	4.25	1.92	0.41	0.71	0.73	0.35	0.03	0.12	0.00	0.07	0.01

Table 2.6 – YLn concentrations (ppt) measured in the leaching solutions during the kinetic experiments at the end of each interaction time.

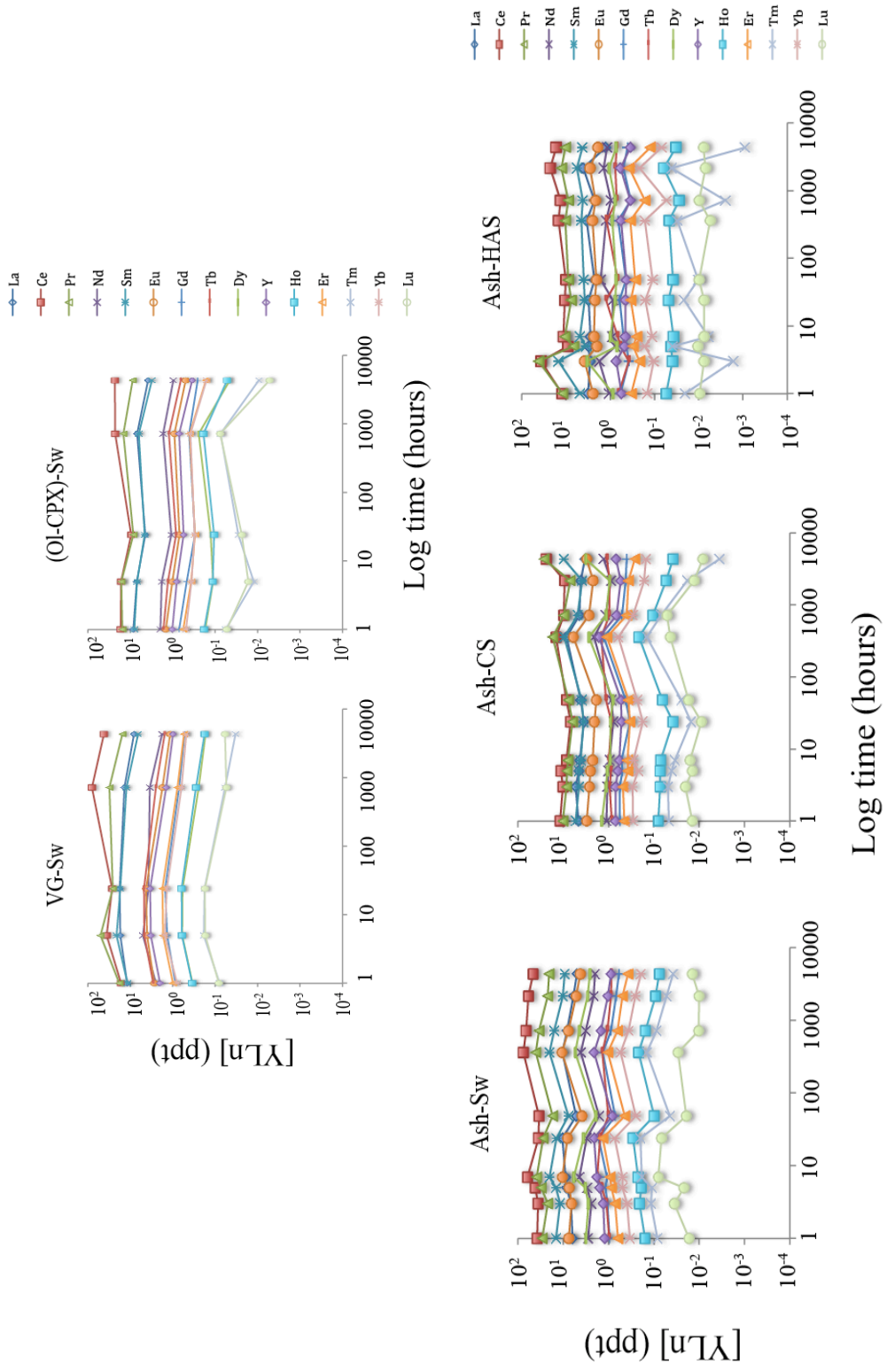

Figure 2.6 – Variation of YLn concentration in dissolved phase during kinetic experiments.

Due to the simultaneous occurrence of unspecific and specific surface coordination sites in montmorillonite-like structures, for pH values larger that 7.5 HREE are preferentially retained onto montmorillonite-like surfaces and Y/Ho increases in parent solution (Coppin et al., 2002) because unspecific sites are solvated by Na^+ and specific sites preferentially coordinate Ho and other HREE, with shorter ionic radii with respect to LREE.

Moreover initial superchondritic Y/Ho values after one hour of interaction suggest an early dissolution of Y enriched materials adsorbed onto surfaces of ash grains. This evidence agrees with AFM observations evidencing soluble fluorides onto surfaces of volcanic ash erupted from Mount Etna during summer 2001 (Delmelle et al., 2007). These phases should form during interactions between ash and hot fluids in the plume before fallout of ash particles and adsorbed onto their surfaces. Recognition of tetragonal and cubic crystals onto ash and mineral surfaces, whose features strongly reflect those typical of Al, Ca and Mg fluorides, also corroborate this suggestion being F-rich fluids and minerals strongly enriched in Y with respect to Ho (Bau, 1996). SEM observations of investigated materials also justify the observed abrupt changes of Y/Ho bahaviour with time. The deposition of FeOOH and/or AlOOH microcrysts onto weathered surfaces usually can induce Y-Ho decoupling due to preferential scavenging of these elements onto mineral surfaces (Ohta and Kawabe, 2001; Quinn et al., 2007). Quinn et al. (2004) demonstrate that Y behaves similarly to an heavy YLn during prevailing ionic interactions occurring with dissolved ligands, whereas it behaves as a light YLn during prevailing covalent interactions with scavenging particulates. Y/Ho increase suggests preferential Ho removal onto Fe-oxyhydroxides (Quinn et al., 2004; 2007). The occurrence of alteration products on the surfaces of the volcanic as was evidenced by scanning electron microscopy (SEM) (Fig. 2.10).

Carbonate addition to Sw, although introducing the complexation variable in the system, does not change features of YLn patterns. This behaviour suggests the higher pH influence on the ash dissolution than carbonate complexing capability. The further HA addition allows us to evaluate the competition between carbonate and humate during YLn leaching from volcanic particles.

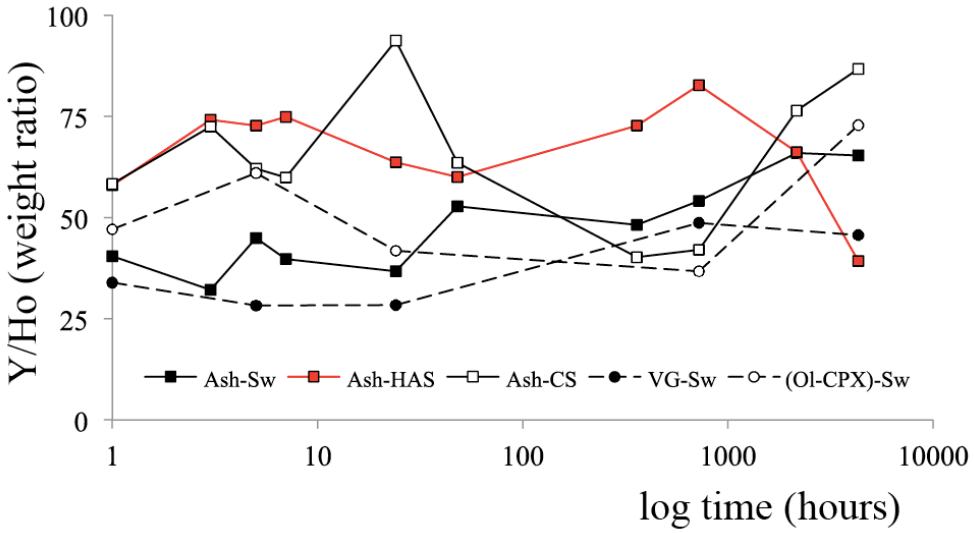

Figure 2.7 a – Y/Ho ratio in dissolved phase during kinetic experiments.

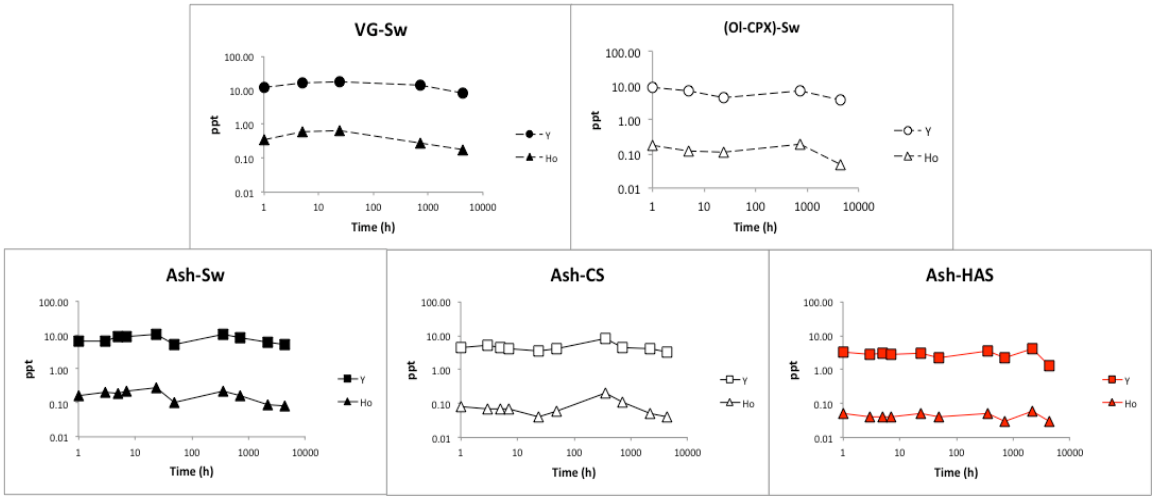

Figure 2.7 b – Y and Ho evolution as function of time in the extraction solutions. The greater tendence of scavenging for Ho than Y is mirrored in the high Y/Ho ratios.

To filtrate from YLn patterns effects related to element leaching from ash, CS and HAS patterns were normalised to those measured in SW experiments and resulting nornalised patterns compared in Figure 2.8. The occurrence of a positive Gd anomaly always occur with time and can be explained by larger dissolved Gd stability induced by the electronic configuration of Gd^{3+} ion ($Xe4f^{7}6s^{0}5d^{0}$). Moreover a HREE fractionation with respect to LREE is very often recognised and significant tetrad effects in La-Nd,

Gd-Ho and Er-Lu intervals are reported from 15 days to the end of experiments. These features correspond to modifications of coordination neighbours along the YLn series according to the Refined spin-pairing energy theory (Jørgensen, 1979; Kawabe, 1992; 1998a; 1998b).

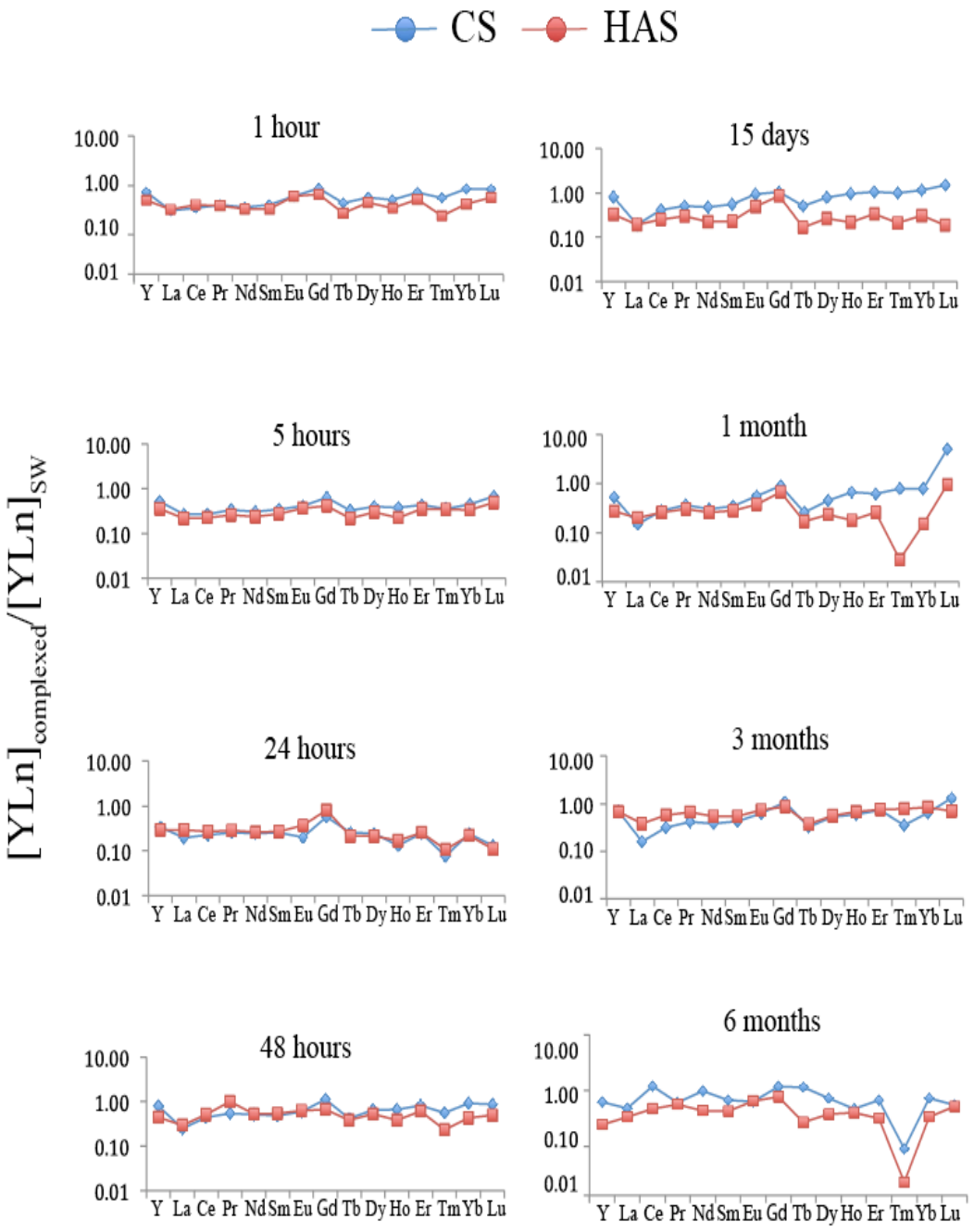

Figure 2.8 – Sw normalized YLn in CS and HAS experiments.

The PAAS-normalised patterns of Lns are showed in Figure 2.9 (a and b). It suggests an important contribution to the Ln fractionation effects due to the alteration of volcanic ash. All samples evidence La enrichments in solution due to the preferential release of light REEs from volcanic ash. This phenomenon is due, according to Bau et al. (1998), to the occurrence of higher concentrations of light Lns in more easily alterable glassy and interstitial materials of volcanic ash. The Ln PAAS-normalised patterns evidence moreover positive Eu anomalies suggesting the partial dissolution of plagioclase, in which crystal structure Eu is usually distributed (McKay, 1989). Moreover dissolved light lanthanides exist as strong dissolved complexes in the studied systems, as suggested by the La–Nd tetrad ($t_1 < 0.7$ for all experiments). On the contrary heavy Ln are mainly involved in adsorption processes on solids surfaces as outer sphere organic complexes (Takahashi et al., 1999; Davranche et al., 2004, 2005).

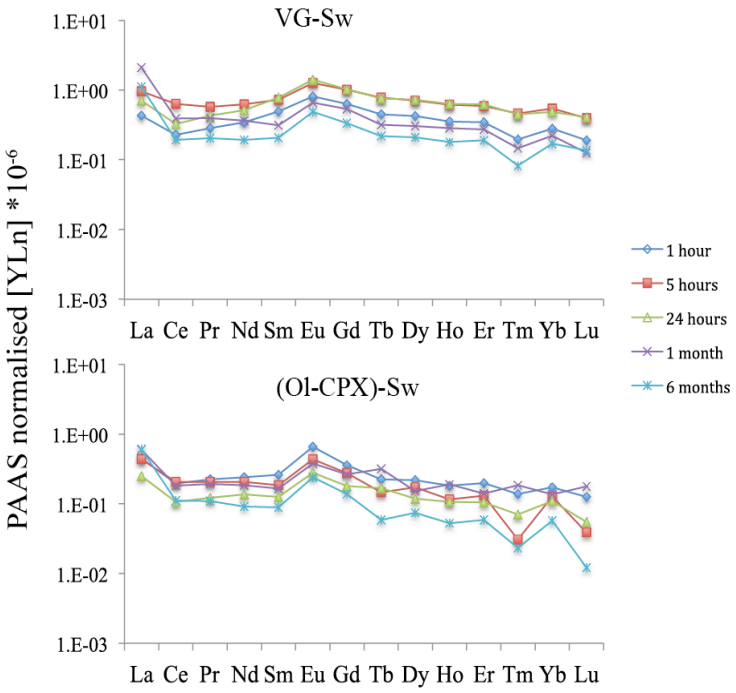

Figure 2.9 (a) – PAAS-normalized YLn contents in dissolved phase during experiments with glass and minerals.

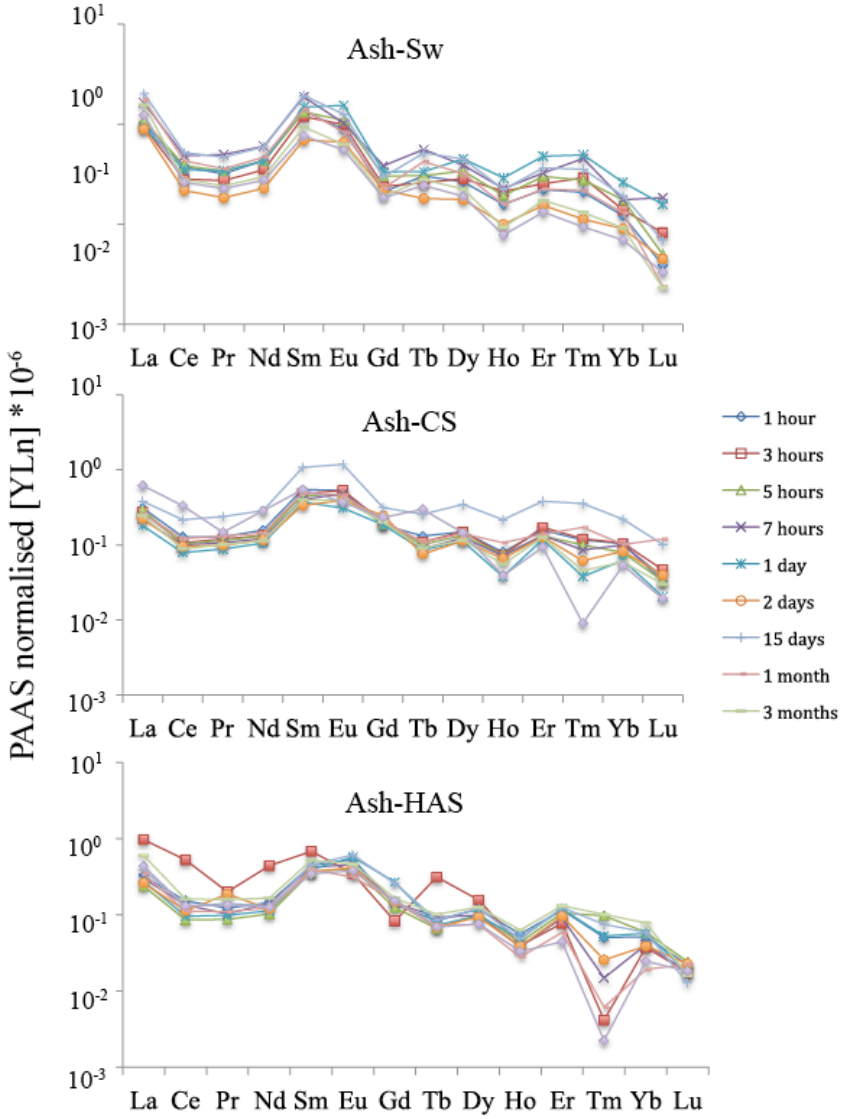

Figure 2.9 (b) – PAAS-normalized YLn contents in dissolved phase during Ash-Sw, Ash-CS and Ash-HAS experiments.

2.3.2. SEM observations

After kinetic experiments, SEM observations of volcanic glass and minerals were carried out and compared with fresh samples, as showed in Fig. 2.10. At the beginning of the experiment, volcanic glass had a smooth bubble surface with many conchoidal fractures and an unaltered surface. Even within the first hours of interaction with synthetic seawater, the presence of micro-spherules on the fractures was evidenced, as well as tubular structures corresponding to the microcrystallization. As interaction

progressed an increasingly thick alteration layer was observed on the surface with incipient crystallization of lamellar microcrystals in 6 months samples.

Starting rounded olivine shows an overall surface roughness and evident "hacksaws" in a selective region of the grain, probably rich of weakness points such as dislocations. After interaction with seawater the surface became rich of ferruginous structures indicating the presence of FeOOH. Augite before interaction shows evident cleavage features and incipient etch pits on the surface that are developed usually parallel to the *c*-axis of the crystal. During interaction process, altered layers cover the mineral surface obscuring sometimes the pristine signs. After 1 and 6 month of interaction with seawater the surface presents fluoride salts and others structures consisting in secondary minerals As alteration continues the cleavages on mineral surface are marked and we can see secondary minerals. The formation of clay minerals is also evidenced by XRD investigations carried out after six months of solid-liquid interaction. Crovisier et al. (2003) report formation of hydrotalcite on volcanic glass surface after interaction with seawater.

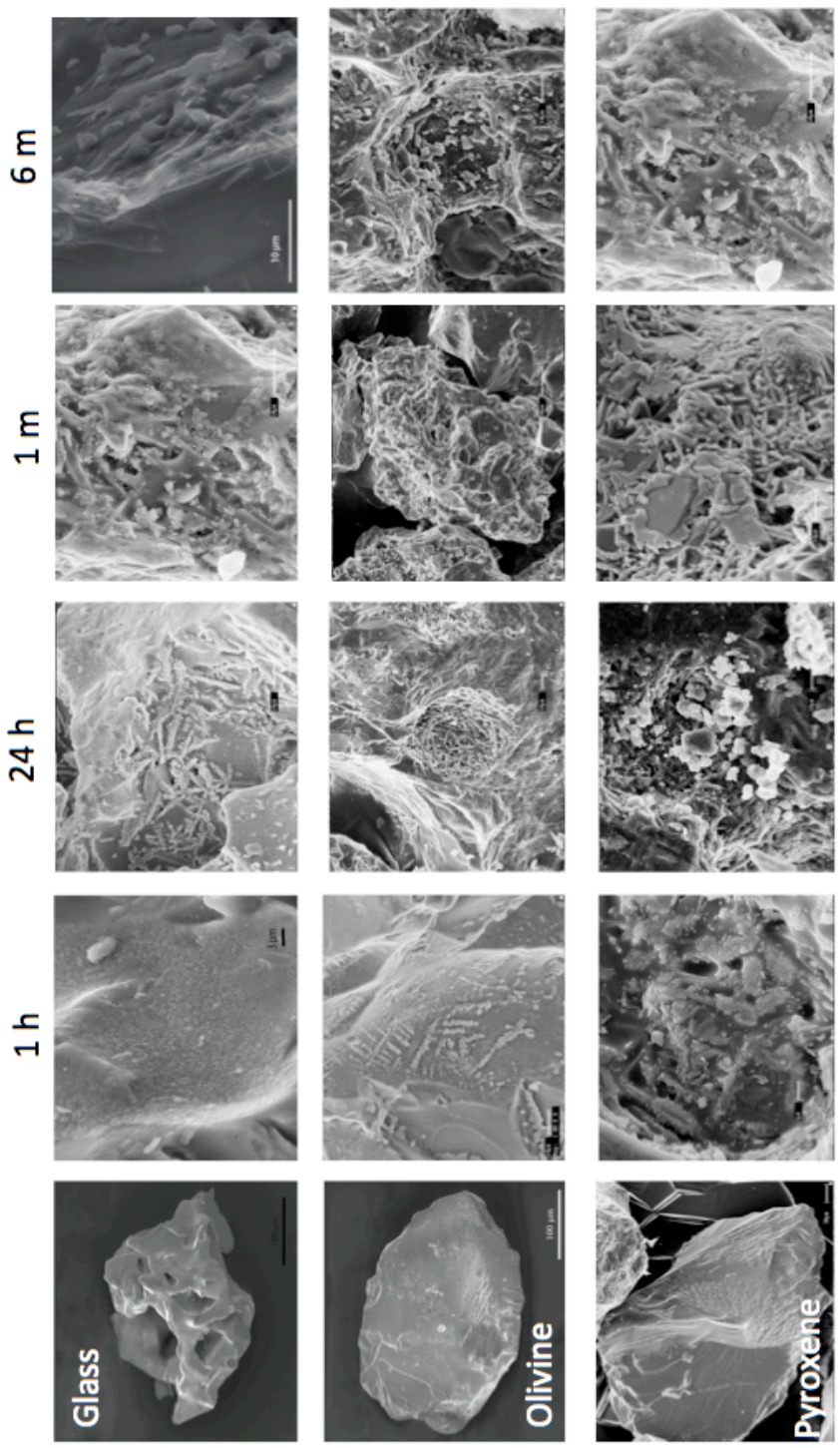

Figure 2.10 - Scanning electron micrographs showing morphologic characteristics of alteration of basaltic glass, olivine (Ol) and clinopyroxene (CPX) on fresh samples and during kinetic experiments. For details see the text.

2.4. Conclusions

Effects of YLn release from different fractions of freshly erupted volcanic ash suggest that these elements are primarily released from glass ash fraction during early solid-liquid processes. A further YLn leaching occurred from weakly soluble fluorides occurring onto surfaces of grains, due to the adsorption of F-rich salts formed after interactions of solid particles with hot plume during eruption. These processes allowed to crystallization of several alteration phases consisting mainly of Al and Fe oxyhydroxides and clay minerals. During these processes extensive changes in Y/Ho ratio were induced in dissolved phase and amplitude of tetrad effects in Gd-Ho interval. Just the relationships recognised between these parameters allowed us to follow the above mentioned process and suggested the occurrence of surface complexation of YLn mainly occurring according to an outer sphere mechanism. This mechanism of YLn surface complexation was possibly induced by large reactivity of glass surface that released large amounts of metals with respect to low concentrations of leached YLn. This process probably induced a quick saturation of specific coordination surface sites and leaving only unspecific negative charged surfaces for interactions with dissolved YLn that were scavenged as outer sphere surface complexes. The addition of ligand species to dissolved media does not increase dissolution rate of volcanic particles but modify the YLn distribution in liquid phase, as well evidenced by Y/Ho ratio. Moreover the availability of altered pyroclastic materials and newly formed clay materials determines fractionation between light and heavy lanthanides.

SEM observation and results of XRD data show that the above mentioned dissolution processes and deposition of newly-formed alteration phases occurred during the experiments with different features depending from the amplitude of interactions and their duration.

References

Alibo, D.S., Nozaki, Y. (1999). Rare earth elements in seawater: Particle association, shale-normalization, and Ce oxidation. Geochimica et Cosmochimica Acta, Vol. 63, No. 3/4, pp. 363–372.

Aubert D., Stille P., Probst A., Gauthier-Lafaye F., Pourcelot L. and Del Nero M. (2002). Characterization and migration of atmospheric YLN in soils and surface waters. Geochim. Cosmochim. Acta 66, 3339–3350.

Bau, M., Dulski, P., Moller, P. (1995). Yttrium and holmium in South Pacific seawater: vertical distribution and possible fractionation mechanisms. Chem. Erde, 55, l-15.

Bau M. (1996). Controls on the fractionation of isovalent trace elements in magmatic and aqueous systems: evidence from Y/ Ho, Zr/Hf, and lanthanide tetrad effect. Contrib. Miner. Petrol. 123, 323–333.

Bau M., Usui A., Pracejus B., Mita N., Kanai Y., Irber W. and Dulski P. (1998). Geochemistry of low-temperature water–rock interaction: evidence from natural waters, andesite, and ironoxyhydroxide precipitates at Nishiki-numa iron-spring, Hokkaido, Japan. Chem. Geol. 151, 293–307.

Byrne, R.H., Sholkovitz, E.R., (1996). Marine chemistry and geochemistry of the lanthanides. In: Gschneidner Jr., K.A., Eyring, L. (Eds.), Handbook on the Physics and Chemistry of Rare Earths. Elsevier, Amsterdam, pp. 497–593.

Brantley, S.L. (2004). Reaction kinetics of primary rock-forming minerals under ambient conditions. In Surface and Ground Water, Weathering, and Soils, Vol. 5 (ed. J. I. Drever), pp. 73–118. Elsevier.

Cantrell K. J. and Byrne R. H. (1987). Rare earth element complexation by carbonate and oxalate ions. Geochim. Cosmochim. Acta 51, 597–605.

Coppin, F., Berger, G., Bauer, A., Castet, S., Loubet, M. (2002). Sorption of lanthanides on smectite and kaolinite. Chemical Geology 182 Ž2002. 57–68.

Crovisier, J.-L., Advocat, T., Dussossoy, J.-L., (2003). Nature and role of natural alteration gels formed on the surface of ancient volcanic glasses (natural analogs of waste containment glasses). J. Nucl. Mater. 321, 91–109.

Delmelle P., Lambert M., Dufrene, Y., Gerin, P., Oskarsson, N. (2007). Gas/aerosol-ash interaction in volcanic plumes: New insights from surface analyses of fine ash particles. Earth and Planetary Science Letters 259, 159-170.

Doe (1994). Handbook of methods for the analysis of the Varius Parameters in sea water; version 2, A. G. Dickinson & C. Goyet, EDS., ORNL/CDIAC-74.

Davranche M., Pourret O., Gruau G. and Dia A. (2004). Impact of humate complexation on the adsorption of REE onto Fe oxyhydroxide. J. Colloid Interf. Sci. 277, 271–279.

Davranche M., Pourret O., Gruau G., Dia A. and Le Coz-Bouhnik M. (2005). Adsorption of REE(III)–humate complexes onto MnO2: experimental evidence for cerium anomaly and lanthanide tetrad effect suppression. Geochim. Cosmochim. Acta 69, 4825–4835.

Elderfield H. (1988). The oceanic chemistry of rare-earth elements. Philos. Trans. R. Soc. London 325, 105–126.

Elderfield H., Upstill-Goddard R. and Sholkovitz E. R. (1990). The rare earth elements in rivers, estuaries, and coastal seas and their significance to the composition of ocean waters. Geochim. Cosmochim. Acta 54, 971–991.

Gautier, J.-M., Oelkers, E.H., Schott, J., (2001). Are quartz dissolution rates proportional to B.E.T. surface areas? Geochim. Cosmochim. Acta 65, 1059–1070.

Ghiara, M.R., Franco, E., Petti, C., Stanzione, D. and Valentino, G.M. (1993). Hydrothermal interaction between basaltic glass, deionized water and seawater. Chemical Geology, 104, 125-138.

Goldberg, E.D., Koide, M., Schmitt, R.A., Smith, R.H., (1963). Rareearth distributions in the marine environment. J. Geophys. Res. 68 (14), 4209– 4217.

Goldstein, S.J. and Jacobsen S.B. (1988). REE in the Great Whale River estuary, northwest Quebec. Earth and Palnetary Science Letters, 88, 241-252.

Greaves M. J., Rudnicki M. and Elderfield H. (1991). Rare earth elements in the Mediterranean Sea and mixing in the Mediterranean outflow. Earth Planet. Sci. Lett. 103, 169–181.

Jørgensen, C.K., (1979). Theoretical chemistry of rare earths. In: Gschneider, K.A., Eyring, L. (Eds.), The Handbook of Physics and Chemistry of Rare Earths, 3, 111-169, North-Holland, Amsterdam.

Hajash, A. and Archer, P. (1980). Experimental seawater/basalt interactions: Effect of cooling. Contrib. Mineral. Petrol. 75, 1-13.

Hannigan R. E. and Sholkovitz E. R. (2001). The development of middle rare earth element enrichments in freshwaters: weathering of phosphate minerals. Chem. Geol. 175, 495–508.

Kawabe, I. (1992). Lanthanide tetrad effect in the Ln^{3+} ionic radii and refined spin-pairing energy theory. Geochemical Journal, 26, 309-335.

Kawabe, I., Toriumi, T., Ohta, A., Miura, N., (1998). Monoisotopic REE abundances in seawater and the origin of seawater tetrad effect. Geochem. J. 32, 213–229.

Koeppenkastrop, D., De Carlo E. H. and Roth M. (1991). A method to investigate the interaction of rare earth elements with metal oxides in aqueous solution. J. Radioanal. Nucl. Chem. 151, 337–346.

Koeppenkastrop, D., De Carlo, E.H. (1992). Sorption of rare-earth elements from seawater onto synthetic mineral particles: an experimental approach. Chem. Geol. 95, 251– 263.

Lasaga, A.C. (1998). Kinetic Theory and Applications in Earth Sciences. Princeton Press, Princeton.

Lerman, A., and Mackenzie, F.T. (1975). Rates of dissolution of aluminosilicates in seawater. Earth and Planetary Science Letters, 25, 82-88.

Lee J. H. and Byrne R. H. (1992). Examination of comparative rare earth element complexation behavior using linear free-energy relationships. Geochim. Cosmochim. Acta 56, 1127–1137.

McKay G. A. (1989). Partitioning of Rare Earth Elements between major silicate minerals and basaltic melts. In Geochemistry and Mineralogy of Rare Earth Elements, Reviews in Mineralogy (eds. B. R. Lipin and G. A. McKay), vol. 21, pp. 45–77.

Millero F. J. (1992). Stability constants for the formation of rare earth inorganic complexes as a function of ionic strength. Geochim. Cosmochim. Acta 56, 3123–3132.

Molinaroli, E., Pistolato, M., Rampazzo, G., Guerzoni, S. (1999). Geochemistry of natural and anthropogenic fall-out (aerosol and precipitation) collected from the NW Mediterranean: two different multivariate statistical approaches. Applied Geochemistry 14, 423-432.

Möller, P., Dulski, P., Luck, J., (1992). Determination of Rare Earth Elements in seawater by inductively coupled plasma-mass spectrometry. Spectrochim. Acta B 47,1379–1387.

Ohta A. and Kawabe I. (2001). REE(III) adsorption onto Mn dioxide (d-MnO2) and Fe oxyhydroxides: Ce(III) oxidation by d-MnO2. Geochim. Cosmochim. Acta 65, 695–703.

Paulson, A.J., (1986). Effects of flow rate and pretreatment on the extraction of trace metals from estuarine and coastal seawater by Chelex-100. Anal. Chem. 58,183–187.

Quinn, K.A., Byrne, R.H., Schijf, J., (2004). Comparative scavenging of yttrium and the rare earth elements in seawater: competitive influences of solution and surface chemistry. Aquat. Geochem. 10, 59–80.

Quinn, K.A., Byrne, R.H., Schijf, J., (2007). Sorption of yttrium and rare earth elements by amorphous ferric hydroxide: Influence of temperature. Environmental Science and Technology, 41 (2), pp. 541-546.

Rikers, R.A., Rem, P., Dalmijn, W. L., Honders, A. (1998). Characterization of Heavy Metals in Soil by High Gradient Magnetic Separation. Soil and Sediment Contamination: An International Journal, 7 (2), 163-190.

Rollinson H. (1993). Using Geochemical Data: Evaluation, Presentation, Interpretation. Longman, Harlow, UK.
Seyfried, W.E. and Bischoff, J.L. (1977). Hydrothermal transport of heavy metals by seawater; the role of seawater basalt ratio. Earth Planet. Sci. Lett., 34, 71-78.

Seyfried, W.E. and Mottl, M.J. (1982). Hydrothermal alteration of basalt by seawater dominated condition. Geochim. Cosmochim. Acta, 46, 985-1002.

Sholkovitz, E.R., (1993). The geochemistry of rare earth elements in the Amazon River estuary. Geochim. Cosmochim. Acta 57, 2181–2190.

Sholkovitz, E. R., Elderfield, H., Smymczak, YLN. and Casey K. (1999). Island weathering: river sources of rare earth elements to the Western Pacific Ocean. Mar. Chem. 68, 39–57.

Standard Methods for the Examination of Water and Wastewate (1992). American Public Health Association, 1015 Fifteenth Street NW, Washington, D.C. 20005

Tachikawa, K., Jeandel, C., Vangriesheim, A. and Dupre, B. (1999). Distribution of rare earth elements and neodymium isotopes in suspended particles of the tropical Atlantic Ocean (EUMELI site). Deep-Sea Res. 46, 733–755.

Takahashi Y., Tada A. and Shimizu H. (2004) Distribution patterns of Rare Earth ions between water and Montmorillonite and its relation to the sorbed species of the ions. Anal. Sci. 20, 1301–1306.

Takahashi Y., Kimura T., Kato Y. and Minai Y. (1999). Speciation of europium(III) sorbed on a montmorillonite surface in the presence of polycarboxylic acid by laser-induced fluorescence spectroscopy. Environ. Sci. Technol. 33, 4016–4021.

Takahashi, Y., Châtellier, X., Hattori, K.H., Kato, K., Fortin, D. (2005). Adsorption of rare earth elements onto bacterial cell walls and its implication for YLN sorption onto natural microbial mats. Chemical Geology, 219 (1-4), pp. 53-67.

Taylor S. R. and McLennan S. M. (1985). The continental crust: Its composition and evolution. An examination of the geochemical record preserved in sedimentary rocks. Blackwell.

Thornton, E.C. and Seyfried, W. E. (1985). Sediment-seawater interaction at 200 and 300°C, 500 bars pressure: The role of sediment composition in diagenesis and low-grade metamorphism of marine clay. Geol. Soc. Am. Bull., 96, 1287- 1295.

Velbel, M. A., (1993). Formation of protective surface layers during silicate-mineral weathering under well-leached, oxidizing conditions. American Mineralogist, v. 78, p. 408–417.

Velbel M.A., (1999). Bond strength and the relative weathering rates of simple orthosilicates. American Journal of Science, vol. 299, p. 679-696.

Wood, S.A. (1990). The aqueous geochemistry of the rare-earth elements and yttrium. Review of available low-temperature data for inorganic complexes and the inorganic REE speciation of natural waters. Chem. Geol. 82, 159– 186.

Chapter III

Yttrium and lanthanides in human lung fluids, probing the exposure to atmospheric fallout.

Censi P.[A,B,C], Tamburo E [A]., Speziale S.[D], Zuddas P.[E], Randazzo L.[A,C,E], Punturo R. [F]., Cuttitta A. [B], Aricò P.[A]

A. *Dipartimento C.F.T.A., Università di Palermo, Via Archirafi, 36 90123 Palermo, Italy*
B. *I.A.M.C.-Consiglio Nazionale delle Ricerche, Via faro, 1, 91021 Torretta Granitola, Campobello di Mazara (Tp), Italy*
C. *En.Bio.Tech. – Via A quileia, 35 90100 Palermo (Italy)*
D. *Deutsches GeoForschungsZentrum, Telegrafenberg, Potsdam, 14473, Germany*
E. *Institut de Génie de l'Environnement Ecodéveloppement and Département Sciences de la Terre, UMR 5125, Université Claude Bernard Lyon 1, 2 rue R. Dubois, Bat GEODE 69622 Villeurbanne Cedex (France).*
F. *Dipartimento di Scienze Geologiche, Università di Catania, Corso Italia, 55 - 95129 Catania, Italy*

Co-supervision Ph. D. thesis - Loredana Antonella Randazzo

Jan 2008 – Dec 2010

Abstract

Inhalation of airborne particles can produce crystallization of phosphatic microcrysts in intraaveolar areas of lungs, sometimes degenerating into pulmonary fibrosis. Results of this study indicate that these pathologies are induced by interactions between lung fluids and inhaled atmospheric dust in people exposed to volcanic dust ejected from Mount Etna in 2001. Here, the lung solid–liquid interaction is evaluated by the distribution of yttrium and lanthanides (YLn) in fluid bronchoalveolar lavages on selected individuals according the classical geochemical approaches. We found that shale-normalised patterns of yttrium and lanthanides have a 'V shaped' feature corresponding to the depletion of elements from Nd to Tb when compared to the variable enrichments of heavy lanthanides, Y, La and Ce. These features and concurrent thermodynamic simulations suggest that phosphate precipitation can occur in lungs due to interactions between volcanic particles and fluids. We propose that patterns of yttrium and lanthanides can represent a viable explanation of some pathology observed in patients after prolonged exposure to atmospheric fallout and are suitable to become a diagnostic parameter of chemical environmental stresses.

3.1. Introduction

Investigating the effects on human health of the exposure to potentially dangerous geological materials represents one of the present issue in our understanding of the Earth dynamics (Sakai, 2007). The human lung system presents interfaces that are exposed to interactions with geological materials by inhalation of atmospheric particulates. Dendriform pulmonary ossification (DPO) and pulmonary microlithiasis (PAM) are two rare diseases that have been recognized in the lungs of individuals who have inhaled atmospheric particles released by industrial practices or hydrocarbon combustion (Baddini Martinez and Ramos, 2008). Both these pathologies generate new phosphatic microcrysts in intraaveolar areas of the lungs (Pracyk et al., 1996; Yoon et al., 2005) that may progress to pulmonary fibrosis (Joines and Roggli, 1989). Both DPO and

PAM are considered difficult to recognize under in vivo observations, whereas their occurrence is usually evidenced only after authoptic examination. Causes of these diseases are not well defined, although the disposal of metal dust with large affinity to phosphate precipitation, such as lanthanides, can represent a suitable possibility. This suggestion agrees with recognition of DPO in people exposed to industrial dust produced during the manufacture of mirrors, optical lenses, and certain electronic components that are usually considered lanthanide-rich materials (Sabbioni et al., 1982; Hirano and Suzuki, 1996).

Trace elements present in atmospheric particles of either natural or anthropogenic origin can dissolve in lung fluid (Luoto et al., 1998; Dias Da Cunha et al., 2009). Since the phosphate (PO_4^{3-}) concentration in lung fluid is approximately 1.175 $mmoll^{-1}$ (Midander and Wallinder, 2007), some cations with an affinity for phosphate, such as those of the lanthanides, can crystallize in interstitial lung spaces. This can be observed using a mildly invasive procedure in which broncho-alveolar lavage (BAL) fluid is analyzed for YLn content using a shale-normalised approach. Techniques borrowed from geochemistry are used to identify dissolved particles and their phosphate crystallizations. This method can be used to assess DPO and PAM induction, and has been texted in human lung fluids of individuals exposed to freshly released volcanic particles by inhalation. This may represent a suitable explaination of DPO and PAM induction and has been tested in human lung fluids of people exposed by inhalation of freshly released volcanic particles.

3.1.1. Briefly description of alveoli anatomy

The alveoli consist of an epithelial layer and extracellular matrix surrounded by capillaries (Saladin et al. 2007). There are three major alveolar cell types in the alveolar wall (pneumocytes):

- Type I (Squamous Alveolar) cells that form the structure of an alveolar wall;
- Type II (Great Alveolar) cells, that are the most numerous cells in the alveoli,

secrete pulmonary surfactant to lower the surface tension of water and allows the membrane to separate, thereby increasing the capability to exchange gases. Surfactant is a mixture of phospholipids and protein that reduces surface tension in the thin fluid coating within all alveoli. The fluid coating is produced in order to facilitate the transfer of gases between blood and alveolar air. Surfactant is continuously released by exocytosis.

- Macrophages that destroy foreign material, such as bacteria.

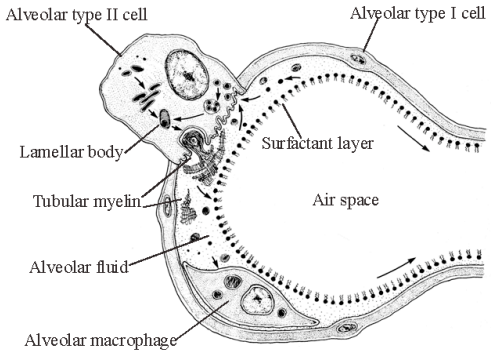

Figure 4.1 – Structure of alveolus.

3.2. Experimental section

3.2.1 *Brief characterization of the fine particulate emitted by Etna volcano in summer 2001*

During Etna eruption in summer 2001 the amount of ejecta was so large to cause the deposition of about 0.39 kg m^{-2} ash between 21 and 24 July 2001 in the interested area (Scollo et al. 2007). Volcanic ejecta typically consisted of a mixture of several solids ranging from particles made of silicate minerals and volcanic glass to soluble salts adsorbed onto those particles (Oskarsson 1980; Frogner et al. 2001; Delmelle et al. 2007). The solid fraction of ejected materials mainly consisted of glass fragments (about 70%) with smaller amounts of clinopyroxene (about 15%) and minor amounts of olivine and spinel (Taddeucci et al. 2004; Viccaro et al. 2006). There is a

soluble ash fraction (SAF) coating solid particles consisted of highly soluble sublimates of acids, metal salts and adsorbed fluids (formed during the rising in the volcanic eruptive plume) (Oskarsson, 1980).

3.2.2 *BAL extraction and chemical processing of the samples*

Six patients in care at the Dipartimento di Medicina Interna e Medicina Specialistica of the Università degli Studi di Catania were subject (after giving their written informed consent) to Bronchoalveolar lavage (BAL) procedure during the summer of 2001, when the city of Catania was exposed to severe delivery of atmospheric particulate matter produced by pyroclastic activity of Mount Etna, the largest European volcano. Due to the particular location of Catania with respect to the eruptive source, this intensively populated urban area was subjected to strong delivery of volcanic particulate mainly consisting of mineral, glass and rock fragments between 1 and 500 μm diameter, with main grain-size in the range of 5-10 μm diameter (Taddeucci et al. 2004; Viccaro et al. 2006; Censi et al. 2007; Scollo et al. 2007). The International Commission on Radiological Protection (ICRP) considers that the percentage of respirable particles within the size range of 5–10 μm is 30–1%, respectively.

BALs were obtained by instillation of four lavages carried out with 30 ml aliquots of physiological solution (SW) using a fibrobronchoscope according to Bargagli et al. (2005). Each aliquot was immediately gently aspirated. From each lavage about 20 ml of sample were rejected and only 10 ml of sample, after filtration with a 0.22 μm Nalgene™ membrane, were used for chemical investigations. BAL samples were treated with 15 ml of hydrogen peroxide, 5 ml of HNO_3 30% solution, HCl 30% solution and 0.1 g of solid NH_4F in a polytetrafluoroethylene (TFM™) reactor. Reactors were sealed and heated in a microwave oven (MARS 5™, CEM Technologies) at 3^x10^5 Pa and 200 °C for 30 minutes. Acid excess was removed from each solution up to incipient dryness using a CEM microvap™ apparatus and HNO_3 solution (5 % v/v) was added to attain final solution volumes of 20 ml. The solutions were finally transferred to previously cleaned polycarbonate vials. The samples were treated under a laminar air flow clean bench to minimize contamination risks.

YLn analyses were carried out with a double focusing magnetic sector field inductively coupled plasma mass spectrometer SF-ICP-MS Thermo-Scientific Element 2,

without gas chromatograph, using an external calibration approach. BAL analyses are reported in Table 3.1.

All the investigated elements were analyzed in medium resolution mode, apart from Y and La that were determined in high-resolution mode, in order to avoid an overestimation of true concentrations due to effects of interferences of polyatomic Ar-bearing species. Although several polyatomic interferences based on Ar-bearing species can influence the correct evaluation of investigated masses, this problem can be avoided using a high-resolution sector field ICP-MS like this used in this research. On the other hand the problem of the over estimation of the mass of interest partially still remains for ^{89}Y which is influenced by $^{49}Ti^{40}Ar$ species also under high resolution mode. According to the Thermo Finnigan Interference Workshop^{TM} this interference can be avoided with $20{,}000M–\Delta M^{-1}$ theoretical resolution that cannot be attained with our SF-ICP-MS. On the other hand a $^{89}Y/^{49}Ti^{40}Ar$ signal-to noise ratio close to 100 has very limited influence of the correct evaluation of the Y content. Although we did not monitor the ^{49}Ti mass, very low Ti concentrations are expected in BAL samples due to the very low solubility of Ti-bearing materials, both of lithogenic and anthropogenic origin where ^{49}Ti represents only 5.5% of the entire Ti abundance. The calibration for each element was based on 7 standard solutions at known concentration. Analytical precision was evaluated using the same physiological solution (SW) used for collection of BAL samples, due to the absence of standard reference materials with certified values for all the investigated elements. Five aliquots of SW solution were added with the same quantities of chemicals used for the BAL samples treatment, they were subject to mineralization procedures and then used as procedural blanks (PBs). YLn contents measured in PBs were used to evaluate the critical values (L_C), the detection limits (L_D) and the limit of quantification (L_Q) for the investigated trace elements (EPA, 2005). Obtained results are reported in Table 3.2. The low L_Q values indicate that the amounts of trace metals lost and/or added during recovery procedures and sample preparation are negligible with respect to the trace elements contents of BAL samples.

All the studied solutions were prepared with Millipore ultrapure water (18.2 MΩ). All used chemicals were Merck ULTRAPUR®. All the materials used to sample and manipulate water samples were plasticware acid cleaned with hot 1:10 HNO_3 solutions.

	Y	La	Ce	Pr	Nd	Sm	Eu	Gd	Tb	Dy	Ho	Er	Tm	Yb	Lu
	µgl l^{-1}	µgl l^{-1}	µgl l^{-1}	µgl l^{-1}	µgl l^{-1}	µgl l^{-1}	µgl l^{-1}	µgl l^{-1}	µgl l^{-1}	µgl l^{-1}	µgl l^{-1}	µgl l^{-1}	µgl l^{-1}	µgl l^{-1}	µgl l^{-1}
AG	10.215	32.822	11.978	0.253	0.983	0.122	0.0316	0.150	0.020	0.1066	0.0316	0.1067	0.028	0.103	0.019
SC	15.549	93.339	30.962	0.229	0.935	0.118	0.0631	0.206	0.024	0.1255	0.0397	0.1102	0.020	0.118	0.023
BR	18.855	85.560	30.016	0.372	0.321	0.030	0.0330	0.165	0.032	0.2100	0.0320	0.1145	0.021	0.182	0.045
CA	14.776	76.408	31.302	0.427	1.666	0.265	0.1309	0.356	0.028	0.2692	0.0475	0.2019	0.028	0.230	0.039
M	22.701	102.718	38.733	0.218	0.401	0.043	0.0170	0.075	0.017	0.1666	0.0370	0.0874	0.026	0.123	0.037
RG	15.786	77.637	30.846	0.399	1.550	0.257	0.0950	0.320	0.039	0.3206	0.0594	0.2733	0.034	0.313	0.046

Table 3.1 - YLn contents measured in BAL solution. The analyzed masses and the used resolutions are also reported. nd: not determined.

	PB-1	PB-2	PB-3	PB-4	PB-5	L_c	L_d	L_Q	SW-1	SW-2	SW-3	SW-4	SW-5	SW_{mean}	σ ±
	ng l^{-1}	ng l^{-1}	ng l^{-1}	ng l^{-1}	ng l^{-1}	ng l^{-1}	ng l^{-1}	ng l^{-1}	ng l^{-1}	ng l^{-1}	ng l^{-1}	ng l^{-1}	ng l^{-1}	ng l^{-1}	ng l^{-1}
Y	0.92	0.72	1.09	0.62	0.70	0.17	0.34	1.05	8.93	10.44	9.87	10.82	9.51	9.91	0.75
La	0.22	0.18	0.34	0.10	0.16	0.05	0.09	0.29	9.89	9.66	9.55	10.18	9.80	9.82	0.24
Ce	0.30	0.47	0.35	0.32	0.46	0.05	0.10	0.32	8.98	9.64	9.01	9.55	9.64	9.36	0.34
Pr	0.28	0.42	0.35	0.32	0.51	0.09	0.18	0.54	9.35	9.67	9.09	9.87	9.73	9.54	0.32
Nd	0.09	0.05	0.12	0.06	0.08	0.02	0.04	0.12	9.74	9.29	9.62	9.46	9.43	9.51	0.17
Sm	0.10	0.08	0.17	0.06	0.09	0.03	0.06	0.19	9.81	9.43	9.46	9.83	9.29	9.56	0.24
Eu	0.10	0.13	0.22	0.14	0.14	0.02	0.04	0.11	10.03	10.17	10.02	9.25	9.08	9.71	0.50
Gd	0.18	0.16	0.33	0.21	0.22	0.04	0.08	0.24	10.53	9.42	10.16	9.97	9.18	9.85	0.55
Tb	0.29	0.55	0.49	0.39	0.60	0.03	0.06	0.19	11.05	9.68	9.51	9.93	9.49	9.93	0.65
Dy	0.35	0.57	0.40	0.33	0.58	0.09	0.18	0.56	9.19	10.13	9.52	9.36	9.73	9.59	0.37
Ho	0.34	0.50	0.43	0.39	0.51	0.02	0.04	0.14	9.65	9.90	11.72	9.37	9.60	10.05	0.95
Er	0.32	0.52	0.45	0.33	0.51	0.07	0.15	0.46	9.28	11.60	11.03	11.09	10.18	10.63	0.91
Tm	0.29	0.60	0.46	0.36	0.64	0.07	0.14	0.44	8.91	9.42	10.07	9.43	11.03	9.77	0.82
Yb	0.30	0.58	0.53	0.37	0.51	0.03	0.07	0.21	9.39	9.55	11.40	9.27	10.47	10.02	0.91
Lu	0.38	0.56	0.54	0.36	0.61	0.08	0.17	0.52	10.21	10.58	11.08	9.81	10.08	10.35	0.49

Table 3.2 - YLN concentrations measured in procedural blanks (PBs) and related critical values (L_C), detection limits (L_D) and limits of quantification (L_Q) for the investigated trace elements. YLn concentrations measured in five repeated analyses of an artificially prepared standard physiological solution having 10 ng l^{-1} nominal concentration of each YLn. nd: not determined.

3.2.3 *Thermodynamic modelling*

In order to evaluate if interactions between lung fluids and volcanic particles could induce crystallization of secondary phases, we followed the modelling approach. Modelling calculations were carried out using the composition of simulated lung fluid (SLF) reported by Wood et al. (2006), taking in account that SLF dissolves soluble-ash fraction (SAF) of suspended volcanic particulates after quick reaction.

Due to the large SAF solubility the rate of the glass dissolution was supposed to be negligible with respect to the rate of SAF dissolution in lung fluids. As a consequence the SLF composition was modified (simulated modified lung fluid, here called SMLF) before interacting with glass and crystalline fractions of volcanic particles. In our calculations the fractionation of YLn induced by the occurrence of colloidal phase was not considered because the colloidal stability in aquatic systems is limited to low salinity conditions (0–6mg l^{-1}) (Sholkovitz, 1992 and 1993). On the contrary, salt contents of lung fluids and the physiological solution used for BAL collection (9.5 and 11.4 mg l^{-1}, respectively) were too high to involve the occurrence of a significant colloidal phase in these fluids. YLn contents in SMLF are reported in Table 3.3. Chemical modifications induced in SMLF by interaction with glassy-ash fraction were evaluated with the aid of the EQ3/6, version 7.2b, software package (Wolery 1979; 1992; Wolery and Daveler 1992) using the LLNL thermodynamic database from the Lawrence Livermore National Laboratory where the same software package was developed.

	Y	La	Ce	Pr	Nd	Sm	Eu	Gd	Tb	Dy	Ho	Er	Tm	Yb	Lu
	µgl l^{-1}	µgl l^{-1}	µgl l^{-1}	µgl l^{-1}	µgl l^{-1}	µgl l^{-1}	µgl l^{-1}	µgl l^{-1}	µgl l^{-1}	µgl l^{-1}	µgl l^{-1}	µgl l^{-1}	µgl l^{-1}	µgl l^{-1}	µgl l^{-1}
SMLF	0.003	0.007	0.010		0.006	0.001	0.0005	0.001		0.0003	0.0001	0.0003	0.004	0.000	0.004
$[YREE]_0$	12.20	41.90	64.10		24.30	518	2.36	3.75		2.43	0.43	1.09	0.16	0.97	0.15

Table 3.3 - YLn contents modelled in simulated modified lung fluids (SMLF) after dissolution of soluble-ash fraction, immediately before to crystallization of YLn-phosphates $[YLn]_0$. nd: not determined.

EQ3/6 algorithm models the chemical evolution of geochemical systems using thermodynamic and kinetic constraints. In order to treat rock-water interactions in a lung system leading to major, minor and trace elements release, the double solid reactant method (DSRM) was adopted according to Accornero and Marini (2008). This approach is usually carried out to model trace elements released to the aqueous solution

during dissolution of host rocks. In fact, thermodynamic models and rate laws based on transition state theory (TST; Eyring 1935a; 1935b) can be used to describe the release during dissolutions of primary minerals. In DSRM, each dissolving solid phase is considered as a double solid reactant, consisting of a pure mineral or a solid mixture (the solid reactant) and another reactant, defined special reactant according to EQ6 nomenclature. Basaltic glass is considered to be a mixture of amorphous silica and cryptocrystalline AlOOH; therefore, the hydrolysis reaction for amorphous silica and gibbsite, rather than for crystalline silica, was used to better simulate natural conditions (Gislason and Oelkers, 2003). Thermodynamic and kinetic properties of the solid reactant are enclosed in the geochemical database and determine analogous proprieties (i.e. equilibrium constant of the hydrolysis reaction), whereas the same features are unknown for the special reactant. The saturation state of the aqueous solution with respect to the solid reactant is calculated during the progressive dissolution of rocks and this process is stopped upon attainment of saturation.

The input parameters utilized in EQ6 thermodynamic model for dissolution of volcanic particle components by lung fluids include: (a) composition and surface area of solid reactant, (b) speciation model consistent with the composition of SMLF and (c) kinetic parameters of the solid reactant. The first two parameters are obtained from analyses of solid and liquid reactants and construction of the speciation model with the aid of the EQ3NR computer code. Reaction path modelling has been carried out according to a kinetic approach based on the transition state theory (TST). Rate-laws are written in the form (Prigogine 1955):

$$r_\varphi = f_i A_{Sj} \sum_{i=1}^{i_{T+j}} k_{+,ij} \left(\prod_{n=1}^{n_{T+ij}} a_n^{-N_{+ij}} \right) (1 - e^{-(A_{+j}/\sigma_{+ij}RT)}) \qquad (1)$$

The terms in brackets are the kinetic activity product taking in account the effect of the dissolved composition and the affinity factor that is influenced by the distance from equilibrium. Symbols used in equation 1 are explained in Table 3.4.

The reaction progress is described by the variable ξ (expressed in moles) that measures the extent of the reactive process (Prigogine 1955; Denbigh 1971). In EQ6, reaction progress variables are used to describe only the reactions that are irreversible (not at equilibrium). The irreversible process is defined by an array of simple irreversible

reactions. A reaction progress (ξ) is associated to each of these reactions. There is in addition an overall reaction progress variable (ξ) for the process as a whole. The investigated system consists of a primary mineral, an aqueous solution and other secondary minerals that can crystallize as a consequence of solid-liquid interactions. The reaction path modeling starts taking into account the dissolution of basaltic glass according to the reaction:

$$SiAl_{0.36}O_2(OH)_{1.08} + 0.36\ H_2O = SiO_2 + 0.36\ Al(OH)_4^- + 0.36H^+$$

Thermodynamic properties were estimated from stoichiometrically weighted sum of hydrolysis reactions for amorphous silica and gibbsite. They were re-computed at the temperature, pressure grid required by the software package EQ3/6 and included in the thermodynamic database. The kinetic parameters used in this simulation correspond to the Gislason and Oelkers estimations (Gislason and Oelkers, 2003).

Inhaled particles interesting the deep lung area should have diameters lower than 3 μm (Baxter et al., 1999). Their shape was suggested by optical observations carried out on the material used for kinetic experiments and revealed wide presence of glass with low porosity and rounded, rather than irregular shape. Therefore we did not measure the specific surface area of these products with a BET approach, according to Wolff-Boenisch et al. (Wolff-Boenisch et al., 2004) who reported that dissolution rates of volcanic glass particles were more closely proportional to geometric surface area rather than their BET surface area. Thus the geometrical surface area of ash was calculated assuming a spherical grain shape (with radius equal to 0.3 μm) with intra-grain porosity equal to 0.3.

Although this can be considered an arbitrary choice and a scalene ellipsoidal form could be more adequate to describe features of ash grains (Dellino et al., 2005), recent investigations suggest that real ash particles have higher surface areas that geometric forms due to their roughness (Ersoy, 2010) and the geometrical approach attains to minimum surface area values. On the other hand Ersoy's results corroborate our choice of a spherical shape of grains in volcanic product because indicate that the spherical assumption of ash shape better than the ellipsoidal for simulates the surface area/volume ratio of natural products, especially for the finest grain size. Clearly, modeling the interface area according to a geometric approach rather than its direct assessment induces an underestimation of interacting solid–liquid surface and

consequently involves an incorrect evaluation of leaching rate of investigated elements. On the other hand the reactivity of volcanic ash in lungs is taking in account only in terms of reaction progress (λ), not in terms of absolute time, to assess if the modeling approach attains to results that corroborate geochemical indications of crystallization of lanthanide phosphate. Trace element concentrations were used to define a special reactant associated with hydrated basaltic glass in DSRM. Model calculations were performed under open-system conditions (being the system in contact with a large external gas reservoir) at 37 °C (body temperature). Simulated physical-chemical conditions, major and minor elemental concentrations in SMLF are reported in Table 3.5. In the reaction path modeling, a set of realistic secondary solid phases has been allowed to precipitate, including the minerals which have been shown to reach saturation at the investigated conditions, and alteration minerals originated from hydrated basaltic glass (gibbsite, kaolinite, chalcedony, saponite and a mechanical mixture of transition metal hydroxides, constituted by ferrihydrite, $Fe(OH)_2$, $Cr(OH)_3$, $Mn(OH)_3$, amorphous $Mn(OH)_2$, $Co(OH)_2$, $Ni(OH)_2$, $Cu(OH)_2$, and e-$Zn(OH)_2$).

Instantaneous equilibrium between these minerals and lung fluids was assumed.

Parameter symbol	Description	Units
$N_{+,ij}$	Mechanism-specific reaction order	
$n_{T+,ij}$	Activity of aqueous species number (iT+ j) of parallel mechanisms, each one comprising a rate constant (k+, ij) a kinetic activity product, and a term	
i	Depending on thermodynamic affinity (A+j)	
r_ϕ	Dissolution rate	$mol\,s^{-1}$
A_{Sj}	Physical surface area of jth solid	cm2
f_j	Ratio of reactive to physical surface area	
$k_{+,iJ}$	Kinetic rate constant	$mol\,cm^{-2}\,s^{-1}$
a_n	Term depending on thermodynamic affinity	
$\sigma_{+,iJ}$	Temkin's coefficient	
T	Absolute temperature	K
A_{+j}	Thermodynamic affinity of jth solid	
R	Gas constant	$J\,mol^{-1}\,K^{-1}$

Table 3.4 - List of the parameters in the thermodynamic modelling.

As regards to YLn, the composition of lung fluids, usually mirrored by

Gamble's solution (Midander et al., 2007), implied that the most suitable lanthanides precipitation phase was the phosphate and this hypothesis also agreed with model calculations carried out by Wood et al. (Wood et al., 2006). However, YLn do not form pure phosphates (Byrne and Kim, 1993). Instead, due to the close similarities in their ionic radii the entire YLn suite in presence of PO_4^{3-} in natural solutions forms coprecipitates (Byrne and Kim, 1993). YLn compositions is related to the composition of parent solution (pf) according to the relationship:

$$\left(\frac{YLn_i}{YLn_j}\right)_{PO_4^{3-}} = \lambda_{ij}\left(\frac{YLn_i}{YLn_j}\right)_{pf} \qquad (2)$$

where $[YLn_i]$ and $[YLn_j]$ denote concentrations of two elements of the suite in co-precipitates (PO_4^{3-} subscript) and coexisting fluid (pf subscript), respectively, whereas λ_{ij} are factors that influ ence the relative YLn fractionations. Therefore, being coexisting fluid represented by SMLF, on the basis of *ij* values measured by Byrne et al. (1996), the consisting YLn concentrations in the hypothetical co-precipitated phosphate were calculated. The YLn phosphate concentration in agreement with SMLF data and λ_{ij} values is $Y_{0.15}La_{0.15}Ce_{0.31}Nd_{0.24}Sm_{0.10}Gd_{0.05}(PO_4)$. This chemical composition to falls in the range of monazites, a common natural phosphate mineral (Nash, 1984) thus, the thermodynamic properties of natural monazite were used during the calculation. During simulations, newly formed authigenic minerals are considered isolated with respect to the residual lung fluid and do not react with it.

pH	Al	Ca	Mg	Fe	Mn	Na	K	Cl	F	SO_4^{2-}	$Ti(OH)_4(aq)$	$SiO_2(aq)$	HPO_4^{2-}	fCO_2
	µgl l^{-1}	µgl l^{-1}	µgl l^{-1}	µgl l^{-1}	µgl l^{-1}	µgl l^{-1}	µgl l^{-1}	µgl l^{-1}	µgl l^{-1}	µgl l^{-1}	µgl l^{-1}	µgl l^{-1}	µgl l^{-1}	Pa
7.4	34	6	0.2	0.01	1	5	0.01	80	3	680	0.01	10	20	500

Table 3.5 - Major and minor element contents, pH and fCO_2 used in SMLF for thermodynamic modelling. Model simulations were carried out at 37 °C. Set values are consistent with those occurring in lung fluids.

3.3. *Results*

YLn cumulative concentrations in the BAL samples analyzed in this study span a range from 56.9 to 165.4 µg l^{-1}. However, the relative abundances of the different elements in the Ln series plus Y are all very similar in all the samples, with Y and light REE (LREE) as the most abundant elements. The overall pattern of YLn abundances in BALs are very different with respect to those of the solid components of volcanic ejecta making it unlikely that the wide range of cumulative YLn contents is caused by residual undissolved inhaled volcanic particles (<6.4 µm, Grainger et al. 2009) mechanically removed from bronchial tissues during BAL lavages.

Comparing shale-normalized YLn patterns of BAL solutions with analogous patterns for SAF, we observe significant differences (Fig. 3.2). While the YLn patterns of SAF are flat, those from BAL lavages are flat only between Pr and Eu. Y and La normalised concentrations are about 50 times higher, whereas Ce is about 4 time higher than Pr–Eu normalised concentrations. Normalised concentrations of heavier elements, from Gd to Lu, progressively increase respect to those measured in Pr–Eu interval, attaining to a Lu enrichment of about 3 times. Furthermore, all YLn concentrations are higher in BALs than in SAF.

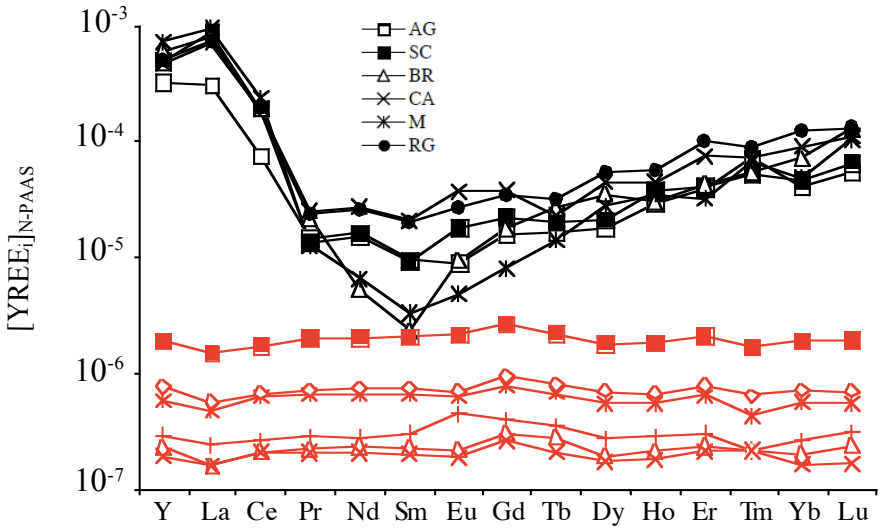

Figure 3.2 - Shale-normalized YLn contents in BAL fluids (black symbols). Concentrations of soluble-ash fractions from Etna (Aiuppa et al. 2003) are reported as reference (red symbols).

Since over-estimation of true concentrations, due to spectral interferences, were avoided by measurements carried out both in high and medium resolution modes for the entire suite of investigated elements, the observed enrichments from Y to Nd can be influenced by co-precipitation of YLn-phosphate from lung fluids in intra-alveolar spaces. Indeed features observed in BAL patterns are very similar to those recognized in solutions that experienced YLn-phosphate co-precipitation (Byrne et al., 1996). As proposed by Byrne and Kim (1993), the co-precipitation of trace elements may follow the relationship:

$$\log\left\{\frac{[YLn_i]}{[YLn_i]_0}\right\} = \lambda_{ij}\ \log\left\{\frac{[YLn_j]}{[YLn_j]_0}\right\} \qquad (3)$$

where $[YLn_i]$ and $[YLn_j]$ denote dissolved concentrations during co-precipitation whereas $[YLn_i]_0$ and $[YLn_j]_0$ are the initial concentrations.

In Fig. 3.3 the behaviour of $\log\{[YLn_i]/[YLn_i]_0\}$ values computed for BAL lavages using SMLF as representative of initial concentrations, are compared with fractionation patterns determined by Byrne et al. (1996) in a study of YLn fractionation during phosphates co-precipitation from solutions at 25 °C and pH close to 4, between 24 and 49 h. Pattern relative to BAL solutions are similar to 49 h phosphate co-precipitation pattern, rather than after 24 h (Byrne et al.,1996).

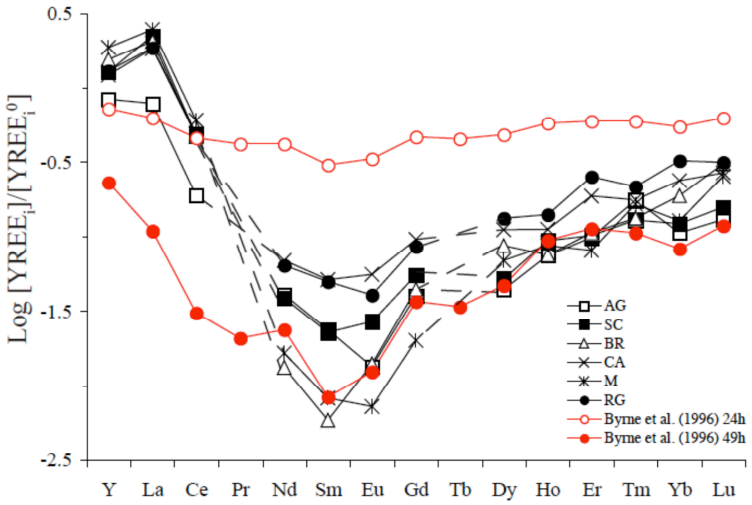

Figure 3.3 - YLn fractionation calculated between initial modeled concentrations of SMLF and BAL solutions. For further details see text. YLN fractionations induced by crystallization of YLN-phosphate after 24-h and 49-h (Byrne et al. 1996) are reported for comparison.

This suggests that phosphate co-precipitation had different amplitude in studied individuals probably as a consequence of different amount of inhaled atmospheric dust. Therefore, if the particle dissolution occurred during a longer time, phosphate co-precipitation had a longer duration and YLn were more intensely fractionated. Since $\log\{[YLn_i]/[YLn_i]_0\}$ BAL values for Y, La and Ce in Fig. 3.3 are often higher than those in phosphate co-precipitation (Byrne et al., 1996), the concurrent presence of an additional particulates source of these elements cannot be excluded (i.e. anthropogenic particulate, Kulkarni et al. 2007).

The recognition of newly formed materials in lungs usually requires micrometric scale observations that need to remove lung tissues by biopsy (Yoon et al., 2005; Hirano and Suzuki, 1996). This is particularly expensive and not easily made in routine hospital analysis in many countries. The results of our calculations indicate that effectively the SMLF-ash interaction produces the precipitation of Al and transition metal hydroxides, cryptocrystalline SiO_2 and phosphates (Fig. 3.4). The precipitation of metal hydroxides and cryptocrystalline SiO_2 does not induce YLn fractionation in parent solution (Coppin et al. 2002; Quinn et al. 2004) because only weak surface complexation processes are involved. On the contrary, YLn have large affinity as regards of phosphates that usually accept in their lattice significant amounts of YLn with large preference for elements, from Sm to Gd, during crystallization of Ca-phosphate. The incorporation of intermediate REE induces REE fractionation in parent solution of newly formed phosphates that consequently assume specular REE features (Hannigan and Sholkovitz 2001). Similarly, if YLn-phosphate co-precipitate as solid solution of YLn, similar YLn behavior is recognized (Byrne and Kim, 1993; Byrne et al., 1996).

3.4. *Implications*

The combination of analytical results and model calculations that we present in this study gives a viable explanation for the occurrence of dendriform pulmonary ossification (DPO), a rare pulmonary pathology affecting people exposed to inhalation of YLn-bearing dust. DPO causes the development of branching bony spicules in the lung parenchyma of people with pulmonary fibrosis that, in the light of results of this

study, can be explained as a consequence of the co-precipitation of YLn-phosphates from YLn-rich lung fluids due to dissolution of atmospheric particles.

We observe a strong similarity between $\log\{[YLn_i]/[YLn_i]_0\}$ patterns of BALs and those produced by co-precipitation of phosphates from parent solution. Such similarity suggests that the amplitude of YLn fractionations in BAL can be used as proxy to investigate the effects of human exposure to inhalation of YLn-bearing atmospheric dust and can represent a tool to develop strategies for the prevention of DPO.

Due to the increasing utilization of YLn for agricultural and industrial applications, the measurement of YLn fractionation in lung fluid (through BAL) has the potential to be a viable tracer of human exposure to heavy fluxes of fine particulates enriched in heavy metals pollutants.

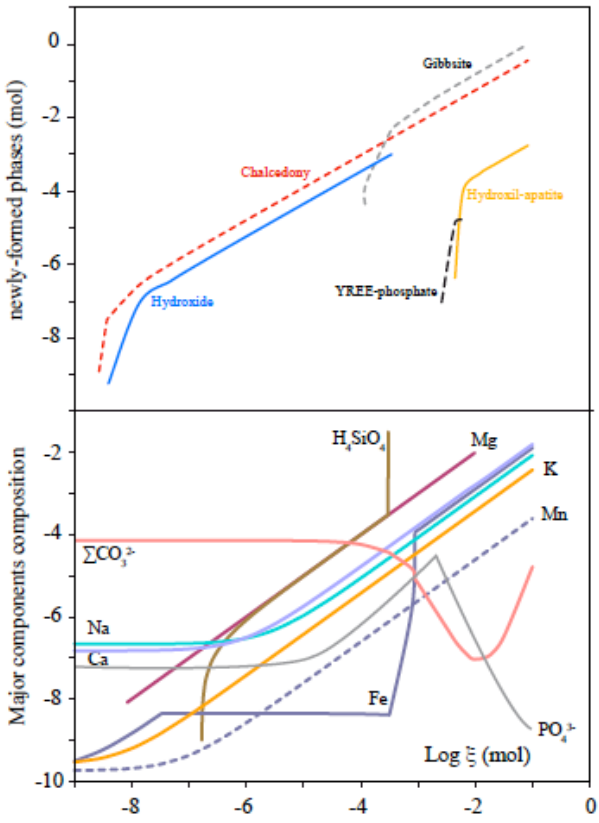

Figure 3.4 – Cumulative moles of secondary minerals precipitated during SMLF-glass interaction. The simulations carried out considering glass-ash as the solid reactant and YLN as the special reactant indicate that gibbsite, hydroxides and chalcedony are the first-formed and the most abundant secondary minerals along the reaction path. Upon increasing extent of reaction, REE-phosphate and hydroxyl-apatite become progressively stable, implying that these minerals act as major sinks for REE elements.

References

Accornero, M, Marini, L., 2008. *The Double Solid Reactant Method for modeling the release of trace elements from dissolving solid phases: I. Outline and limitations.* Environmental Geology 55, 1627-1635.

Aiuppa, A, Dongarrà, G, Valenza, M, Federico, C, Pecoraino, G., 2003. *Degassing of trace volatile metals during the 2001 eruption of Etna.* In: Volcanism and the Earth‟s Atmosphere Geophysical Monograph 139 (Robock A. and Oppemheimer C. eds.). American Geoph Union, Washinghton DC, 41-54.

Baddini Martinez, J.A., Ramos, S.G., 2008. *Inhalation of hydrocarbon combustion products as a cause of dendriform pulmonary ossification*. Medical Hypoth. 71, 981-982.

Bargagli, E, Bigliazzi, C, Leonini, A, Nikiforakis, N, Perari, MG, Rottoli, P. 2005. *Tryptase concentrations in bronchoalveolar lavage from patients with chronic eosinophilic pneumonia.* Clin. Sci. 108, 273-276.

Bargagli, E, Monaci, F, Bianchi, N, Bucci, C, Rottoli, P. 2008. *Analysis of trace elements in bronchoalveolar lavage of patients with diffuse lung diseases*. Biol. trace elem. Res. 124, 225-235.

Byrne, RH, Kim K., 1993. *Rare earth precipitation and co-precipitation behavior: The limiting role of PO4 3- on dissolved rare earth concentrations in seawater.* Geochim. Cosmochim. Acta 57, 519-526.

Byrne, RH, Liu, X, Schijf, J. 1996. *The influence of phosphate co-precipitation on rare earth distributions in natural waters.* Geochim. Cosmochim. Acta 60, 3341-3346.

Censi, P, Sprovieri, M, Larocca, D, Aricò, P, Saiano, F, Mazzola, S, Ferla, P., 2007. *Alteration effects of volcanic ash in seawater: Anomalous Y/Ho ratios in coastal waters of the Central Mediterranean sea.* Geochim. Cosmochim. Acta 71, 5405-5422.

Coppin, F., Berger, G., Bauer, A., Castet, S., Loubet, M. 2002. *Sorption of lanthanides on smectite and kaolinite.* Chem. Geol. 182, 57-68.

Delmelle, P., Lambert, M., Dufrêne, Y., Gerin, 304 P., Óskarsson., N., 2007. *Gas/aerosol-ash interaction in volcanic plumes: New insights from surface analyses of fine ash particles*. Earth Plan. Sci. Lett. 259, 159-170.

Denbigh, K., 1971. *The principles of chemical equilibrium*. 3rd ed. Cambridge University Press.

Dias da Cunha, K., Santos, M., Zouain, F., Carneiro, L., Pitassi, G., Lima, C., 2009. Dissolution Factors of Ta, Th, and U Oxides Present in Pyrochlore, Water, air, and soil pollution 1-7.

Duarte, A.O, Nakatani, J, Rigueiro, M.P., Saad, T., 2006. *Dendriform pulmonary ossification.* J Bras. Pneumol. 32, 270–273.

Eyring, H., 1935a. *The activated complex in chemical reactions*. J. Chem. Phys. 3, 107-115.

Eyring, H., 1935b. *The activated complex and the absolute rate of chemical reactions*. Chem Rev 17: 65-77.

Forde. S., Hynes, M.J., Johnson, B., 2008. *Dissolution of glass compositions containing no added lead in simulated lung fluid.* Int. J. Hyg. Environ. Health 211, 357-366.

Frogner, P. , S.R. , N., 2001. *Fertilizing potential of volcanic ash in ocean surface water*. Geology 29, 487-490.

Galle, P., Berry, J.P., Galle C. 1992. *Role of alveolar macrophages in precipitation of mineral elements inhaled as soluble aerosols*. Environ. Health Perspect. 97, 145-147.

Gislason, S.R., Oelkers, E.H., 2003. *Mechanism, rates, and consequences of basaltic glass dissolution: II. An experimental study of the dissolution rates of basaltic glass as a function of pH and temperature*. Geochim. Cosmochim. Acta 67, 3817-3832.

Grainger, C. I., Greenwell, L. L., Martin, G. P., Forbes, B., 2009. *The permeability of large molecular weight solutes following particle delivery to air-interfaced cells that model the respiratory mucosa.* Eur. J. Pharm. Biopharm. 71, 318-324.

Hannigan, R.E., Sholkovitz, E.R., 2001. *The development 331 of middle rare earth element enrichments in freshwaters: Weathering of phosphate minerals*. Chem. Geol. 175, 495-508.

Helgeson, H.C., 1968. *Evaluation of irreversible reactions in geochemical processes involving minerals and aqueous solutions-I. Thermodynamic relations.* Geochim. Cosmochim. Acta 32, 853-877.

Kulkarni, P., Chellam, S., Fraser, M. P., 2007. *Tracking petroleum refinery emission events using lanthanum and lanthanides as elemental markers for* $PM_{2.5}$. Environ. Sci. Technol. 41, 6748-6754.

Luoto, K., Holopainen, M., Kangas, J., Kalliokoski, P. & Savolainen, K., 1998. *Dissolution of short and long rockwool and glasswool fibers by macrophages in flow through cell culture*. Environ res. 78, 25-37.

Muller, K.M., Friemann, J, Stichnoth, E., 1980. *Dendriform pulmonary ossification*. Pathol Res Pract. 168, 163–172.

Oskarsson, N., 1980. *The interaction between volcanic gases and tephra: fluorine adhering to tephra of the 1970 Hekla eruption*. Jour. Volcanol. Geoth. Res. 8, 251-266.

Prigogine, I., 1955. *Introduction to Thermodynamics of Irreversible Processes.* Wiley, New York.

Quinn, K.A., Byrne, R.H., Schijf, J., 2004. *Comparative scavenging of yttrium and the rare earth elements in seawater: Competitive influences of solution and surface chemistry*. Aq. Geochem.10, 59-80.

Sakai, N., 2007. *Medical Mineralogy and Geochemistry: an interfacial sciences*. Elements 3 381-384

Scollo, S., Del Carlo, P., Coltelli, M., 2007. *Tephra fallout of 2001 Etna flank eruption: Analysis of the deposit and plume dispersion*. Jour. Volcanol. Geoth. Res. 160:147-164.

Taddeucci, J., Pompilio, M., Scarlato, P., 2004. *Conduit processes during the July-August 2001 explosive activity of Mt. Etna (Italy): Inferences from glass chemistry and crystal size distribution of ash particles.* Jour. Volcanol. Geoth. Res. 137 (SPEC. ISS.), 33-54.

Takaya, M., Shinohara, Y., Serita F., Ono-Ogasawara, M., Otaki, N., Toya, T., 2006. *Dissolution of functional materials and rare earth oxides into pseudo alveolar fluid*. Ind. health. 44, 639-644.

Viccaro M, Ferlito C, Cortesogno L, Cristofolini R, Gaggero L. 2006. *Magma mixing during the 2001 event at Mount Etna (Italy): Effects on the eruptive dynamics*. Jour Volcanol Geoth Res 149:139-159.

Wolery, T.J., 1979. *Calculation of chemical equilibrium between aqueous solutions and minerals: the EQ3/6 software package, Report UCRL-52658*. Lawrence Livermore National Livermore, California.

Wolery, T.J., 1992. *EQ3NR, A Computer Program for Geochemical Aqueous Speciation-Solubility Calculations: Theoretical Manual, User's Guide, and Related Documentation (Version 7.0). Report UCRL-MA-110662 PT III*. Lawrence Livermore National Laboratory, Livermore, California.

Wolery, T.J., Daveler, S.A., 1992. *EQ6, A computer program for reaction path modeling of aqueous geochemical systems: theoretical manual, users guide, and related documentation (version 7.0), Report UCRL-MA-110662 pt IV*. Lawrence Livermore National Laboratory, Livermore, California.

Wood, S.A., Taunton, A.E., Normand, C., Gunter, M.E., 2006. *Mineral-fluid interaction in the lungs: Insights from reaction-path modeling.* Inhal. Toxicol. 18, 975-984.

Yoon, H. K. Moon, H.S., Park. S.H., Song, J.S., Lim, Y., Kohyama, N., 2005. *Dendriform pulmonary ossification in patient with rare earth pneumoconiosis.* Thorax 60, 701-703.

Chapter IV

Origin of trace elements in human bronchoalveolar lavages during the Etna 2001 eruption.

P. Censi [A, B, C], P. Zuddas[D], L.A. Randazzo [A,C,D],
E. Tamburo[A], A. Cuttitta[B], R. Punturo[E], P. Aricò[A], R. Santagata[F].

A. Dipartimento C.F.T.A. Università di Palermo, Via Archirafi, 36 90123 - Palermo (Italy).
B. I.A.M.C.-CNR –UOS di Capo Granitola, Via del Mare, 3 - 91026 Torretta Granitola, Campobello di Mazara (TP) (Italy).
C. En.Bio.Tech. – Via Aquileia, 35 90100 Palermo (Italy)
D. Institut de Génie de l'Environnement Ecodéveloppement and Département Sciences de la Terre, UMR 5125, Université Claude Bernard Lyon 1, 2 rue R. Dubois, Bat GEODE 69622 Villeurbanne Cedex (France).
E. Dipartimento di Scienze Geologiche, Università di Catania, Corso Italia, 55 - 95129 Catania (Italy)
F. Dipartimento Biomedico di Medicina Interna e Specialistica, sezione di Pneumologia (DI.BI.M.I.S.), Università degli Studi di Palermo - Via Trabucco n° 180, 90146 Palermo

Abstract

Rapid volcanic eruptions quickly ejecting large amount of dust provoke accumulation of heavy metal in people living in the rounding areas. Analyses of bronchoalveolar lavages (BAL) collected on people exposed to the paroxysmal 2001 Etna eruption reveal a strong enrichment on many heavy toxic metals. Comparing the BAL to the dust composition of the South-eastern Sicily, we found that only the V, Cr, Mn, Fe, Co and U enrichment is related to the volcanic event while the Ni, Cu, Cd and Pb is related to the dissolution of particle having an anthropogenic origin. Furthermore, analyses of anomalous La and Ce enrichments in studied BAL solutions reveal the composite nature of the inhaled ambient airborne particles of anthropogenic origin consisting of a mixture of road dust and emissions of petroleum refineries. According with obtained results trace element distribution in BAL represents a suitable tracer or human exposure to different inhaled atmospheric particulates and allows to investigate the origin of source materials inhaled by people subjected to atmospheric fallout.

4.1. Introduction

Can bronchoalveolar fluids be used to identify the sources of the atmospheric dust inhaled by people living in highly anthropized areas? Can this goal be attained using classical solid-liquid geochemical approaches?

The behaviour of minor and trace elements in human pulmonary fluids is a poorly understood. We do know that atmospheric dust can react with lung fluids dissolving atmospheric particles of different types (Luoto et al., 1998; Takaya et al., 2006; Forde et al., 2008). Moreover, investigations on the effect of dust particle dissolution in human lung systems and on the delivery of trace elements to bronchial fluids are quite uncommon as well are studies that use trace element distributions in broncho-pulmonary fluids as probes of the exposure of humans to particular environments. This investigation was initially carried out to assess whereas the elemental composition of BAL could be considered a tool in identification of pathology of diffuse lung diseases. People living

urban areas are primarily exposed to inhalation of atmospheric dust from both anthropogenic and/or lithogenic origin. Furthermore, suspended anthropogenic particulate matter can have both an automotive or industrial origin and sometimes it can be difficult to univocally differentiate between them. The recognition of origin and nature of inhaled dust particles is fundamental to evaluating potential health risks for exposed people due to differences in chemical reactivity of the atmospheric dust. In summer 2001 Catania, a town of 500000 inhabitants located southward the Mount Etna, was the focus of this study because of the largest pyroclastic eruptions of Etna recent history. The eruption allowed us to investigate the simultaneous occurrence in the atmospheric column of suspended particles from lithogenic (volcanic and sedimentary origin) and anthropogenic sources. We take this opportunity to investigate the trace element distribution in bronchoalveolar lavages (BAL) of some volunteers exposed people to clarify wherever trace element distributions in BAL could be used as proxy for the origin and nature of atmospheric dust. In this work we used an original geochemical approach bases on the assumption that BAL solutions can be treated as natural fluids that interacted with different solids. According to this assumption trace element compositions in BAL are influenced by interactions with different materials inhaled by the investigated people and can be used as a proxy of the environmental exposure of individuals.

4.2. *Experimental section*

4.2.1 *Fine particulate emitted by Etna volcano in summer 2001*

During the Etna eruption in summer 2001, the amount of ejecta was so large that it caused the deposition of about 0.39 kg m^{-2} ash between 21 and 24 July 2001 in the interested area (Scollo et al., 2007). Volcanic ejecta typically consisted of a mixture of several solids ranging from particles made of silicate minerals and volcanic glass to soluble salts adsorbed onto those particles (Oskarsson, 1980; Frogner et al., 2001; Delmelle et al., 2007). The solid fraction of ejected materials mainly consisted of glass fragments (about 70%) with smaller amounts of clinopyroxene (about 15%) and minor amounts of olivine and spinel (Taddeucci et al., 2004; Viccaro et al., 2006). Soluble ash

fraction (SAF) coating solid particles consisted on highly soluble sublimates of acids, metal salts and adsorbed fluids formed during the uprising in the volcanic eruptive plume (Oskarsson, 1980). More recently Delmelle et al. (2007) demonstrated that coatings, consisting of chlorides, sulphates, sulphosalts, sulphides and native elements, were produced, with added large amounts of fluorides. The last compounds could be originated by high temperature alteration of thin glass surface for interaction with plume fluids.

4.2.2 BAL extraction and chemical sample processing

Six patients (volunteers) in care at the Dipartimento di Medicina Interna e Medicina Specialistica of the Università degli Studi di Catania were subjected (after giving their written informed consent) to Bronchoalveolar lavage (BAL) during the summer of 2001. Due to the particular location of Catania with respect to the eruptive source, this intensely populated urban area was subjected to intense delivery of volcanic particulate mainly consisting of mineral, glass and rock fragments between 1 and 500 μm diameter, with main grain-size in the range of 5-10 μm diameter (Taddeucci et al., 2004; Viccaro et al., 2006; Censi et al., 2007; Scollo et al., 2007).

Bronchoalveolar lavages were obtained by instillation of four lavages carried out with 30 ml aliquots of physiological solution (SW) using a fibrobronchoscope (Bargagli et al. 1995) where every aliquot was immediately gently aspirated. From each lavage, about 20 ml of sample were rejected, and only 10 ml of sample, were used for chemical investigations. After filtration with a 0.22 mm Nalgene™ membrane, BAL were treated with 15 ml of hydrogen peroxide, 5 ml of HNO_3 30 % solution, HCl 30% solution and 0.1 g of solid NH_4F in a polytetrafluoroethylene (TFM™) reactor. Reactors were sealed and heated in a microwave oven (MARS 5™, CEM Technologies) at 3^x105 Pa and 200 °C for 30 minutes. Acid excess was removed from each solution up to incipient dryness using a CEM microvap™ apparatus and HNO_3 solution (5 % v/v) was added to attain final solution volumes of 20 ml. The solutions were finally transferred to previously cleaned polycarbonate vials. The samples were treated under a laminar airflow clean bench to minimize contamination risks.

Trace element analyses were carried out with a sector field SF-ICP-MS Thermo-Fisher Element 2 using an external calibration approach. BAL analyses are reported in Table 4.1. The calibration for each element was based on 7 standard solutions at known concentration.

	Units	BAL-1	BAL-2	BAL-3	BAL-4	BAL-5	BAL-6	Average	σ±	Variation (%)
Al	mg l^{-1}	67.57	143.19	194.92	189.65	102.42	229.36	154.52	61.43	39.76
V	µgl l^{-1}	34.33	28.51	21.32	33.70	4.78	17.36	23.33	11.31	48.47
Cr	µgl l^{-1}	78.48	126.46	136.45	107.52	74.60	180.79	117.38	39.77	33.88
Mn	µgl l^{-1}	179.59	181.60	150.93	303.21	66.60	150.74	172.11	76.64	44.53
Fe	mg l^{-1}	8.28	9.19	6.25	10.48	5.95	7.08	7.87	1.77	22.47
Co	µgl l^{-1}	6.81	7.07	4.26	6.89	4.30	5.39	5.79	1.31	22.67
Ni	µgl l^{-1}	82.54	152.61	77.42	165.84	470.04	143.36	181.97	145.89	80.17
Cu	µgl l^{-1}	211.49	176.45	61.31	969.32	112.93	238.87	295.06	336.64	114.09
As	µgl l^{-1}	24.67	69.53	139.40	279.63	93.36	157.59	127.36	88.64	69.60
Y	µgl l^{-1}	10.22	15.55	18.86	14.78	22.70	15.79	16.31	4.19	25.67
Cd	µgl l^{-1}	3.76	3.76	1.93	1.40	16.26	17.13	7.38	7.29	98.82
La	µgl l^{-1}	32.82	93.34	85.56	76.41	102.72	77.64	78.08	24.28	31.09
Ce	µgl l^{-1}	11.98	30.96	30.02	31.30	38.73	30.85	28.97	8.92	30.80
Pr	µgl l^{-1}	0.25	0.23	0.37	0.43	0.22	0.40	0.32	0.09	29.48
Nd	µgl l^{-1}	0.98	0.94	0.32	1.67	0.40	1.55	0.98	0.56	57.36
Sm	µgl l^{-1}	0.12	0.12	0.03	0.27	0.04	0.26	0.14	0.10	73.02
Eu	µgl l^{-1}	0.03	0.06	0.03	0.13	0.02	0.10	0.06	0.04	71.04
Gd	µgl l^{-1}	0.15	0.21	0.17	0.36	0.08	0.32	0.21	0.11	50.48
Tb	µgl l^{-1}	0.02	0.02	0.03	0.03	0.02	0.04	0.03	0.01	30.34
Dy	µgl l^{-1}	0.11	0.13	0.21	0.27	0.17	0.32	0.20	0.08	41.78
Ho	µgl l^{-1}	0.03	0.04	0.03	0.05	0.04	0.06	0.04	0.01	25.86
Er	µgl l^{-1}	0.11	0.11	0.11	0.20	0.09	0.27	0.15	0.07	48.89
Tm	µgl l^{-1}	0.03	0.02	0.02	0.03	0.03	0.03	0.03	0.01	19.70
Yb	µgl l^{-1}	0.10	0.12	0.18	0.23	0.12	0.31	0.18	0.08	45.73
Lu	µgl l^{-1}	0.02	0.02	0.05	0.04	0.04	0.05	0.03	0.01	32.50
Pb	µgl l^{-1}	76.51	165.07	57.30	140.38	145.89	118.98	117.36	42.19	35.95
U	µgl l^{-1}	0.32	1.42	2.03	1.74	0.20	2.66	1.39	0.97	69.65

Table 4.1 - Minor and trace element contents measured in BAL solutions. The analysed masses and the used resolutions are also reported. La and Ce analyses are reported from Chapter 3.

The accuracy of the different procedures was evaluated analysing five aliquots of CASS-4 and NASS-5 standard reference seawaters (National Research Council of Canada; Ottawa, Ontario, Canada) and reported in Table 4.2.

NASS-5

	Resolution	*Measured values (μg l^{-1})*					*MEAN*	*± σ*	*Reference*
^{51}V	Medium	1.163	1.173	1.128	1.145	1.074	1.136	0.039	1.200
^{52}Cr	Medium	0.099	0.104	0.098	0.107	0.097	0.101	0.004	0.110
^{55}Mn	Medium	0.888	0.886	0.864	0.896	0.951	0.897	0.033	0.919
^{57}Fe	High	0.199	0.218	0.196	0.206	0.208	0.205	0.009	0.207
^{59}Co	Medium	0.010	0.010	0.011	0.010	0.011	0.010	0.001	0.011
^{58}Ni	Medium	0.241	0.228	0.234	0.234	0.232	0.234	0.005	0.253
^{63}Cu	High	0.265	0.255	0.259	0.246	0.247	0.254	0.008	0.297
^{75}As	High	1.198	1.231	1.194	1.008	1.483	1.223	0.170	1.270
^{111}Cd	High	0.026	0.024	0.021	0.028	0.025	0.025	0.003	0.023
^{208}Pb	High	0.010	0.012	0.008	0.016	0.014	0.012	0.003	0.008
^{238}U	Medium	2.506	2.523	2.526	2.567	2.609	2.546	0.042	2.600

CASS-4

	Resolution	*Measured values (μg l^{-1})*					*MEAN*	*± σ*	*Reference*
^{51}V	Medium	1.096	1.076	1.108	1.112	1.022	1.083	0.037	1.180
^{52}Cr	Medium	0.134	0.125	0.134	0.135	0.127	0.131	0.005	0.144
^{55}Mn	Medium	2.797	2.701	3.019	3.028	2.756	2.860	0.153	2.780
^{57}Fe	High	0.706	0.758	0.765	0.662	0.732	0.725	0.042	0.714
^{59}Co	Medium	0.024	0.025	0.025	0.024	0.025	0.025	0.001	0.026
^{58}Ni	Medium	0.296	0.311	0.285	0.302	0.315	0.302	0.012	0.314
^{75}As	High	0.952	1.034	1.192	1.005	1.056	1.048	0.090	1.110
^{63}Cu	High	0.542	0.503	0.512	0.536	0.581	0.535	0.030	0.592
^{111}Cd	High	0.616	0.627	0.574	0.568	0.643	0.606	0.034	0.023
^{208}Pb	High	0.010	0.015	0.012	0.008	0.007	0.010	0.003	0.0098
^{238}U	Medium	2.844	2.850	2.681	2.889	2.788	2.810	0.081	3.000

Table 4.2 – Minor and trace element concentrations measured in NASS-5 and CASS-4 standard reference materials. The analysed masses and the used resolutions are also reported.

	SW-1 μg l^{-1}	SW-2 μg l^{-1}	SW-3 μg l^{-1}	SW-4 μg l^{-1}	SW-5 μg l^{-1}	SW_{mean} μg l^{-1}	σ ± μg l^{-1}	L_c μg l^{-1}	L_d μg l^{-1}	L_Q μg l^{-1}
^{27}Al	6.849	6.994	7.012	7.031	6.916	6.960	0.076	0.177	0.354	0.761
^{51}V	0.009	0.012	0.014	0.010	0.008	0.011	0.002	0.006	0.011	0.024
^{52}Cr	0.037	0.028	0.031	0.034	0.047	0.035	0.007	0.017	0.034	0.073
^{55}Mn	0.057	0.096	0.085	0.064	0.048	0.070	0.020	0.046	0.092	0.199
^{57}Fe	2.770	1.981	1.917	1.873	2.529	2.214	0.408	0.952	1.899	4.084
^{59}Co	0.002	0.007	0.008	0.012	0.004	0.007	0.004	0.009	0.018	0.038
^{58}Ni	0.097	0.121	0.118	0.095	0.089	0.104	0.014	0.034	0.067	0.145
^{63}Cu	0.058	0.079	0.095	0.079	0.093	0.081	0.015	0.034	0.068	0.146
^{75}As	0.006	0.005	0.011	0.013	0.031	0.013	0.011	0.024	0.049	0.105
^{111}Cd	0.000	0.012	0.008	0.009	0.011	0.008	0.005	0.011	0.022	0.047
^{208}Pb	0.068	0.073	0.081	0.104	0.194	0.104	0.052	0.122	0.243	0.522
^{238}U	0.007	0.012	0.011	0.021	0.038	0.018	0.012	0.029	0.058	0.124

Table 4.3 - Measured concentrations in physiological solutions (SW) repeated to assess critical values (LC), detection limits (LD) and limits of quantification (LQ) for investigated elements.

Analytical precision was evaluated using the same physiological solution (SW) used for collection of BAL samples. In particular, to five aliquots of SW solution were added the same quantities of chemicals used for the BAL samples treatment, they were subject to mineralization procedures and these represented our procedural blanks used to evaluate critical values (LC) and detection limits (LD) for the investigated trace elements according to the expressions:

$$L_C = 2.33 * \sigma_{PBs} \qquad (1)$$
$$L_D = 4.65 * \sigma_{PBs}$$

where σPBs is the standard deviation of procedural blank measurements. LQ was calculated as ten times the amount of σPBs according to EPA procedures (EPA, 2005).

The obtained results are reported in Table 3.3. The low LQ values indicate that the amounts of trace metals lost and/or added during sample collection and preparation are negligible with respect to the trace elements contents of BAL samples.

All the studied solutions were prepared with Millipore ultrapure water (18.2 MΩ). All used chemicals were Merck ULTRAPUR®. All the materials used to sample and manipulate water samples were plasticware acid cleaned with hot 1: 10 HNO_3 solutions.

4.3. *Results and discussion*

4.3.1 BAL composition

The amplitude of Etna's eruption during July-August 2001 was so large that it exposed all the population of south-eastern Sicily to inhalation of volcanic particles. This fact made it virtually impossible to carry out a typical comparative study on BAL composition between exposed people and control subjects. Therefore results of minor and trace element compositions in BAL of people exposed to the inhalation of volcanic particles are compared with the few minor and trace element analyses from published work (Bargagli et al., 2008). The amount of minor and trace elements measured in this study, reported in Table 1, spans between 0.02 μg l^{-1} for Tm and Lu and 229.36 mg l^{-1}

for Al. The latter, together with Fe, is the most abundant studied element in BAL solutions. Variation coefficients of investigated minor and trace elements, calculated as ratio between standard deviation and average values of every element, are larger for Cu, Cd, Ni, As and U, ranging from 114% and 70%, and are lower for other investigated elements falling between 48% (V) and 20% (Tm).

Many of these values are different both in terms of concentration and in terms of the observed variability with respect to analogous data of BAL carried out on people exposed to inhalation of airborne particles, showing sarcoidosis, idiopathic pulmonary fibrosis, and Langerhans cell histiocytosis and healthy (smoking and non-smoking) controls (Bargagli et al., 2008), as reported in Fig. 4.1.

Trace element concentrations reported in Bargagli et al. (2008) are always lower than those measured in our study, especially for iron that is the most enriched element in their data. On the other hand recognised concentrations in Bargagli et al. (2008) often span on larger ranges with respect to our data. The above mentioned evidences suggest that trace element leaching from inhaled atmospheric fallout influenced trace element contents in studied BAL solutions. In order to clarify if the inhaled particles came from atmospheric fallout of volcanic nature alone, a typical geochemical approach based on the amplitude of enrichment factors of studied trace elements in BAL was carried out.

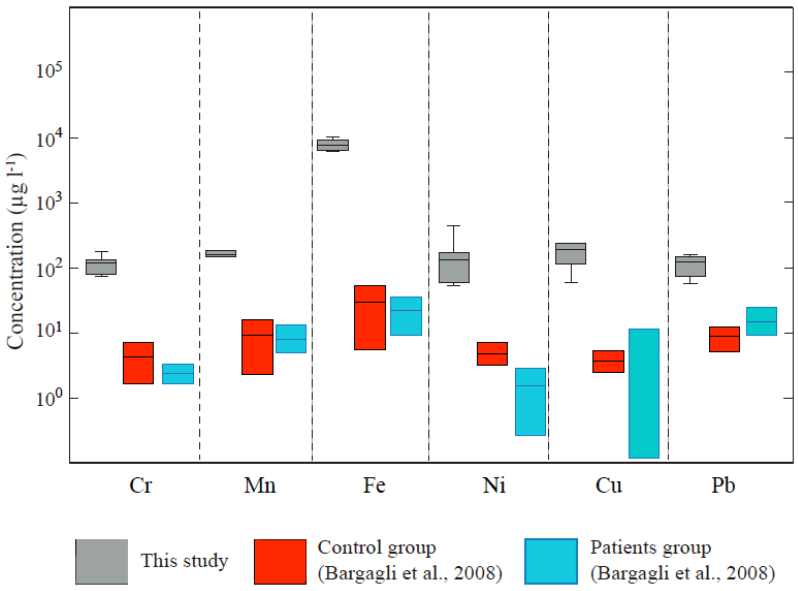

Figure 4.1 – Concentrations of studied minor and trace elements in BAL compared with values reported by Bargagli et al. (2008) for people with extensive lung diseases (patients group) and people unaffected by lung patologies (control, group).

4.3.2 Enrichment factors (EFs)

Enrichment factor values represent a suitable geochemical tool to evaluate the provenance of selected elements from a given source comparing their ratios, with respect to a normalizing element (usually Al). Therefore EFs are calculated according to the following equation (Puckett and Finegan, 1980):

$$EF_X = \frac{[X]_{BAL}}{[Al]_{BAL}} \Big/ \frac{[X]_{REF}}{[Al]_{REF}} \qquad (2),$$

where $[X]$ is the concentration of a given element in the BAL sample (BAL) or in a hypothetical source material (REF) taken as reference (Salomons and Förstner 1984). Generally EF values smaller than 10 indicate that the X element is not significantly enriched in the BAL with respect to the selected reference, whereas an EF value larger than 10 implies an enrichment of the X element in the studied materials with respect to the chosen source (Chester et al. 1999).

Volcanic ash mainly consists of a mixture of glass and crystalline particles that are coated by soluble products consisting of sublimates of acids, metal salts and adsorbed fluids formed as a consequence of interactions between ash grains with volcanic fluids (Rose, 1977; Oskarsson, 1980) with a variable reactivity with respect to aqueous fluids (Delmelle et al., 2007 and references therein). Therefore elemental releases from volcanic ash can occur from the soluble ash fraction and/or from solids, both glass and crystalline materials, under the action of macrophages (Sulotto et al., 1986; Luoto et al., 1998).

In order to establish if the investigated elements were released from volcanic products alone we compared both SAF of erupted ash and BAL samples with respect to the composition of the parent Etna magma of 2001 activity, taken as reference. Calculated EF_{PM} values, reported in Fig. 4.2a, showed that many lanthanides, V, Cr, Fe, Cu, As, Pb and U had EF values similar both in BAL and in SAF, suggesting that these elements could have a volcanic origin probably related to the dissolution of soluble

fraction of pyroclastic materials during interactions with lung fluids. On the contrary La, Ce, Y, Mn, Co, Ni and Cd showed EF values different in BAL with respect to corresponding value measured in SAF. This evidence suggests a different source for these elements. In order to assess if lithogenic materials could represent this further source of inhaled La, Ce, Y, Mn, Co, Ni and Cd from non-volcanic origin EF values for latter elements were recalculated with respect to the composition of the Upper Continental Crust (UCC, from Taylor and McLennan, 1995) and reported in Fig. 4.2b.

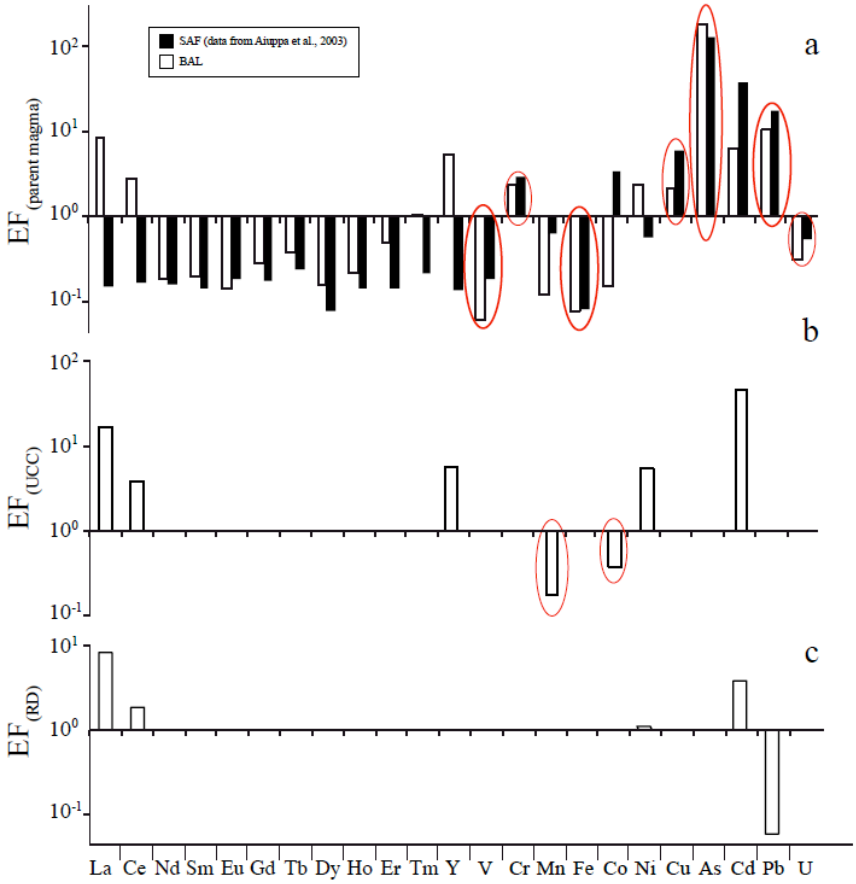

Figure 4.2 - Enrichment factors calculated for studied elements with respect to different possible parent materials: Etna's magma of 2001 eruption (a), upper continental crust (b), road dust (c). Red circles highlight elements whose source is suggested (see text). Data of Etna's parent magma and soluble ash fraction (SAF) are reported in Aiuppa et al. (2003). Data of UCC are reported in Taylor and McLennan (1995). Composition of road dust parent material is reported in Dongarrà et al. (2003).

These EF_{UCC} values are lower than 1 for Mn and Co, suggesting an origin of these elements from partially leached non-volcanic lithogenic materials. On the contrary EF_{UCC} values higher than 10 or falling between 1 and 10 calculated for La, Ce, Y, Ni, Cu, Cd

and Pb involve a non-lithogenic origin for these elements. This source could have an anthropogenic nature that would agree with the intense automotive traffic occurring in Catania and the presence of large industrial sites in south-eastern Sicily (Ausili et al. 2008). To confirm the presence of this anthropogenic contribution to the budget of atmospheric fallout, EF values La, Ce, Ni, Cu, Cd and Pb were recalculated with respect to trace element compositions measured in road dust (RD) collected in the Messina area, that is subjected to a high automotive traffic and is located at about 60 km far from Catania under similar climatic conditions (Dongarrà et al. 2003). Calculated EF_{RD} values for Ni, Cu, Cd and Pb are not far from 1 or lower suggest that atmospheric suspended matter in Catania during Etna's eruption in summer 2001 consisted also of a road dust component. Moreover, amplitudes of these EF values could reflect the labile fraction of Ni, Cu, Cd and Pb in the road dust component of atmospheric fallout in Catania. This hypothesis is consistent of linear relationship observed between calculated EF_{RD} values for Ni, Cu, Cd and Pb and labile fraction of these elements reported by Voutsa and Samara (2002) for atmospheric particulates collected in urban sites (Fig. 4.3), depending from the cleaning capabilities of human bronchial system as regards of inhaled particles containing these elements.

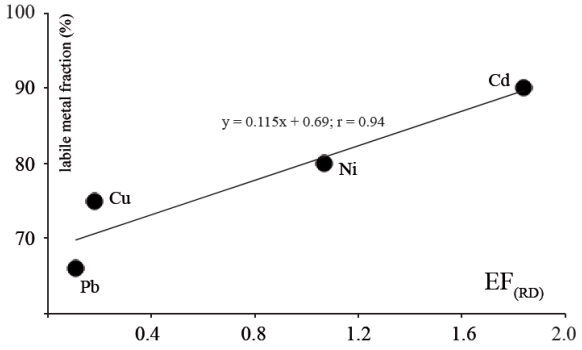

Figure 4.3 – Correlation between EF values calculated respect to the road dust as reference composition for Ni, Cu, Cd and Pb and their bioaccessible fraction measured in airborne materials from urban sites (data from Voutsa and Samara, 2002).

4.3.3. Contribution of the anthropogenic sources

Enrichments in La and Ce disagree with their origin from dissolution of a road dust component. On the contrary La and Ce enrichments in the environment usually

involve delivery of particulates from hydrocarbon refinery industry where La-Ce rich carbonates and zeolites are employed as catalytic converters that are released during hydrocarbon combustion in power stations (Kulkarni et al. 2007; Moreno et al. 2008). Typical geochemical character of these materials is the stronger La enrichment respect to Ce with respect to lithogenic products (Olmez and Gordon 1985; Kitto et al. 1992; Kulkarni et al. 2007) that can be enhanced using a La-Ce-Sm triangular diagram according to Moreno et al. (2008). In this diagram BAL samples fall closely to particulates collected in refinery and oil power station emissions (Moreno et al. 2008), suggesting that particulates emitted from oil refineries in the Augusta-Priolo area interest the air column in Catania (Fig. 4.4a). Further confirmation of a not-lithogenic nature of La and Ce is also given in a $La_{3.1}Ce_{1.54}V$ diagram (Fig. 4.4b). Here, BAL solutions are scattered along a linear trend falling between linear arrays identifying crustal materials and products coming from oil refinery industry reported by Moreno et al. (2008). This evidence confirms that a strong anthropogenic contribution to the budget of inhaled particulate occurred together with volcanic particles ejected from Mount Etna and this contribution can be identified also in zeolitic catalytic converters used in oil refinery.

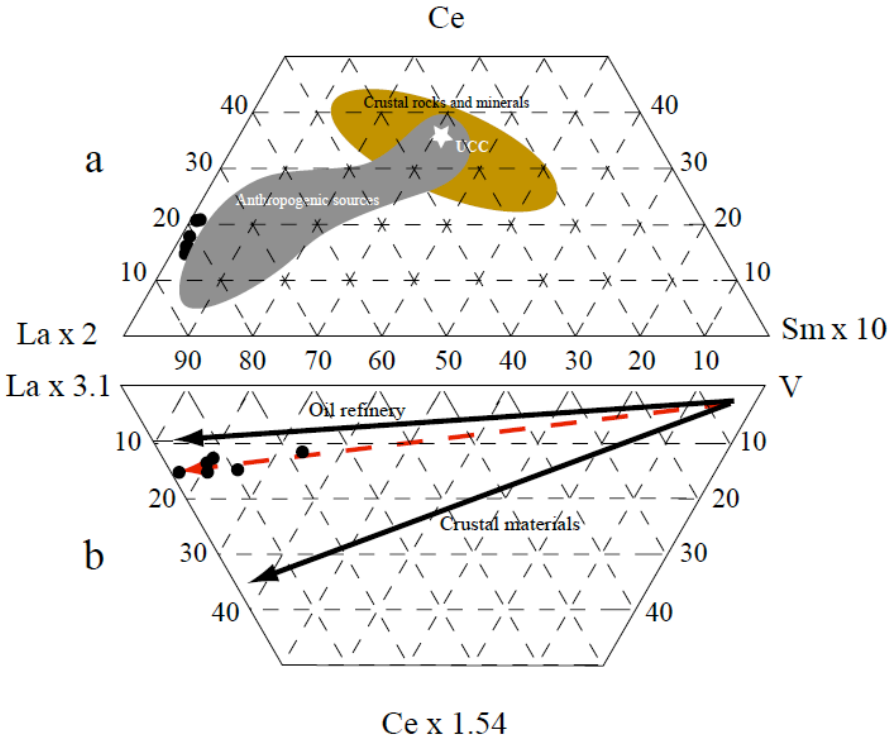

Figure 4.4 – La-Ce-Sm plot for BAL samples compared with crustal materials, anthropogenic source materials (Moreno et al., 2008) and UCC (Taylor and McLennan, 1995).

4.4. *Conclusions*

The study of minor and trace element distributions in bronchoalveolar lavages collected from people subject to inhalation of atmospheric dust particles of different origins can represent a powerful tool for environmental researches. This evidence rises from the results of this study that show as an approach based on the analysis of EF calculated with respect to different source materials is suitable to recognise the nature of inhaled materials. This goal was achieved in a very complicated context, in terms of an urbanised environment where studied individuals were exposed to the continuous inhalation of road dust together with suspended materials from oil refineries and power plants near located. A further episodic contribution of volcanic ash erupted from Mount Etna in summer 2001 was added to this scenario for a period of one month. Collected data indicate that V, Cr, Mn, Fe, As and U have a lithogenic origin due to partial dissolution of different fraction of volcanic ash during interactions with lung fluids, whereas Ni, Cu, Cd and Pb are probably originated by incomplete dissolution of anthropogenic originated road dust. The occurrence of the further industrial input is detected by means of La enrichment in BAL solutions.

References

Aiuppa A, Dongarrà G, Valenza M, Federico C, Pecoraino G. 2003. Degassing of trace volatile metals during the 2001 eruption of Etna. Geophysical Monograph, 19: 41-55.

Ausili A, Gabellini M, Cammarata G, Fattorini D, Benedetti M, Pisanelli B, Gorbi S, Regoli F. 2008. Ecotoxicological and human health risk in a petrochemical district of southern Italy. Marine Environmental Research, 66: 215-217.

Bargagli E, Bigliazzi C, Leonini A, Nikiforakis N, Perari MG, Rottoli P. 2005. Tryptase concentrations in bronchoalveolar lavage from patients with chronic eosinophilic pneumonia. Clinical Science, 108: 273-276.

Bargagli E, Monaci F, Bianchi N, Bucci C, Rottoli P. 2008. Analysis of trace elements in bronchoalveolar lavage of patients with diffuse lung diseases. Biology and trace elements Research 2008, 124: 225-235.

Censi P, Sprovieri M, Larocca D, Aricò P, Saiano F, Mazzola S, Ferla P. 2007. Alteration effects of volcanic ash in seawater: Anomalous Y/Ho ratios in coastal waters of the Central Mediterranean sea. Geochim Cosmochim Acta, 71: 5405-5422.

Censi P., Tamburo E., Speziale S., Zuddas P., Randazzo L. A., Punturo R, Cuttitta A, Aricò P. 2010. Rare Earth Elements and yttrium in human lung fluids probing the exposure to atmospheric fallout. Journal of Hazardous Materials. In press.

Chester R, Nimmo M, Preston MR. 1999. The trace metal chemistry of atmospheric dry deposition samples collected at Cap Ferrat: A coastal site in the Western Mediterranean. Marine Chemistry, 68: 15-30.

Delmelle P, Lambert M, Dufrêne Y, Gerin P, Óskarsson. N. 2007. Gas/aerosol-ash interaction in volcanic plumes: New insights from surface analyses of fine ash particles. Earth Planetary Science Letters, 259: 159-170.

Dongarrà G, Sabatino G, Triscari M, Varrica D. 2003. The effects of anthropogenic particulate emissions on roadway dust and Nerium oleander leaves in Messina (Sicily, Italy). Journal of Environmental Monitoring, 5: 766-773.

Forde. S., Hynes MJ, Johnson B. 2008. Dissolution of glass compositions containing no added lead in simulated lung fluid. International Journal of Hygiene Environmental Health, 211: 357-366.

Frogner P., Gislason S.R., N. O. 2001. Fertilizing potential of volcanic ash in ocean surface water. Geology, 29: 487-490.

Goddu SR, Appel E, Jordanova D, Wehland F. 2004. Magnetic properties of road dust from Visakhapatnam (India) - Relationship to industrial pollution and road traffic. Physics and Chemistry of the Earth, 29: 985-995.

Kitto ME, Andersen DL, Gordon GE, Olmez I. 1992. Rare earth distributions in catalysts and airborne particles. Environmental Science and Technology, 26: 1368-1375.

Kulkarni P, Chellam S, Fraser MP. 2007. Tracking petroleum refinery emission events using lanthanum and lanthanides as elemental markers for PM2.5. Environmental Science and Technology, 41: 6748-6754.

Luoto K, Holopainen M, Kangas J, Kalliokoski P, Savolainen K. 1998. Dissolution of short and long rockwool and glasswool fibers by macrophages in flow through cell culture. . Environmental research, 78: 25-37.

Moreno T, Querol X, Alastuey A, Gibbons W. 2008. Identification of FCC refinery atmospheric pollution events using lanthanoid- and vanadium-bearing aerosols. Atmospheric Environment, 42: 7851-7861.

Olmez I, Gordon GE. 1985. Rare earths: Atmospheric signatures for oil-fired power plants and refineries. Science, 229: 966-968.

Oskarsson N. 1980. The interaction between volcanic gases and tephra: fluorine adhering to tephra of the 1970 Hekla eruption. Journal of Volcanology and Geothermal Research, 8: 251-266.

Puckett, K.J. and Finegan, E.J., 1980. An analysis of the element content of lichens from the Northwest Territories, Canada. Can. J. Bot. 58, 2073-2088.

Rose, W.I. R. 1977. Scavenging of volcanic aerosol by ash: atmospheric and volcanologic implications. Geology, 5: 621-624.

Salomons, W. and Förstner, U., 1984. Metals in the hydrocycle. Springer, Berlin Heidelberg Tokyo.

Scollo S, Delcarlo P, Coltelli M. 2007. Tephra fallout of 2001 Etna flank eruption: Analysis of the deposit and plume dispersion. Journal of Volcanology and Geothermal Research, 160: 147-164.

Sulotto F, Romano C, Berra A, Botta GC, Rubino GF, Sabbioni E, Pietra R. 1986. Rare-earth pneumoconiosis: a new case. Am J Ind Med, 9: 567-575.

Taddeucci J, Pompilio M, Scarlato P. 2004. Conduit processes during the July-August 2001 explosive activity of Mt. Etna (Italy): Inferences from glass chemistry and crystal size distribution of ash particles. Journal of Volcanology and Geothermal Research, 137: 33-44.

Takaya M, Shinohara Y, Serita F., Ono-Ogasawara M, Otaki N, Toya T. 2006. Dissolution of functional materials and rare earth oxides into pseudo alveolar fluid. Industrial health, 44: 639-645.

Taylor SR, Mclennan SM. 1995. The Geochemical Evolution of the Continental-Crust. Reviews of Geophysics, 33: 241-265.

Viccaro M, Ferlito C, Cortesogno L, Cristofolini R, Gaggero L. 2006. Magma mixing during the 2001 event at Mount Etna (Italy): Effects on the eruptive dynamics. Journal of Volcanology and Geothermal Research, 149: 139-159.

Voutsa D, Samara C. 2002. Labile and bioaccessible fractions of heavy metals in the airborne particulate matter from urban and industrial areas. Atmospheric Environment, 36: 3583-3590.

Yu, RC and Rappaport, SM. 1996. Relation between pulmonary clearance and particle burden: A Michaelis- Menten-like kinetic model. Occupational and Environmental Medicine, 53:567-572.

Concluding Remarks

CONCLUDING REMARKS

The dissolution of volcanic ash in seawater carried out under closed system laboratory controlled conditions evidenced the crystallization of newly-formed alteration phases as Al, Fe oxyhydroxides and clay minerals. Lanthanum showed the largest leaching capability among the studied elements evidenced in dissolved phase. YLn dissolved composition is influenced by early dissolution of glass ash fraction and fluorides, formed during high temperature interactions between ejected particles and plume fluids. Y/Ho ratio demonstrates an useful tool to discriminate between YLn scavenging process onto Al and Fe oxyhydroxides. Moreover the modification of dissolved phase adding carbonate and carbonate and humate species influence the YLn behaviour especially during scavenging. SEM observations corroborate these suggestions showing the crystallization of Fe and Al oxyhydroxides.

In the light of these results the effects of YLn leaching in human bronchial fluids, the first world-carried out, assume a large relevance. YLn concentrations in pulmonary fluids originated by inhalation of volcanic particles strongly suggest that bronchial fluids were the parent solution of crystallizing phosphates in bronchoalveolar spaces. Observed large Y and Eu, positive anomalies in these fluids suggest that fluorides dissolution was the early stage of interaction process that was followed by dissolution of ash glass fraction. On the contrary La and Gd anomalies were probably induced by the same larger tendency of these lanthanides for the dissolved phase. Obtained results indicate that geochemical evaluation of bronchoalveolar lavages are able to detect evidences of pulmonary microlithiasis and could represent a not conventional approach to medical pulmonary investigations.